1-2-2013

Multiplexed Photometry And Fluorimetry Using Multiple Frequency Channels

Khaled M. Dadesh
Wayne State University,

MULTIPLEXED PHOTOMETRY AND FLUORIMETRY USING MULTIPLE FREQUENCY CHANNELS

by

KHALED M. DADESH

DISSERTATION

Submitted to the Graduate School

of Wayne State University,

Detroit, Michigan

in partial fulfillment of the requirements

for the degree of

DOCTOR OF PHILOSOPHY

2013

MAJOR: ELECTRICAL ENGINEERING

Approved by:

_____

Advisor Date

_____

_____

_____

DEDICATION

I dedicate my humble work to the soul of my father who encouraged and supported me to be in the right path, my mother who raised me and still prays for me to be a successful person to people and community, my wife and kids, and all my family members and friends who gave me support and help to finish my dissertation.

ACKNOWLEDGEMENTS

I would like to express my sincere appreciation to Dr. Amar Basu, who contributed tremendous time and valuable support to my research. I also appreciate Dr. Yang Zhao, Dr. Mark Ming-Cheng, and Dr. Jessica Back for their constructive comments and precious suggestions and support. I extend my appreciation to our group members in the MB laboratory. Lastly, I acknowledge all the ECE-department's faculty and staff and the machine-shop's technical staff for help and support.

TABLE OF CONTENTS

LIST OF FIGURES

LIST OF TABLES

ABBREVIATIONS

FDM: Frequency division multiplexing.

TDM: Time division multiplexing.

WDM: Wavelength division multiplexing.

LIF: Laser induced fluorescence.

KCRC: Karmanos Cancer Research Center.

DMC: Detroit Medical Center.

APD: Avalanche Photo Diode.

PD: Photo Diode.

PMT: Photomultiplier Tube.

LIA: Lock-in Amplifier.

NIA: Non Inverting Amplifier.

TIA: Trans-Impedance Amplifier.

LOD: Limit of Detection.

SMD: Surface Mount Device.

EMI: Electromagnetic Interference.

DIP: Duel In-Line Package.

LED: Light Emitting Diode.

LD: Laser Diode.

CCD: Charge Coupled Devices.

AM: Amplitude Modulation.

FM: Frequency Modulation.

DSB: Double Side Band.

PSD: Phase Sensitive Detection.

DC: Direct Current.

AC: Alternating Current.

GBP: Gain Bandwidth Product.

PBS: Phosphate Buffer Solution.

HV: High Voltage.

UV: Ultraviolet.

CY: Cyanines.

PDMS: PolyDiMethylSiloxane.

MEMS: Micro Electro Mechanical Systems.

DWS: Dual Wavelength Spectrophotometer.

LPF: Low Pass Filter.

FMM: Frequency Modulation Multiplexing.

EOM: Electro-Optical Modulator.

VCO: Voltage Controlled Oscillator.

PCB: Printed Circuit Board.

FET : Field Effect Transistor.

IC: Integrated Circuit.

MLCC: Multilayer Ceramic Capacitors.

FD&C: Food Dye and color.

S/N: Signal to Noise ratio.

CHAPTER 1: INTRODUCTION

1.1 Problem Statement and Motivation

Spectrophotometry and fluorimetry are ubiquitous techniques in analytical chemistry, and they are widely used in applications ranging from health sciences, environmental monitoring, and homeland security. Basically, spectrophotometers measure light absorption and scattering, while fluorimeters measure fluorescence light signals. For example, light emitting diodes (LED) spectrophotometers are used for the direct determination of the oxy and deoxy-hemoglobin content in tissues [1], and fluorimeters are used to quantify hepatitis C virus [2]. The need for in-situ, low cost, point-of care devices has motivated designers to use miniature semiconductor light sources such as light emitting diodes (LED) and laser diodes (LD), and light detectors including photodiodes (PD), avalanche photodiodes (APD), and photomultiplier tubes (PMT). The benefits of LEDs and LDs include their low cost, low power consumption, long lifetimes, and flicker-free operation. In addition, LEDs provide good chromaticity (50-100 nm spectral bandwidth), while laser diodes provide absolute chromaticity (5-10 nm spectral bandwidth). Chromaticity is important because it can mitigate or eliminate the need for excitation filters that are typically used with the wide spectrum light sources like mercury or halogen lamps. Such filters are needed in applications like laser-induced fluorescence (LIF).

The most basic type of photometer or fluorimeter uses a single wavelength (i.e., a single light source and single light detector) for detection [3]. Although useful in many basic chemical analysis measurements, single wavelength photometry lacks the ability to

differentiate between multiple analytes. By contrast, multi-wavelength photometry and fluorimetry offers additional specificity, as *n* parameter measurements can differentiate up to 2^n unique species. The tradeoff, however, is that multispectral photometry and fluorimetry require more complex optical designs. Spectrometers, for example, require gratings and arrayed light detectors (CCDs, photodiode arrays). Multi-wavelength systems can also have a lower sensitivity due to losses in the grating and the poor low-light performance of CCD based detectors compared to PMTs. In microfluidic systems, the reduced sensitivity is particularly problematic due to the small path lengths, and the integration of multiple optical paths is also a challenge [4].

Multi-color fluorimetry is used in numerous applications, but perhaps the most common is in multi-spectral cell cytometry, where cells tagged with multiple fluorophores are passed single file through a detection window. Multi-color cytometers use a single light detector per wavelength which makes the overall system more complex and expensive. For example, a popular cell cytometer from Beckton Dickinson, model BD LSR II, has eleven PMTs. Each PMT requires a band pass filter, dichroic mirror, and high voltage power supply associated to it. In addition, cytometers must include a flow cell, flow control system, signal conditioning, and data acquisition systems. The number and complexity of the optical components contributes to the high cost for multicolour cytometers, ranging from $200,000 to $400,000 depending on the number of parameters to be detected. More details can be found in section 2.1.7.

In this dissertation, we propose the use of frequency multiplexing to accommodate multiple fluorophores on a single PMT. Other multi-color detection techniques found in

the literature employed either time or frequency division multiplexing. These techniques can reduce the cost and complexity of multispectral photometry and fluorimetry instruments; however, to the current implementations do not respond fast enough to multi-parameter high throughput systems [5], [6], or require bulky and expensive electro optical modulators [7]–[11].

Many multi-color multi-parameter applications, like cell cytometers and sorters, operate at very high flow velocity, which requires high speed detection electronics. In cell cytometers, for example, the exposure time of stained cells in the detection window is ~4 μs, so the detection time must take place in < 4 μs. This mandates that the time constant of our detection system is sufficiently small to allow such fast measurement. The engineering challenge of this work is to provide a detection system which can not only multiplex, but simultaneously provide high speed detection. The combination of the two has not been achieved in the prior literature.

1.2 Research Objectives and Contributions

In order to minimize the cost and reduce the complexity of multi-color spectrophotometry and fluorimetry systems without sacrificing bandwidth necessary for high throughput systems, we are introducing the application of the frequency division multiplexing (FDM) technique in conjunction with lock-in and heterodyne technology to be able to utilize only a single light detector for multiple wavelengths. Both LEDs and LDs are used as light sources. PD, APD or PMT can be used as light detectors. When using frequency multiplexing, the minimum frequency separation between modulation frequencies of different channels determines the speed of the detection system; i.e., the

channel bandwidth. In the case of flow cytometry, our target is to operate at modulation frequencies up to 100 MHz to allow for channel bandwidths of > 1MHz. Our proof of concept system operated at modulation frequencies <10 KHz, allowing 2 KHz frequency separation and channel bandwidth [12]. We then improved our setup to operate at an order of magnitude higher frequency separation [13]. Finally, we improved our designs to culminate in our third generation circuit, which operates in the 100s of MHz range so that it can be used in high speed cell cytometry applications. From the biochemical point of view, we tested our system to perform simultaneous multi-color absorbance photometry to distinguish between three different analytes and fluorescence measurements to distinguish between two different analytes. RF circuit designs which control light sources and implement phase-sensitive or heterodyne detection are developed. Finally, the FDM system is deployed in a commercial cell cytometry system to demonstrate its utility. The detection system is also tested with several microfluidic flow focusing designs in anticipation the long term goal of creating a fully miniaturized multicolor cytometer.

CHAPTER 2: BACKGROUND PRINCIPLES AND LITERATURE REVIEW

2.1 Background Principles

The principle of FDM-based photometry can be explained using frequency domain analysis. The following subsections outline the principles of FDM and lock-in detection, and how they are utilized for multiplexed photometry.

2.1.1 FDM Principle

In radio broadcasting, frequency-division multiplexing (FDM) is defined as the assignment of signal spectra into non-overlapping frequency channels [14] Each signal spectrum can be extracted using a band pass filter. We can consider N signals, each band limited to f_m Hz, and each modulated (e.g., AM or FM) with a carrier frequency f_{C1}, f_{C2}, …, f_{CN}. If the modulation method results in double side band (DSB) the spectral density of each modulated signal has a bandwidth of $2f_m$ and each is centered at different carrier frequencies f_{C1}, f_{C2},…, f_{CN}. These carrier frequencies are chosen far enough apart such that the signal spectral densities do not overlap. Figure 1 illustrates the concept for three different signals of arbitrary shapes.

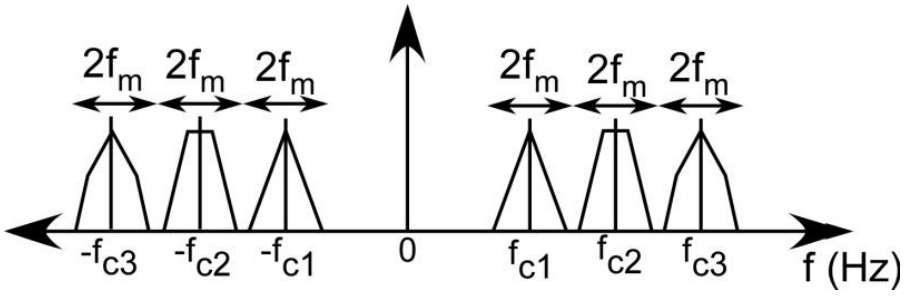

Figure 1: Frequency domain of a FDM signal.

2.1.3 Avalanche Photo diode (APD)

An avalanche photodiode is a PN-junction semiconductor device that uses the photoelectric effect and avalanche phenomenon to operate as a very high sensitivity light detector. We used a Perkin Elmer type C30902E avalanche photodiode with a high responsivity between 400 and 1000 nm. Due to the fast rise and fall times at all wavelengths, this APD can detect light signals with modulation frequency up to 800 MHz, well above our target frequency range of 200 MHz [15]. Instrumentation applications usually use APDs because their speed and high sensitivity compared to conventional PDs, and their quantum efficiencies at > 400 nm exceed PMT quantum efficiencies [16].

2.1.4 Photomultiplier Tubes (PMT)

Photomultiplier tubes are part of the vacuum phototube families, and they possess an extremely high light sensitivity in the range from ultraviolet to infrared light spectrum. Figure 2 shows photocathode spectral responses of some PMTs made by Hamamatsu Company. They have a photocathode at the input that generates an electron when a photon strikes it. A focusing electrode directs the generated electron towards a biased dynode which will generate secondary electrons. These electrons strike another dynode to generate extra electrons. A high voltage power supply is connected across these dynodes via a voltage divider circuitry. The multiplication process continues until the last dynode. Eventually, all generated electrons are collected by the last anode and delivered to the front- end circuit for signal conditioning. PMTs can multiply the electron current

generated from the incident light by a factor of 100 million times in multiple dynode stages [17][18].

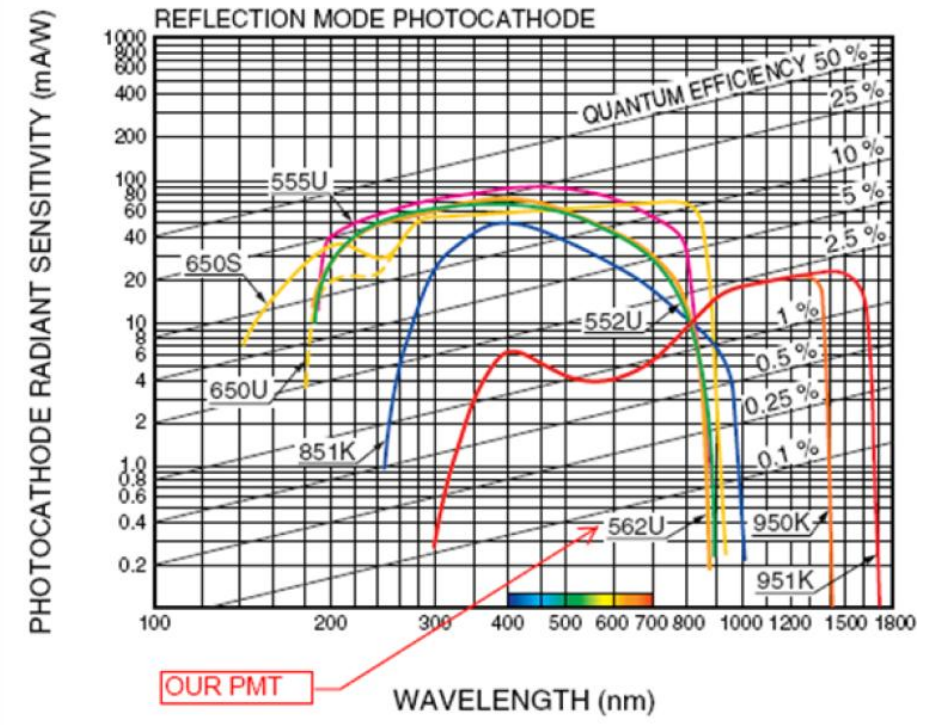

Figure 2: *Photocathode radiant sensitivity of reflection mode PMTs that are made by Hamamatsu-Photonics Company. The PMT we use is from the 562U category.*

2.1.5 Lock-in/Phase Sensitive Detection

Lock-in detection is a low-noise measurement technique commonly used in scientific studies. In a typical radio transmitter, the amplitude or the frequency of a carrier wave is modulated according to the transmitted signal, and later demodulated by synchronous detection circuits at the receiver. By contrast, in lock-in detection, a reference signal with fixed frequency and amplitude applies a periodic stimulus to the experimental system. The system responds with a periodic output, but the amplitude is effectively modulated by the system measurand. The changes in amplitude, reflecting the

changes in the measurand, are extracted by a phase sensitive detector (PSD). PSDs can extract a signal of known frequency from a highly noisy system output, providing a high signal to noise ratio [8].

The core principle behind PSD relies on the orthogonality of sine waves. Any periodic signal with a fundamental frequency f_o can be expanded to its Fourier series, a summation of sine waves which are harmonics of f_o. A PSD multiplies the system output $V_s(t)$ by an electrical reference signal $V_r(t)$, which both have fundamental frequency f_o, and integrates the product over a specified period of time $\tau >> T$, where $T=1/f_o$ [19]. Due to the orthogonality of sine waves, all sinusoidal terms which are integer harmonics of f_o, will integrate to zero. Therefore, the output of a lock-in amplifier is a DC signal given by [8]:

$$U_{out} = \frac{1}{\tau}\int_0^{\tau} V_r sin[2\pi f_o t + \emptyset]\, V_s(t)dt \qquad (1)$$

Where ϕ is the phase of the reference signal.

It is worthwhile to consider the special case where both $V_s(t)$ and $V_r(t)$ are simple sinusoids with frequency f_0 and f_1, respectively. In this case, the product of the two functions is found using the trigonometric relation $\sin(A)\sin(B) = 1/2(\cos(A-B) - \cos A+B$. The output of the PSD is

$$U_{out} = \frac{1}{\tau}\int_0^{\tau}\left\{\frac{V_r V_s}{2}\right\}\{cos[2\pi(f_o - f_1)t] - cos\,[2\pi(f_o + f_1)t]\}dt \qquad (2)$$

If $f_o = f_1$, one of the sinusoidal components of U_{out} will be a DC signal proportional to $(V_r Vs/2)$.

2.1.6 Lock-in Detection in Spectrophotometry

In our spectrophotometry system (Figure 6), which utilizes a lock-in amplifier, the electrical reference signal is a square wave with the following Fourier expansion [20]:

$$\boldsymbol{V_r(t) = \sum_{n=0}^{\infty} \frac{4V_r}{(2n+1)} sin[(2n+1)2\pi f_o t + \varphi_n]} \quad (3)$$

The reference signal drives an LED emitter. The modulated light passes through the detection cell and generates a phase-locked square wave output signal at the photodetector. Both the electrical reference V_r and photodetector signal V_s have the same fundamental frequency f_o and integer harmonics (eq. 3). However, the harmonics in V_s are attenuated due to light absorption by the sample. The frequency spectra are illustrated in Figure 3A-3B. Multiplication of the two signals produces a permutation of the sum and difference of the harmonics of the input signal (Figure 3C). However, after the integration (or low pass filtering), the only component that remains is the DC term, which includes only the product of identical frequency harmonics from the reference and photodetector signal (Figure 3D), respectively. Thus, the DC output is proportional to the amplitude of the photodetector signal.

The DC component can be selectively extracted using a narrow band low pass filter with cutoff frequency $<f_0$. This removes the other harmonics and as well as the wideband system noise, resulting in the high signal-to-noise ratio of lock-in amplifiers. The measurement speed of the system increases with modulation frequency f_0.

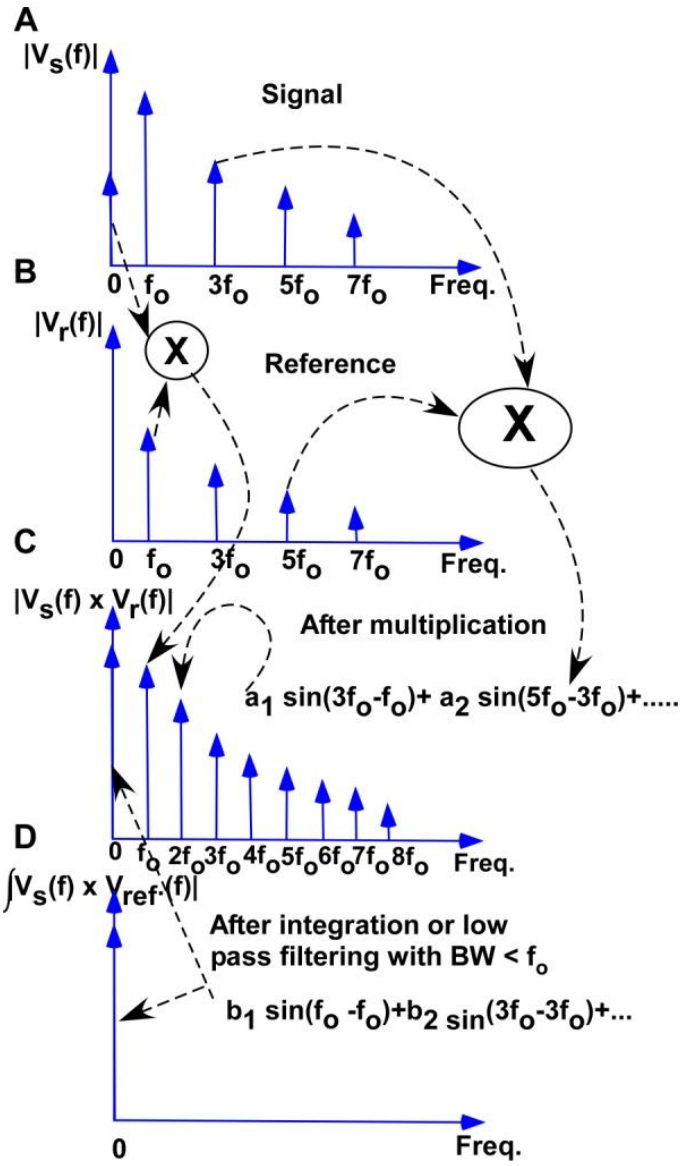

Figure 3: Lock in amplifier concept applied for a square wave sample signal (A) and another square wave reference signal (electrical not optical) (B). (C) is the product of the two signals. (D) is the lock in output after integration. Note. Signal A has a DC component, but B does not.

2.1.7 Multiplexed Lock-in Detection

Additional light signals can be multiplexed by modulating each light source at a unique reference frequency, and by adding a dedicated multiplier and low pass filter per

frequency channel. In order to remove interfering harmonics from adjacent frequency channels, the cut-off frequency of the low pass filter (LPF) must be less than the frequency separation between the channels f_s. Furthermore, one must exercise caution in choosing the reference frequencies: if any of the reference frequencies or their harmonics overlap, the multiplication step will generate a DC interference which cannot be removed by the LPF.

Given the constraints above, the LPF must have a time constant of $1/f_0$ or $1/f_s$, whichever is greater. In other words, the measurement bandwidth of the FDM system is the smaller of f_0 and f_s. This underscores the importance of utilizing high frequencies in the FDM system. By having a high fundamental frequency f_0 and a large frequency separation between adjacent channels, it is possible to improve the measurement time of the system while avoiding interchannel crosstalk.

2.1.8 Laser Light Modulation and Heterodyne Detection Principles

Light is propagating electromagnetic energy, so the time varying electric filed component of such energy can be expressed as [21]:

$$E = E_o \cdot \exp[\, j(2\pi \cdot f_o \cdot t)] \tag{4}$$

Where E_o is the amplitude and f_o is the light frequency. The wavelength of this light is $\lambda = c/f_o$. In our approach, lights from laser diodes are modulated by modulating the diode current with a modulating signal *m(t).* Modulating a laser diode current causes the light signal to be AM and FM modulated simultaneously [22]. The AM signal usually written as [14]:

$$v_{AM}(t) = A_C[1 + m(t)]\exp[j \cdot 2\pi \cdot f_o \cdot t] \tag{5}$$

And the FM signal usually written as [14]:

$$v_{FM}(t) = A_c \exp[j \cdot 2\pi \int_0^t f(\tau) \cdot d\tau] \tag{6}$$

Assume:

$$m(t) = M \cdot \cos(2\pi \cdot f_m t) \tag{7}$$

Then the time varying FM frequency can be written as [23]:

$$f(t) = f_o + \Delta f \cdot m(t) \tag{8}$$

Where Δf is the maximum frequency. From equations (5)-(8), the AM/FM light signal can be written as [22-24]:

$$E = E_o\{1 + M \cdot cos(2\pi \cdot f_m \cdot t)\} \cdot exp[j \cdot \{2\pi \cdot f_o \cdot t + \beta \cdot sin(2\pi \cdot f_m(t)\}] \tag{9}$$

And the frequency of the modulated signal is[23]:

$$f = f_o + \Delta F \sin(2\pi \cdot f_m t) \tag{10}$$

Where, $\beta = \Delta f / f_m$.

Expanding E in terms of *Bessel function* bases of first kind $J_\alpha(x)$ yields [23]:

$$E(f_o) = J_o E_o \cdot \exp\{j \cdot (2\pi \cdot f_o t)\} \tag{11}$$

$$E(f_o \pm f_m) = [(M/2) \cdot \{J_2(\beta) + J_o(\beta)\} \pm J_1(\beta)\} \cdot \exp\{j \cdot 2\pi(f_o \pm f_m) \cdot t\} \tag{12}$$

Where,

$$J_\alpha(x) = \sum_{m=0}^{\infty} \frac{(-1)^m}{m!\Gamma(m + \alpha + 1)} (\tfrac{1}{2}x)^{2m+\alpha} \tag{13}$$

Because we are interested in the energy of the light beam, we will only consider the real part of the electromagnetic field of equations (11) and (12). Therefore,

$$\mathrm{Re}[E(f_o)] = J_o(\beta)\cdot E_o \cdot \cos(2\pi\cdot f_o t) \tag{14}$$

$$\mathrm{Re}[E(f_o \pm f_m) = [(M/2)\cdot\{J_2(\beta) + J_o(\beta)\} \pm J_1(\beta)\}\cdot\cos\{2\pi(f_o \pm f_m)\cdot t\} \tag{15}$$

The real field can be written as:

$$E = A_o \cdot \cos[2\pi\cdot f_o \cdot t] + A_+ \cdot \cos[2\pi(f_o + f_m)\cdot t] + A_- \cdot \cos[2\pi(f_o - f_m)\cdot t] \tag{16}$$

Where,

$$A_0 = J_o(\beta)\cdot E_o \tag{17}$$

$$A_\pm = [(M/2)\cdot\{J_2(\beta) + J_o(\beta)\} \pm J_1(\beta)\}\,] \tag{18}$$

Or,

$$E = E(f_o) + E(f_o + f_m) + E(f_o - f_m) = E_o + E_+ + E_- \tag{19}$$

If we have two coupled modulated light beams E_1 and E_2, because light obeys the superposition principle, we can write the total field as[25]:

$$E = E_1 + E_2 \tag{20}$$

Writing E_1 and E_2 in the form of equation (15) as follows:

$$E_1 = E_{1o} + E_{1+} + E_{1-} \tag{21}$$

$$E_2 = E_{2o} + E_{2+} + E_{2-} \tag{22}$$

For a square law detector, generated electric current (I) is proportional to light energy (E^2), so

$$E^2 = E_1^2 + E_2^2 + 2\cdot E_1 \cdot E_2 \tag{23}$$

From equation (17),

$$E_1^2 = E_{10}^2 + E_{1+}^2 + E_{1-}^2 + 2\cdot E_{10}\cdot E_{1+} + 2\cdot E_{10}\cdot E_{1-} + E_{1+}\cdot E_{1-} + E_{1-}\cdot E_{1+} \tag{24}$$

From equation (12), and eliminating all frequencies that are $\geq f_o$, yields:

$$E_1^2 = A_{10}^2 + A_{1+}^2 + A_{1-}^2 + 2\cdot A_{10}\cdot A_{1+}\cos(2\pi f_{1m}t) + 2\cdot A_{10}\cdot A_{1-}\cos(2\pi f_{1m}t) + 2\cdot A_{1+}\cdot A_{1-}[\cos(2\pi\cdot 2 f_{1m}t)] \tag{25}$$

Simplifying equation (25) yields,

$$E_1^2 = DC_1 + AC_{10+}\cos(2\pi f_{1m}t) + AC_{10-}\cos(2\pi f_{1m}t) + AC_{1+-}[\cos(2\pi\cdot 2 f_{1m}t)] \tag{26}$$

Where,

$$DC_1 = A_{10}^2 + A_{1+}^2 + A_{1-}^2 \tag{27}$$

$$AC_{10+} = 2\cdot A_{10}\cdot A_{1+};\quad AC_{10-} = 2\cdot A_{10}\cdot A_{1-};\quad AC_{1+-} = 2\cdot A_{1+}\cdot A_{1-} \tag{28}$$

Similarly, from equation (22),

$$E_2^2 = A_{20}^2 + A_{2+}^2 + A_{2-}^2 + 2\cdot A_{20}\cdot A_{2+}\cos(2\pi f_{2m}t) + 2\cdot A_{20}\cdot A_{2-}\cos(2\pi f_{2m}t) + 2\cdot A_{2+}\cdot A_{2-}[\cos(2\pi\cdot 2 f_{2m}t)] \tag{29}$$

$$E_2^2 = DC_2 + AC_{20+}\cos(2\pi f_{2m}t) + AC_{20-}\cos(2\pi f_{2m}t) + AC_{2+}[\cos(2\pi\cdot 2 f_{2m}t)] \tag{30}$$

And the product,

$$E_1\cdot E_2 = A_{20}\cdot A_{10}\cdot\cos[2\pi(f_{10} - f_{20})t] \tag{31}$$

By summing all above terms and eliminating terms that have frequencies greater than $2f_{m1}$ and $2f_{m2}$, the total field can be written as:

$$E^2 = DC_1 + [AC_{10+} + AC_{10-}]\cos(2\pi f_{1m}t) + AC_{1+-}[\cos(2\pi\cdot 2 f_{1m}t)] + DC_2 + [AC_{20+} + AC_{20-}]\cos(2\pi f_{2m}t) + AC_{2+-}[\cos(2\pi\cdot 2 f_{2m}t)] + A_{20}\cdot A_{10}\cdot\cos[2\pi(f_{10} - f_{20})t] \tag{32}$$

Applying a heterodyne detection principle to frequency stage *i*, we multiply Equation (32) by the same modulating signal $m_i(t) = A_{ref} cos(2\pi f_{im} t)$ with frequency f_{im} and integrate with a time constant $\gg 1 / f_{1m}$. For the first stage *i=1*, we multiply Equation (32) by $m_1(t)$ and eliminate all frequencies apart from zero frequency. The result is:

$$E^2 \cdot A_{ref} \cos(2\pi f_{1m}) = \frac{[AC_{10+} + AC_{10-}] \cdot A_{ref}}{2} \tag{33}$$

This is proportional to the fluorescence light intensity. Note that we do not use optical signal as reference, but all reference signals are electrical signals.

2.1.9 Noise and Bandwidth Analysis

In this section, we provide a theoretical analysis of noise and bandwidth of the FDM detection system. We are primarily concerned with the amplifier front end which converts the modulated light signals to a voltage. Since the frequency range that we are expected to work with is in the 100s of MHz, we select a wide band operational amplifier (OPA657, Texas Instruments). Two opamps are used, one configured in the transimpedance mode, and the second in the non-inverting amplifier mode of operation. Even though we are not going to use the amplifier in the inverting mode, our final circuit allows the use of inverting amplifier configuration for future expansion. Because noise analysis for inverting and non-inverting amplifiers is the same, we will perform noise and bandwidth analysis for transimpedance amplifier and non-inverting amplifier modes of operation.

Figure 4 shows a transimpedance amplifier noise model [26]. Three noise sources are treated as current noise (I_{Nth}=Johnson noise, I_{NS}=Shot noise, and I_{Namp}= Amplifier current

noise) and the forth is treated differently as a voltage noise (e_{Namp}=Amplifier voltage noise).

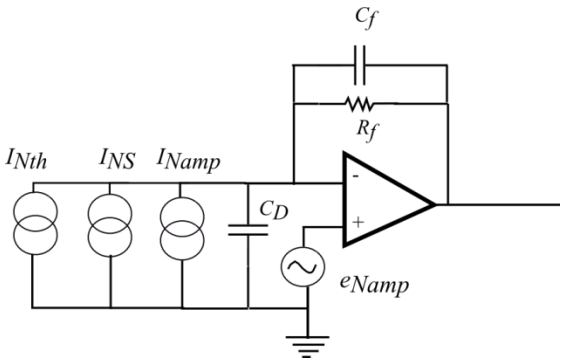

Figure 4: Transimpedance amplifier noise model. Three noise sources are current sources and one is a voltage source

The four components can be expressed in terms of an equivalent noise current as follows [27]:

$$I_{EQ} = \sqrt{I_{Namp}^2 + \frac{4KT}{R_f} + \left(\frac{e_{Namp}}{R_f}\right)^2 + \frac{\left(e_{Namp} * 2\pi * C_D * F\right)^2}{3}} \tag{34}$$

Where C_D is the total capacitance components for the photodetector and the differential and common mode capacitances of the amplifier; F is the band limiting frequency in Hz determined by post-filtering circuits. For the OPA657 (Texas Instruments) amplifier that we are, the voltage amplifier noise is e_{Namp}= 4.8nV/√Hz and the current amplifier noise I_{Namp}= 1.3fA/√Hz. For the capacitance of a typical silicon PD and the parasitic capacitances of the amplifier OPA657 (Texas Instruments), C_D =15.2 *pf* [28].

The parameters which determine the bandwidth of a transimpedance amplifier is gain bandwidth product *GBP*, C_D, and the feedback impedance $R_f \| C_f$. To have maximum flat

2nd-order Butterworth frequency response, we have to satisfy the following relation for the feedback pole:

$$\frac{1}{2\pi R_f C_f} = \sqrt{\frac{GBP}{4\pi R_f C_D}} \tag{35}$$

That will lead to the -3dB bandwidth as:

$$f_{-3dB} = \sqrt{\frac{GBP}{4\pi R_f C_D}} \quad Hz \tag{36}$$

Using the *GBP* of the OPA657 (Texas Instruments) (1.6 GHz), setting R_f=10KΩ, and using the C_D=15.2 pF for the OPA657 (Texas Instruments) and typical silicon PD we obtain f_{-3dB}=100 MHz. However, we are not able to use the transimpedance amplifier mode with a PMT because the PMT caused the amplifier to oscillate. At high frequency operation, the capacitances of C_D and C_f determine the stability of the amplifier. Therefore, the value of the C_f and the PMT capacitance must be carefully selected to avoid oscillations. Using the non-inverting amplifier mode allows us to use a PMT with the OPA657 (Texas Instruments) amplifier without any oscillation problems.

Figure 5 shows the noise model of the non-inverting amplifier configuration [27, p. 6]. Although the OPA657 (Texas Instruments) amplifier is a low input noise amplifier, other noise sources have to be carefully minimized to maintain low overall circuit noise. Using superposition to all spot noise powers, the total output noise voltage can be calculated as [27, p. 6]:

$$E_O = \sqrt{(E_{NI}^2 + (I_{BN}R_s)^2 + 4KTR_S)G_N^2 + \left(I_{BI}R_f\right)^2 + 4ktR_fG_N} \tag{37}$$

Where $G_N = 1 + R_f/R_G$ is the gain of the non-inverting amplifier. Dividing Equation (37) by the gain yields the equivalent total noise, E_N at the non-inverting input of the OPA657 (Texas Instruments) amplifier as:

$$E_N = \sqrt{E_{NI}^2 + (I_{BN}R_s)^2 + 4KTR_S + \left(\frac{I_{BI}R_f}{G_N}\right)^2 + \frac{4KTR_f}{G_N}} \tag{38}$$

This equation tells us that the use of low resistor values will make the total equivalent input voltage noise will be low as will. To achieve the maximally flat 2nd-order Butterworth frequency response, the parallel combination $R_f \| R_G$ must be kept <150, and a compensation capacitor can be used in parallel with R_f. For a OPA 657 (Texas Instruments) non-inverting amplifier configuration gain of 10, it is possible to achieve a bandwidth of about 275 MHz [27, p. 6].

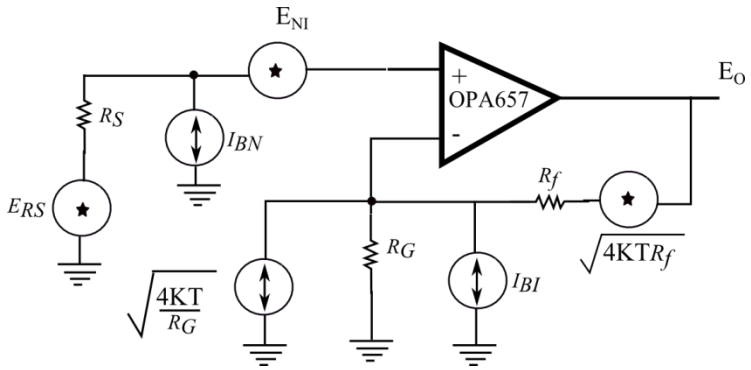

Figure 5: Noise model of a non-inverting amplifier configuration. We use the OPA 657 (Texas Instruments) amplifier because it has a very low input noise voltage noise [27].

2.1.10 Multi-Color Flow Cytometry

Figure 6 shows a picture of the BD LSR II cell analyzer, which can be configured with up to 7 wavelengths. In such cytometers, fluorescently labeled particles or cells are

hydrodynamically focused in a sheath of PBS (Phosphate Buffer Solution) and flown across a detection window where they are illuminated and detected.

Figure 6: PD LSR II cell analyzer, which can be configured with up to 7 wavelengths chosen from 11 different wavelengths.

Figure 7 shows a picture and schematic (inside) of a flow cell used in the BD LSR II flow analyzer. Focused into a small aperture, the excitation light can be either scattered or absorbed by those passing particles or cells. If any of them is stained by fluorochrome molecules, it will emit a light signal that has a higher wavelength than the wavelength of the excitation source.

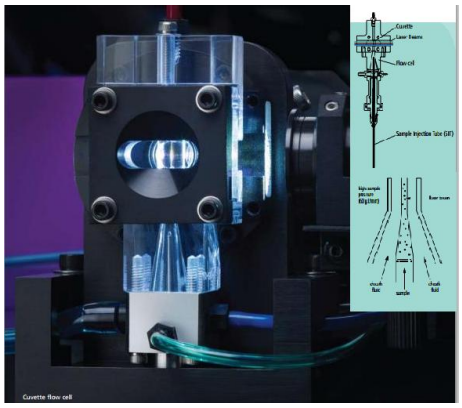

Figure 7: A picture and schematic (inside) of a flow cell used in the PD LSR II flow analyzer.

According to the type and size of the fluorochrome molecules, multi-parameter data can be acquired and investigated using cytometers to discriminate distinct populations of particles or cells. The data can also be used to quantify the type, status, etc of such distinct populations [29].

To increase the number of parameters that need to be investigated, one has to add more different excitation sources and/or different fluorochrome molecules. Accordingly, the complexity and cost of traditional multi-color cell cytometers will increase dramatically. Each newly added fluorophore requires a dedicated dichroic mirror, filter, PMT or APD with a HV power supply. Figure 8 shows both octagons and trigons detection cells of the model BD LSR II flow analyzer, which are surrounded by precisely angled mirrors, band pass filters, and PMTs. This analyzer contains 11 PMTs, which we hope to minimize using the FDM technique.

Since 1990's multiparameter flow cytometry has largely advanced from hardware, reagents, and data analysis tools. Multiparameter analysis is important because it provides information about cells with complex phenotypes, enabling the isolation and detection of rare cell populations. It is commonly used in detecting T-4 cell counts in AIDS diagnostics, and cell immunity in vaccine [30].

As described earlier, multiparameter cytometry relies on a single PMT for each fluorophore to be detected. This allows multiple fluorophores, excited by the same laser, to be detected simultaneously. However, PMT's are expensive and bulky. Over the last decade, laser diode technology has advanced to the point where multiple lasers can be integrated in a system in an economical manner. Therefore, we propose to allocated a

single laser diode per fluorophore. If each laser is modulated at a different wavelength, all the fluorophores can be detected with a single PMT. . Lasers like UV 350 nm, Violet 408nm, blue 488, green 532, yellow 560 nm, orange 610 nm, and red 633 nm are commercially available [30]. Laser

A

B

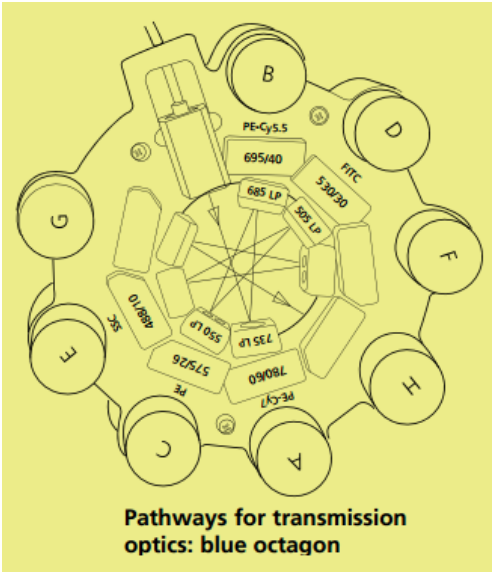

Figure 8: A) A picture of the detection cell of BD LSR II cell analyzer. It contains both octagons or trigons cell, which are surrounded by precisely angled mirrors, band pass filters, and PMTs. B) is a schematic of the octagons cell shows 8 PMTs, 8 filters ,and 8 dichroic mirror.

diodes can be customized for specific wave length, and lasers with 558 nm, 561 nm 580 nm, and 592 nm have been commercially integrated in cytometers. These laser technologies (diode and diode-pumped solid state, DPSS) are capable of producing any required wave length needed for fluorophore excitation [31].

Fluorochrome reagent technologies have broadened within the last four decades at which resonance energy tandem dyes have been produced. Such dyes are excitable by wide spectrum lasers, which engorge the use of considerable number of laser lights to simultaneously excite them. Classical organic fluorochromes like PE and APC can be coupled with cyanines (Cy5, Cy5.5 and Cy7) and Alexa dyes to produce the tandem dyes [30].

In addition to the usual phenotypic measurements that multi-parameters cytometers can perform, they can measure cell functions like cytokine production and cyrotoxicity. They can also distinguish death cells. Example of flow cytometry applications are to analyze:

1. DNA content and cell cycle distribution.
2. Cellular viability.
3. Apoptosis.
4. Calcium flux.
5. Intracellular pH and membrane potential.
6. Expression of cell surface and/or intracellular antigens and markers.
7. Fluorescent reporter proteins.

8. Chromosomes.

One common approach is to conjugate fluorescent dyes to specific antibodies against antigens expressed in a target cell population. Expression of fluorescent marker proteins injected or transfected into target cells is another popular flow cytometric approach. For this purpose, Green, Yellow, Cyan, and Red fluorescent proteins have been used in flow cytometric studies. Fluorescence-activated cell sorters can be used to identify and isolate viable labeled cells, chromosomes, or cell organdies from complex populations for further studies [29].

2.1.11 Microfluidic Chip Preparation

In order to miniaturize future cytometers, the flow cell must be minimized as well. Microfluidic technologies are promising techniques to do so. We use a silicone rubber material known as Polydimethylsiloxane (PDMS) to make microfluidic chips using soft lithography [32]. Such PDMS chips have many advantages over traditional MEMS micromachining. These advantages are [33]:

2 Optically transparent.

3 Mechanically flexible.

4 Simple to manufacture.

5 Low cost.

6 It can be applied to large varieties of channel geometries.

To prepare a microfluidic chip, we perform three main steps:

I. Chip design and Simulation

According to a specific need, we start our design with a geometry that we expect will serve our need. Simulation software such as COMSOL is usually used to assess the operation of the suggested geometry. Some traditional designs and simulation results can be found in the literature [34]–[36].

II. AutoCAD Drawing and Mask Preparation

Based on simulation results, AutoCAD software is used to draw the selected design geometry to scale as shown in Figure 9. The AutoCAD drawing is then printed on a transparency using a high resolution laser printer (Thin Metal Parts). The final mask is shown in Figure 10.

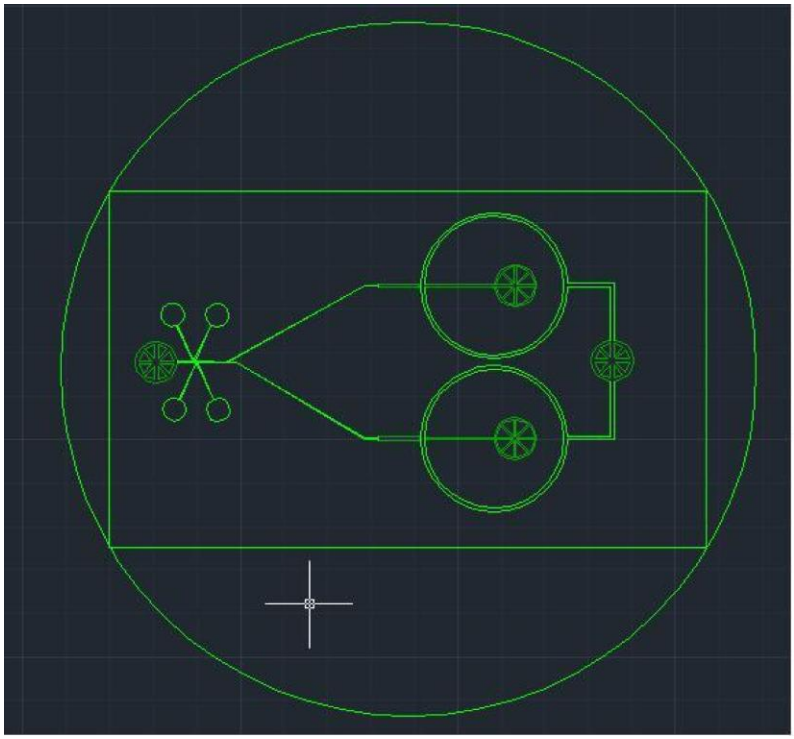

Figure 9*: Sample microfluidic chip design drew using AutoCAD 2013 software.*

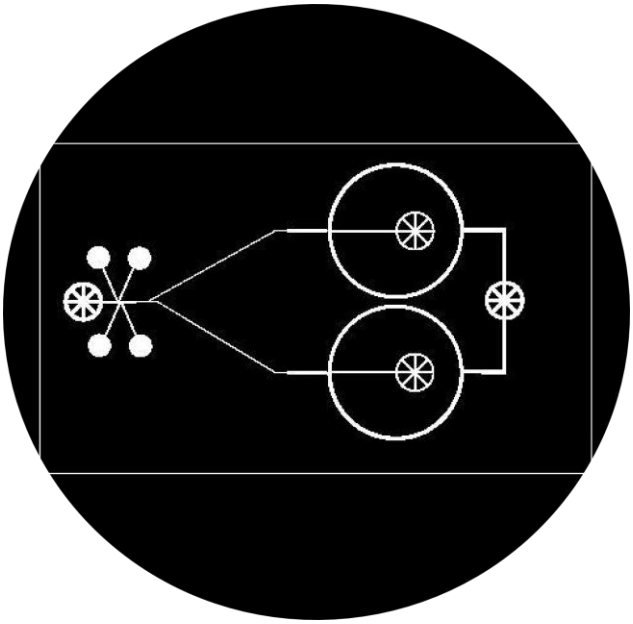

Figure 10: A black and white picture that resembles the final mask. The black side will be opaque while the white side will transparent to UV light. This mask will be used to manufacture the master mold using soft lithography technology.

III. Master Mold and PDMS Chip Preparation

At this stage, the process of preparing the master mold in the ECE clean room begins. The soft lithography procedure presented in table 1 is followed to print the channel design on silicon wafer using the SU-8 material.

After preparing the master mold in the clean room, the next step is to print this mold on a transparent PDMS layer. The following general procedure has to be followed for making functional microfluidic PDMS chips:

1. Mix PDMS and curing agent in the ratio of 10:1. The quantity of each should be very precise. The ratio of PDMS to curing agent can determine the hardness of the cured PDMS. Mix both chemicals thoroughly for about 5-10 minutes.
2. Pour about 2-3mm of the mixture over a master mold wafer which is located in a Petri-dish and desiccate it until all air bubbles disappear.

3. After all air bubbles are removed from the PDMS, put it on a hotplate for 50-60 minutes at a temperature of 75 degree Celsius.
4. Carefully cut the chip using a sharp knife or razor blade. Be sure not to scratch the Si/SU-8 mold. Keep 3-5 mm away from channels.
5. Punch inlets and outlets. Use metal punches slightly smaller than the connection tubes
6. Take a glass plate or flat PDMS plate, and clean it with methanol, or ethanol, or IPA, and dry it with nitrogen gun or filtered air before bonding. The surface should be dry and should have no dust particles. Scotch tape can be used to remove dust.
7. Bond the PDMS to the glass or PDMS plate using corona bonder. Move the corona bonder back and front on the glass chip and PDMS for about 3 minutes each. (optional) Add 1-2 drops of methanol to the sides of the chip to be bonded. This acts as a lubricant, so the two layers can be aligned. Press both of them together gently. Avoid any dust particles and contamination.
8. After bonding, place the chip on a hot plate for about 10 hours for baking at 50 degrees Celsius.
9. Clean all used beakers and tools, and any spills.
10. Switch off the hot plate when you finish.

After making the chip successfully the following surface treatments can be applied:

1. Treating PDMS with SDS can make a hydrophobic surface hydrophilic. (SDS is an aqueous surfactant). Use this to make PDMS hydrophilic for electrophoresis or double emulsions. Glass can be treated with Aquapel to make it hydrophobic.

Table 1: Clean room soft lithography procedure to print the channel design on silicon wafer using the SU8 material.

• **Substrate Pretreatment** Wafers must be cleaned with a solvent, rinsed with dilute acid and DI water and dried before applying the SU8. A piranha etch /clean may be used. Put the cleaned wafer on a hotplate at 200˚C for 5 min to dehydrate.	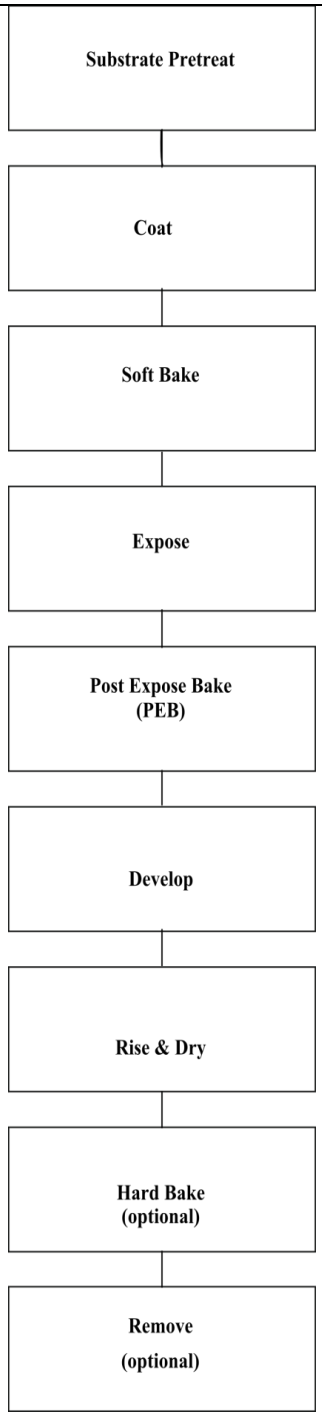
• **Coat** The thickness of the SU8 can be controlled by the coater speed, time and acceleration. Plots and tables for such parameters for a specific SU8 can be found in [37].	
Soft Bake Once the appropriate SU8 thickness has been achieved, it should be baked on a hotplate or a convection oven. The bake time and temperature for optimum solvent evaporation conditions for either a hot plate or an oven can be found in [37].	
Expose The optimum light absorption for SU-8 is in the UV range between 350 and 400nm. The optimum UV dose depends on the exposed film thickness.	
Post Expose Bake To overcome adhesion failure problems, both exposure and post exposure bake (PEB) times must increased. The PEB is also used to cross-link the exposed portions of the film.	
Develop Many developer solutions can be found in the market. One may use immersion, spray or spray- puddle processes. High aspect ratio can be achieved with strong agitation. Approximate develop times can be found in [37].	
Rinse and Dry Rinse with isopropyl alcohol (IPA) and dry with filtered air or nitrogen immediately after development.	
Hard Bake (cure) Because the SU8 is a part of the final master mold, it has to be ramp/step hard baked using either a hot plate or an oven between 150-200 ^{o}C. Depending on a film thickness and the type of baking, the baking times can be determined.	
Remove Different removal processes has to be applied depending on SU8 type and preparation conditions.	

2. PDMS can be cleaned with non-swelling solvents (methanol, ethanol) or HCl.

2.1.12 Droplet Generation

In order to test the FDM detection system, we need to generate droplets in certain manners to quantify the FDM system response. First, we used the trinity-channel microfluidic chip shown in Figure 11 to generate alternating droplets of Fluorescein and Rhodamine 6G as a proof of concept of the low speed FDM-LIF system. Because of its large channel size (about 1mm) it cannot generate high speed alternating droplets.

To test the high speed FDM system, we used the design suggested by Anna et al., 2003 to generate high speed droplets (about 2,800 drops/sec) [35]. Figure 12 shows the chip design that we are using. It is not possible to generate high speed alternating droplets, and the maximum achieved speed using this design was 10 drops/sec.

In the middle channel we injected fluorescein in water solution and in the outer two channels we injected Fluorinert FC-40 oil with 2% Krytox surfactant. The oil and water are immiscible liquids, so when forced to flow in a tiny orifice downstream the three channels, the oil exerts pressure and viscous stress that breaks the water flow into a train of droplets. The size and velocity of these droplets can be controlled by the relative oil/water flow rates [35].

In order to quantify the operation of our high speed FDM-LIF system, we used the chip design shown Figure 13 to generate alternating droplets (about 300 drops/sec) of Fluorescein and Alexa 680 with Fluorinert FC-40oil with 2% surfactant as a carrier fluid. The chip design can generate three alternating droplets of three different analytes, but we used only two channels, and we blocked the third one. In each side, a standard T-junction

is used to generate droplets of each analyte. The generated droplets are then forced to flow sequentially in the outlet channel. The small channel size (about 100 µm) helps in achieving a throughput of 300 droplets/sec. To generate higher speed of alternating droplets, the designs shown in Figures 14 & 15 are suggested.

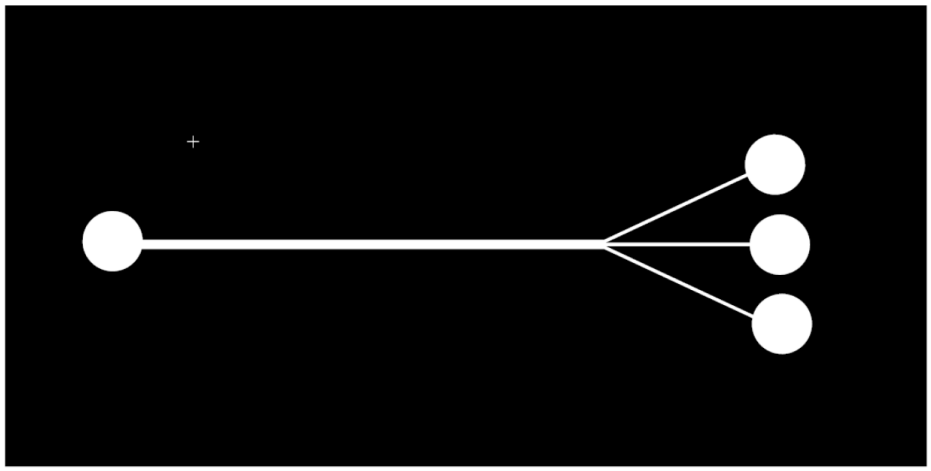

Figure 11: A trinity-channel microfluidic chip used to generate alternating droplets of Fluorescein and Rhodmine 6G as a proof of concept of the low speed FDM-LIF system.

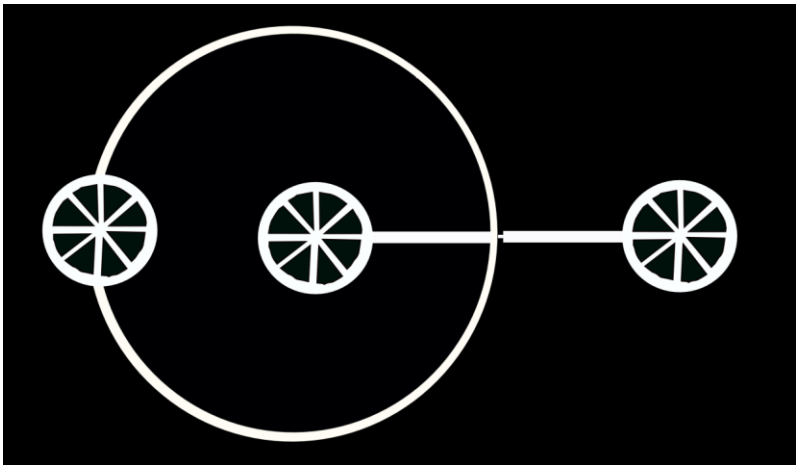

Figure 12: High speed droplet generator suggested by Anna et al., 2003. In the middle channel we injected fluorescein in water solution and in the outer two channels we injected fluorinate oil with 2% Krytox surfactant.

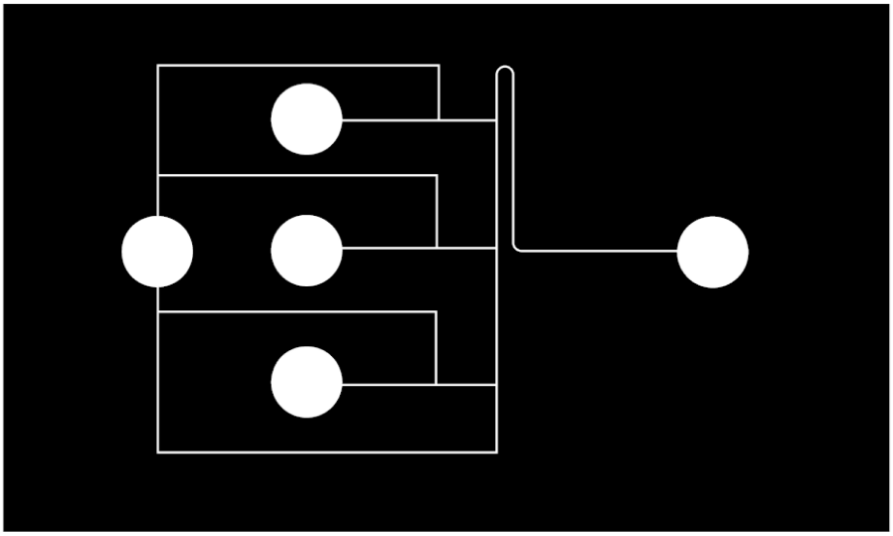

Figure 13: A chip design to generate high speed alternating droplets (about 300 drops/sec) of Fluorescein and Alexa 680 with fluorinate oil as a carrier fluid.

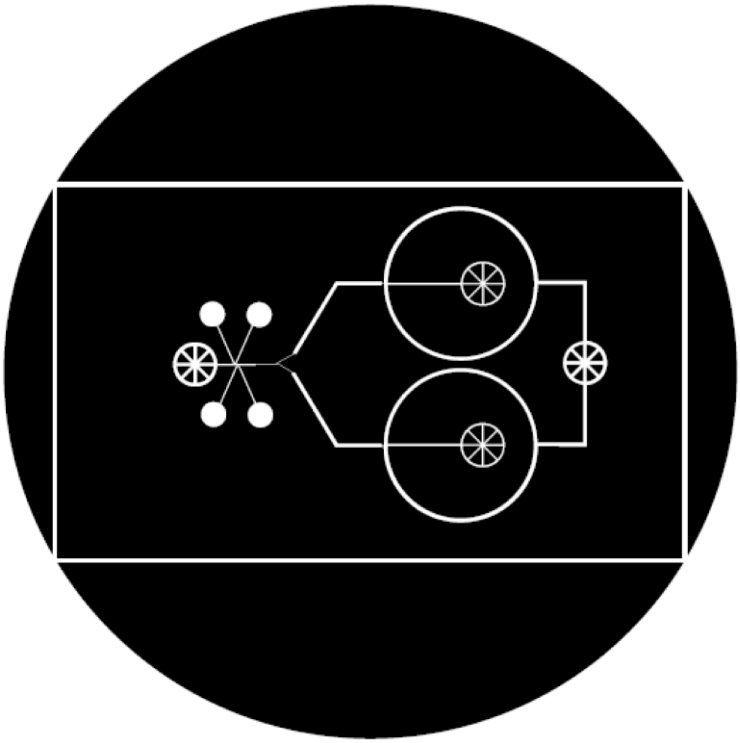

Figure 14: High speed alternating droplet generator. The design combines two high speed single droplet generators shown in Figure 12.

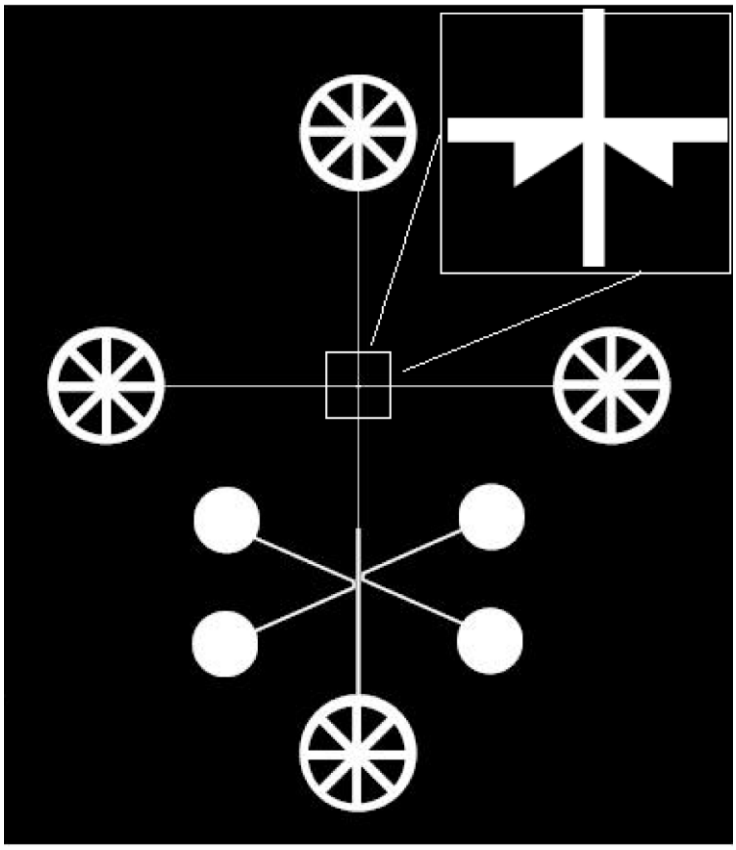

Figure 15: Alternating droplet generator suggested by Hung et al. [36].

However, the ultimate target of our system is in cell cytometry, so we need to generate a hydrodynamically focused, single file stream of cells. To accomplish that, flow focusing techniques must be applied.

2.1.13 Flow Focusing

Most of the previously mentioned techniques, when used with miscible fluids are regarded as two dimensional (2D) focusing techniques, and they were proven to be useful in some cell/particle sorting and counting and DNA analysis systems [38]. However, to overcome some drawbacks of the 2D focusing such as decontamination [39] of surfaces

and flowing particles/cells in a non fixed depth within the channel, three-dimensional (3D) flow focusing must be employed.

Many 3D focusing techniques for PDMS microfluidic chips can be found in the literature [25-28]. Among these, we select two designs at which one comprises a single PDMS layer whereas the other comprises a double PDMS layer. The single layer design depends on microfluidic drifting mechanism in focusing cells/particles three dimensionally. The advantage of this design is that it is a single layer chip design which requires no alignment. The mask for this design is shown in Figure 16. The zoomed diagram shows the curvature part that makes use of the centrifugal force on cells/particles flow and causes it to be vertically focused. The final cross junction focuses the drifted flow in the horizontal direction. Accordingly, cells/particles flow will be centred horizontally and vertically in the middle of the channel [41].

Figure 17 shows a two-PDMS layer design that was first suggested by [39] and then modified by [38]. The design has four inputs and one output. The first step is the vertical focusing of the sample flow then the horizontal focusing using the final cross junction. The two PDMS layers have to be aligned together to form the complete microfluidic chip. Figure 18 shows 2D view of the 3D duople layer microfluidic chip. The water flow is focused vertically between two oil flows. Figure 19 shows the masks of the two PDMS layer design of 3D focusing technique. The two layers have to be aligned together to form a microfluidic chip.

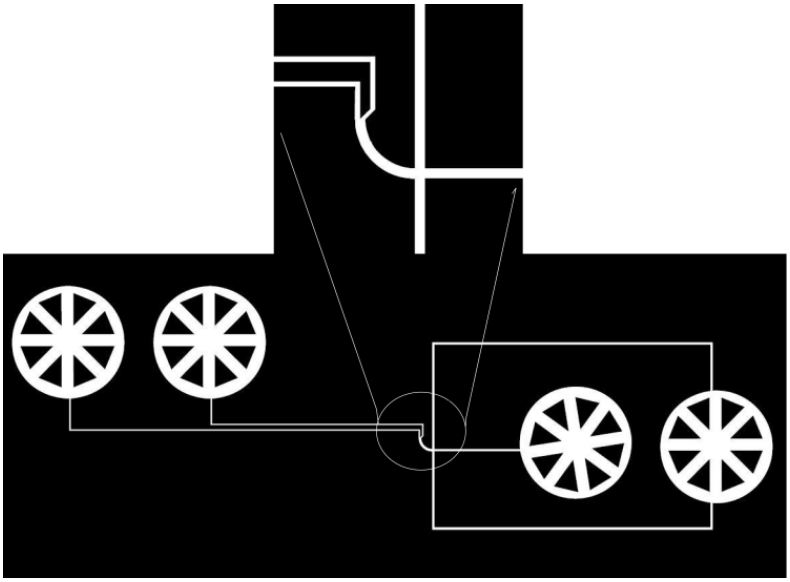

Figure 16: Microfluidic drifting single PDMS layer chip design for 3D focusing of cells/particles. The design uses a 90^{o} curved channel to focus cells/particles vertically using the centrifugal force exerted on cells/particles flow.

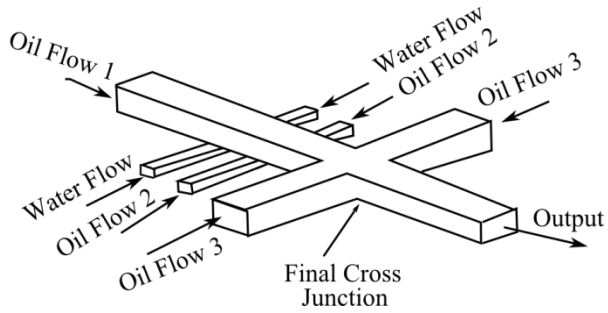

Figure 17: Double layer PDMS 3D focusing microfluidic chip. Three oil inputs and one water input required to focus cells/particles vertically and horizontally.

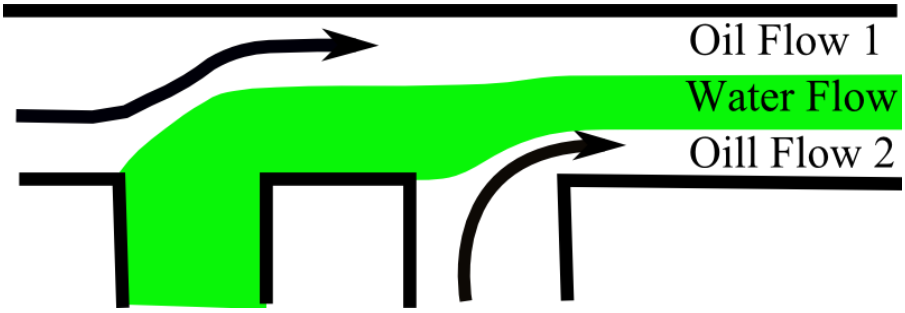

Figure 18: 2D View of the 3D duople layer microfluidic chip. The water flow is focused vertically between two oil flows.

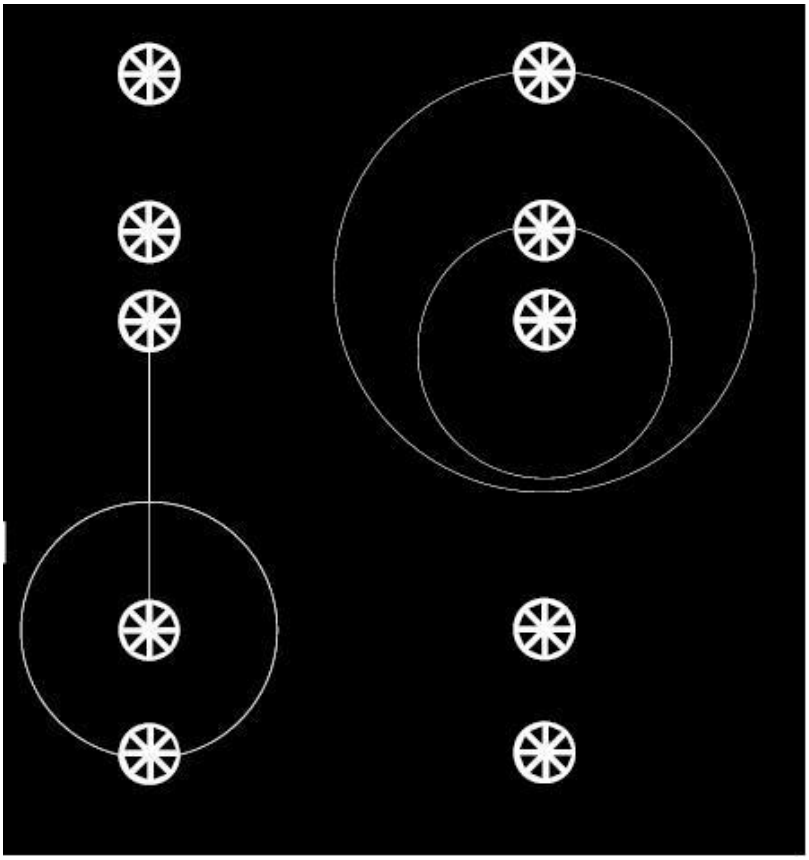

Figure 19: Two PDMS layer design of 3D focusing technique. The two layers have to be aligned together to form a microfluidic chip.

2.1.14 Literature Review of Existing Multiplexing Techniques

Early multi-wavelength spectrophotometry and fluorimetry setups were constructed with expensive and complex optical components. In addition, they require a dedicated light detector (e.g., PMT, APD, etc) per wavelength, and it is usually called wavelength division multiplexing (WDM) [42], [43].

To reduce complexity, cost, and size problems of the early multi-wavelength spectrophotometry and fluorimetry setups, several efforts have demonstrated multi-color

setups that use either time (TDM) or frequency (FDM) division multiplexing. Light multiplexing offers means to perform multicolor detection in a single optical window. For example, Chance and Graham proposed the first commercial dual wavelength spectrophotometer (DWS) [44]. A time-multiplexing technique was accomplished using a rotating wheel (60 Hz) with properly selected interference filters; the measurement time constant was 20 ms. Totschnig, Baer et al. proposed a time-division multiplexing strategy that they used to record the ringdown absorption traces of multiple species from two lasrer diodes. They used a trigring frequency of 20 Hz alternatively between the two lasers [45]. Werner also used two selecting interference filters, but with a small vibrating mirror as the time sharing unit [46]. The vibrating frequency was 104 Hz, resulting in a time constant of 10 ms. Werner, again, reported a micro-DWS using electronic time multiplexing, where two LED's were controlled with alternating 2 KHz rectangular pulses. The reflected light signals were detected using a single photomultiplier, lock-in amplifier, and a low pass filter (LPF) with a 30 ms time constant. The 30 ms time constant was chosen because the maximum bandwidth of the LPF must be substantially smaller than the modulation frequency (more details are given in the Theory section). This time constant was large because they used 2 KHz as the chopping frequency. Arroyo, Birbeck et al. used 3 KHz triangular signals to time multiplex two laser diodes to simultaneously make two line-shape measurements in different spectral regions and facilitate the selection of appropriate line pairs for thermometry for a water-vapor flow field generated in a shock tube [47].

To improve measurement speed, other multiplexed detection systems have used order of magnitude higher modulation frequencies, in the 10's of KHz. This is suitable for moderate throughput systems, but it is still not sufficient for high speed detection in flow cytometry or high throughput microfluidic systems. Gianfrani, Gagliardi et al. developed a novel laser diode spectrometer using FDM technique at 18 and 27 KHz. They used two analog and two digital lock in amplifiers with 30 ms and 10 ms time constants, respectively. This setup was used for high-precision and simultaneous measurements of three different isotope ratios in water [48]. Oh, Paige et al. performed a simultaneous detection of multiple gases (i.e., CO and CO_2) using frequency modulation multiplexing (FMM) with diode lasers modulated at 40 and 50 kHz, respectively. Two lock-in amplifiers were used to extract each FMM signal, and the measurement time constant was 16 ms [49]. Suzuki et al. used the same technique to measure absorbance with a flow-injection analysis system. They used four different LEDs with four different frequencies. The highest frequency was <10 KHz, resulting in a measurement time constant of 10 ms [5].

Eom and Dasgupta used the FDM technique but at a low frequency range. They modulated two LEDs with 700Hz and 1KHz square wave, and the final stage time constant was 2 s [50]. Izquierdo, Puyol et al. reported a novel compact FDM dual-wavelength system to measure the absorbance of chemically active polymeric membrane. They used two low frequencies as reference signals of 1.2 KHz and .48 KHz. They incorporated digital lock-in amplifiers with 30 ms time constant [51].

We also previously reported the use of multispectral absorbance photometry of organic dyes [12]; the maximum frequency used was 10 KHz, and our measurement time constant was 10ms. In another work we presented a multispectral and high-speed absorbance detection system which improved the measurement time constant of the previous efforts by more than one order of magnitude (i.e., about 1ms). To do this, we operated at high frequencies (> 100 KHz), and maintained a large frequency separation (50 KHz) between modulation channels.

In addition to absorbance photometry, the FDM technique has been used in many fluorescence detection applications. Wu, Zhang et al. proposed an FDM multichannel fluorescence confocal microscope. They simultaneously encoded different fluorescence signals from different locations into the frequency domain. In their experiment, the two modulated light signals were 340Hz and 400Hz ; they used lock in amplifiers to extract the fluorescence signals [52]. We also demonstrated a frequency-division-multiplexed laser-induced- fluorescence (FDM-LIF) system which can perform two-color detection with a single PMT. Fluorescein and rhodamine-6G samples were excited by two inexpensive laser diodes modulated with two square waves at 1 KHz and 1.5 KHz. Fluorophores were distinguished by the frequencies at which they fluoresce. The system successfully distinguished water-in-oil droplets containing fluorescein or rhodamine-6G alternately generated in a microfluidic junction [53]. The FDM-LIF system identifies fluorophores based on their excitation frequency; therefore it can distinguish fluorophores with overlapping emission spectra.

Carlsson and his group published many articles at which they used an electro-optical modulator, EOM, to utilize the FDM technique to perform simultaneous multi-wavelength fluorescence detection using a confocal microscope. Although they operated at high frequencies up to 3MHz, their optical setup was bulky and complex due to the use of the EOM to modulate light beams. In addition to the added complexity, EOM are expensive [8]–[11].

Recently we published our high frequency and high speed developed FDM-LIF in microTAS 2013 conference. In this work, we demonstrate a high speed frequency multiplexed electronic detector for multicolor flow cytometry. The system's key benefit is that it can detect multiple fluorophores on single photomultiplier tube, rather than one per fluorophore. The system implements a 3 channel heterodyne demodulator operating at 40 MHz, enabling a multi-channel bandwidth of >200 KHz necessary for cell cytometry.

The objective of this work is to provide multiplexed photometry and fluorimetry setups with high bandwidth and, therefore, high speed. When utilizing frequency division multiplexing (FDM), the measurement bandwidth and system throughput are directly related to the difference between light source modulation frequencies. A larger frequency separation will allow for a higher bandwidth filter after demodulation. More details are given in the following sections.

CHAPTER 3: CONTROL CIRCUIT DESIGN AND EMPLEMENTATION

In the process of developing our FDM system, we have developed two different systems: The first system uses a lock in amplifier chip (AD630, Analog Devices). This chip has gain bandwidth product of 350 KHz which enables us to develop our first FDM photometry system at which we operated three LEDs up to 250 KHz. The second system uses the heterodyne demodulation technique using high frequency (500MHz) analog multiplier. This technique allowed us to run our FDM-LIF experiments up to 40 MHz. The design, implementation, and testing of both systems will be discussed in the following sections, and the experimental results will be presented in the two subsequent chapters.

3.1 Photometry-FDM System

In this section we are going to explain the design of the control circuit and the PCB layout of the FDM system which is used for absorbance photometry.

3.1.1 Control Circuit of Photometry-FDM System

Figure 20 shows a schematic diagram of the electronic circuit of the FDM system. The three LEDs (red, blue and green) are modulated using independent voltage controlled oscillators (VCO) (SN74LS629N, Texas Instruments). The VCO is chosen because of its good voltage to frequency linearity and wide range. The VCOs provide three independent square wave electrical reference signals ($V_{r1,}$ $V_{r2,}$ *and Vr3*) to high-speed voltage comparators (LM311, Texas Instruments) which drive the respective LED's through their open collector outputs. Three current limiting resistors are used to adjust

the relative intensity of the respective LEDs to compensate for non-uniform spectral sensitivity of the photodetector. The modulation frequencies of 150 KHz, 200 KHz, and 250 KHz drive the green (574 nm), red (636 nm), and blue (470 nm) LEDs, respectively. The frequency separation between channels is 50 KHz. To further minimize the possibility of crosstalk, we utilized a low pass filter with a 160 Hz bandwidth.

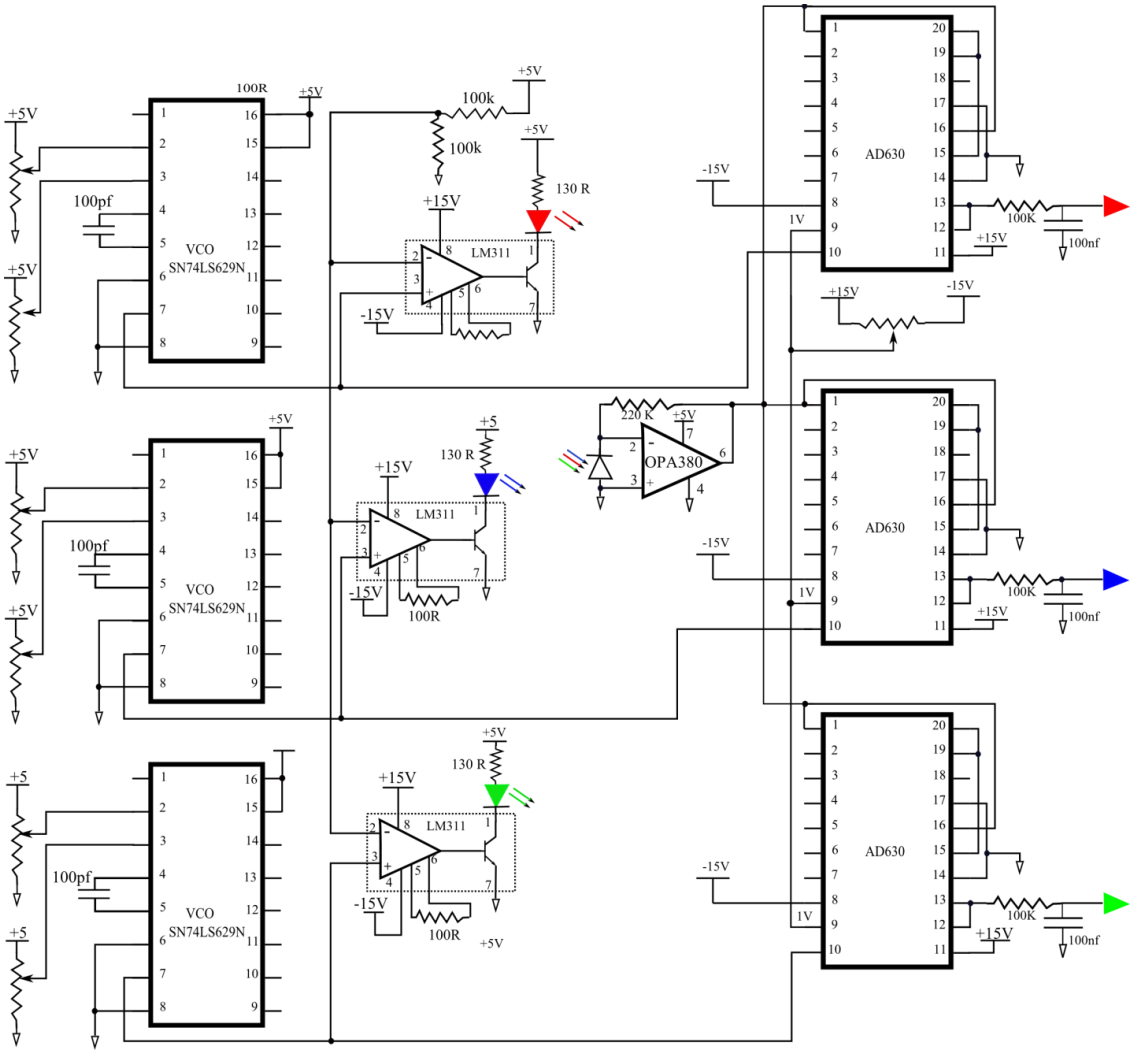

Figure 20: Schematic diagram of the electric circuit of the FDM photometry system. The system consists of three stages; each stage has a VCO, comparator, lock in amplifier, and low pass filter. A PD/transimedance amplifier stage is used to detect and amplify the multiplexed light signal.

The photocurrent generated in the PD is converted to a voltage signal using a transimpedance amplifier (TIA) which must have a bandwidth >300 KHz, more than 10X larger than our previous efforts [12]. In our previous design, the frequency was limited by a low frequency pole formed at the amplifier input by the parasitic capacitance of the photodiode C_{PD} (about 4 pF) and the large feedback resistance R_f (2MΩ) in the TIA. The corresponding bandwidth was $f_c = 1/(2\pi R_f C_{PD}) \sim 20KHz$. Here, we use a high-speed, high gain-bandwidth product (GBP) TIA (OPA380, Texas Instruments). In this setup, the cutoff frequency becomes $f_C = \sqrt{GBP/4\pi R_f C_{TOT}}$ [26], where C_{TOT} is the total input capacitance consisting of the photodiode capacitance (C_{PD}) plus the parasitic common-mode and differential-mode input capacitance (3pF + 1.1pF for the OPA380, Texas Instruments). Using R_f= 2MΩ, C_{PD}=4 pF, and GBP =90 MHz, the cutoff frequency is f_C=21 MHz. The detection system therefore is more than sufficient for working with frequencies well above 100 KHz.

The multiplexed voltage signal at the TIA is distributed simultaneously to three lock-in amplifiers (AD630, Analog Devices). It is a relatively a low-cost component which provides phase-sensitive demodulation in a frequency range up to 350 KHz that is suitable for our application. As shown in Figure 20, each lock-in amplifier is tuned to a specific LED by providing the LED's drive signal as the reference. The AD630 (Analog Devices) internally provides the multiplication step required for demodulation. The output of each lock-in amplifier is then passed through a 1 KHz low pass filter to eliminate any cross-talk between channels. To successfully reduce crosstalk, the low

pass filter must be substantially less than the frequency separation between channels, which is 50 KHz in this case.

3.1.2 PCB Layout

Figure 21 shows the PCB layout of the schematic shown in Figure21. The Pad2Pad software package version 1.9.66 is used to generate the PCB layout on two layers, and this is our first PCB design. We use foot prints of both surface mount devices (SMD) and dual in-line package (DIP) devices. The PCB has 61.3 mm in width and 72.2 mm in height, 1 oz copper weight, 0.062" material thickness, and FR4 material type. However, it lacks a grounding plan, power plan, and electromagnetic interference (EMI) suppression measure. This caused this circuit to have distortions and interferences. Such measures are considered in the next generations.

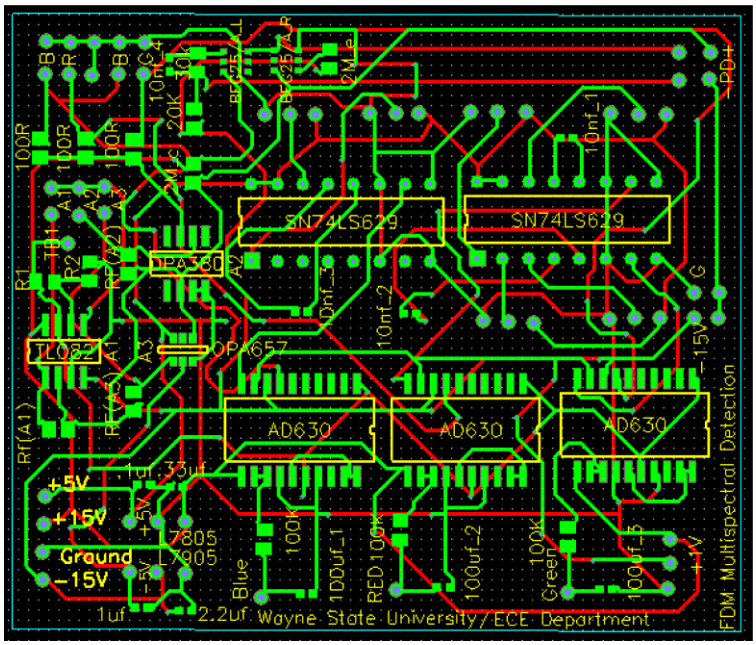

Figure 21: Double-layer PCB layout of the FDM photometry system. This is our first PCB design. Surface mount devices (SMD) and Dual In-Line Package (DIP) devices are used.

3.2 Fluorimetry-FDM System

3.2.1 Control Circuit of Fluorimetry-FDM System

Because our ultimate target is to apply the FDM technique to cell cytometry analysis instruments, the FDM system bandwidth must be high to allow enough time for the modulated light to run certain number of periods within the exposure time of the targeted stained-cell or molecule. For standard cytometers, the normal exposure time for cells stained with fluorophores is 4μs. To allow at least 40 periods of the modulation signal to take place within the 4 μs time, the modulation frequency must be at least 10 MHz. In order to be able to operate on speeds that is an order of magnitude higher than this minimum limit, we develop a high frequency FDM fluorimetry system that modulates lights of red, greed, and blue laser diodes with sine waves up to 100 MHz using high performance laser drivers that provide controlled current to a grounded laser diodes (EL6245C, Elantec). The driver has an on-chip 500 MHz oscillator that provides an output current modulation up to 100 mA peak to peak [54]. The driver also allows the use of external square wave oscillator to modulate laser diode current with square wave signals. In our developed system, lights from three lasers are combined using an optical combiner and the multiplexed light is directed towards the sample via a microscope cube or alignment optics that has a specific dichroic mirror and emission filter.

Part of the multiplexed light signals will be absorbed by an analyte under investigation, and the other part will be scattered. If the sample contains fluorophores, each fluorophore will absorb a specified light (excitation light), and will fluoresce a light signal proportional to the excitation light signal but with a higher wavelength. Due to the

short fluorescence lifetime, 0.5 to 20 ns, the emitted fluorescence light signal will have the same shape as the modulation signal generated either by the internal sine wave oscillator or the external square wave. Because fluorescence signals are expected to be weak, the emitted multiplexed light signal will be detected using either an APD or PMT that have internal gain. Either light detector will generate a current that is proportional to the fluorescence light intensity. This current will be converted to a voltage signal using either a wide band TIA configuration or a 50 ohm resistor with a wide band non-inverting amplifier configuration. In both configurations, we use the wide band amplifier (OPA657, Texas Instruments). This amplifier has a high gain bandwidth product (1.6 GHz), low distortion voltage-feedback op amp, and low voltage noise FET input stage [27].

To demodulate the modulated light signals, we must have electrical reference signals. In our case, the reference signals will be extracted from voltages at the anodes of each laser diode, and they will be similar to the modulation signals. In the demodulation scheme, the reference signal corresponding to one of the light sources is multiplied with the detected light signal using a 500 MHz analogue multiplier AD834 (Analog Devices), and the result is passed through a passive low pass filters [55]. Figures 23 and 24 show the schematics of two modified high speed circuit designs, respectively.

The modifications to the first design are as follows:

1. Instrumentation amplifier to magnify the weak differential output of heterodyne demodulator circuit.
2. Four VCOs to allow future square wave modulation of laser diodes.

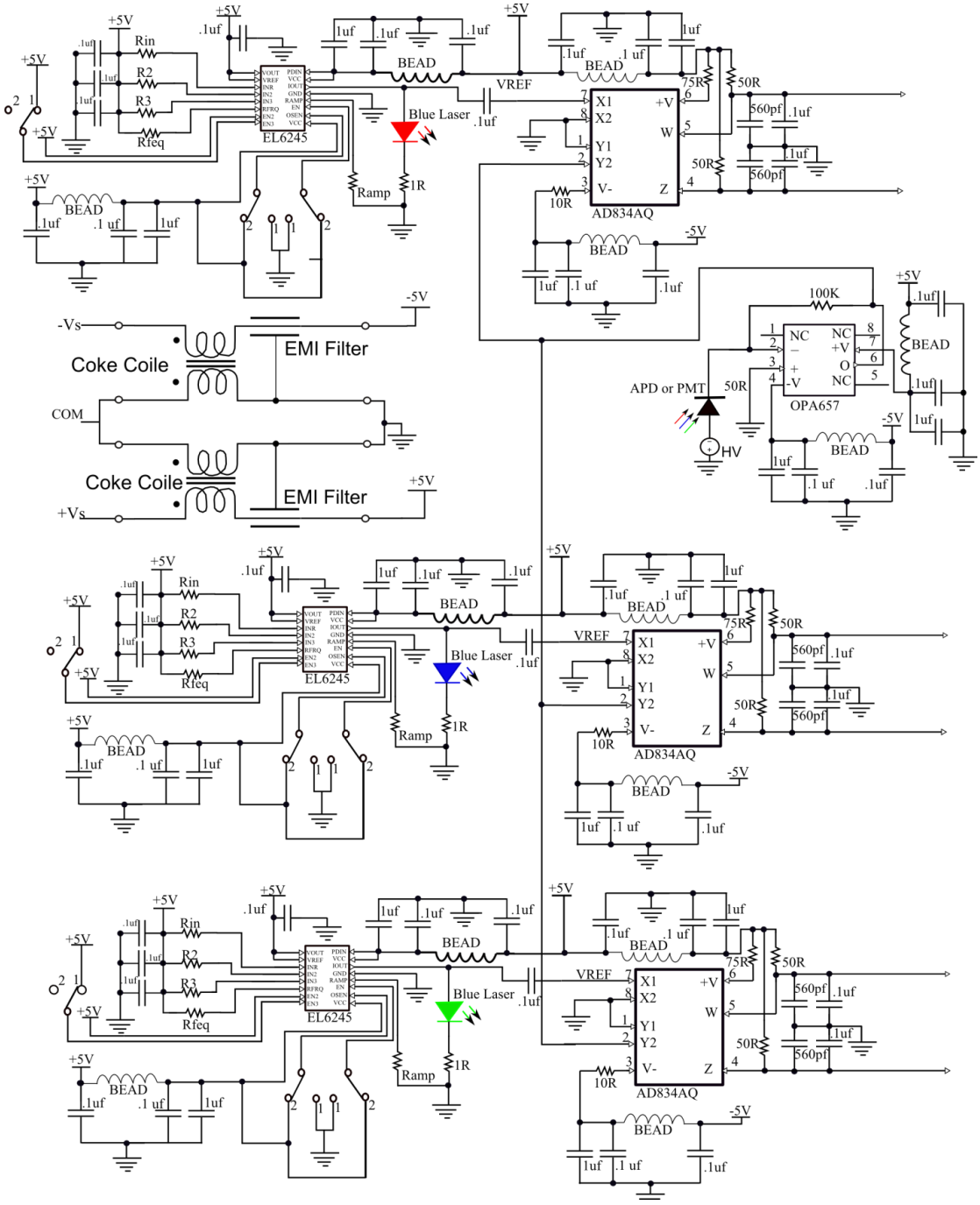

Figure 22: High speed FDM circuit schematic. The circuit is designed to work in the 100s MHz range. EMI suppression measures are used in this design.

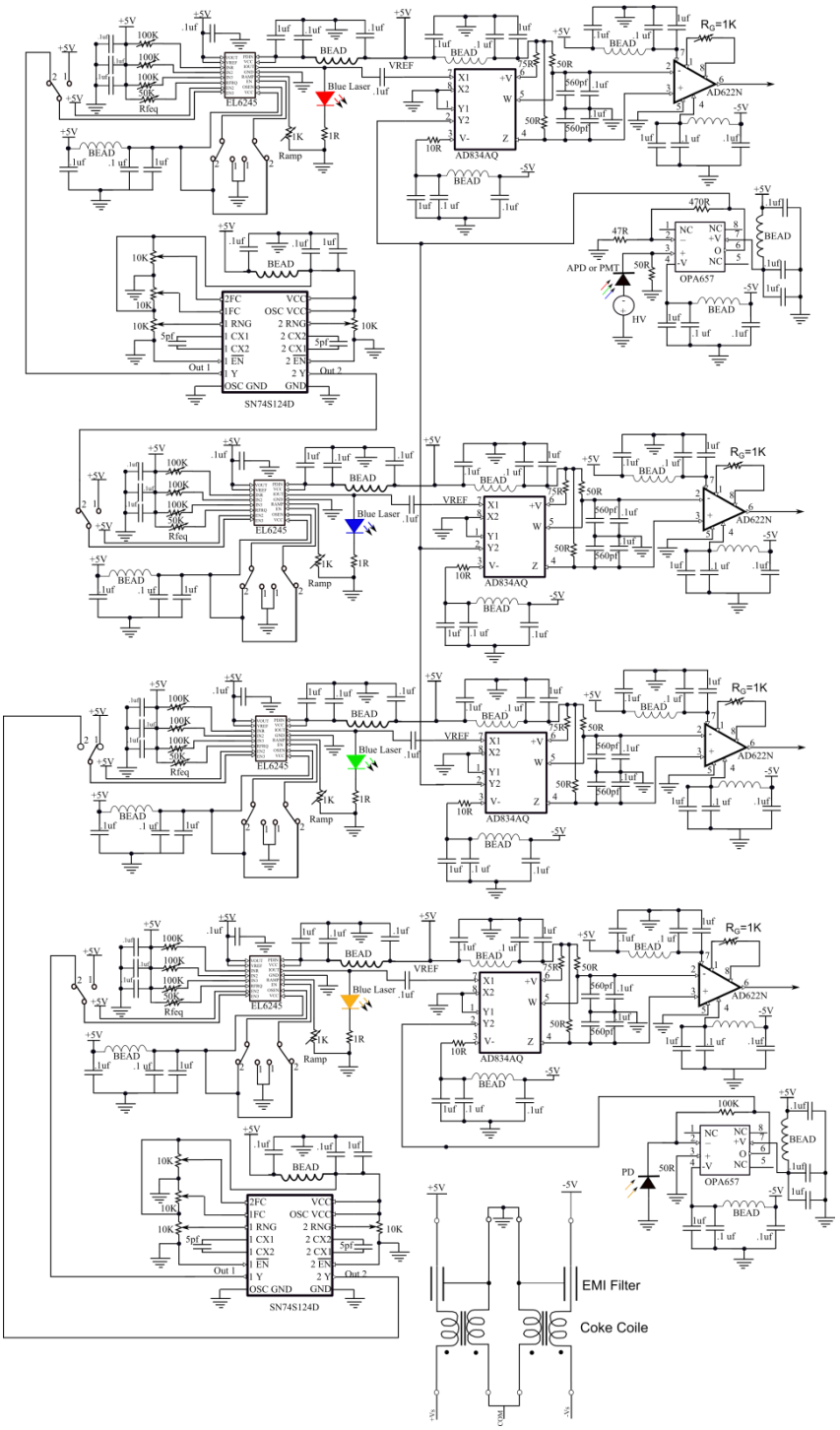

Figure 23: Second version of the high speed FDM circuit schematic. Some additions and modifications to the previous version are made such as adding a fourth stage for forward scatter measurements and instrumentation amplifier circuits.

3. Complete stage with amplifier circuit to be used for forward scatter measurements.
4. Use of variable resistors to allow easy adjustment of system parameters like modulation frequency and amplitude, lasing threshold level, the gain of the instrumentation amplifier circuit, etc.
5. Larger footprints of choke coils and chip EMI filters.
6. Use of SMA connectors in all inputs and outputs to reduce noise interferences and ease of connection to the external world.
7. Make cutouts in power and ground plans underneath every IC to eliminate possible stray capacitances between IC pin and those plans.
8. Allow the configuration of the amplifier in to different operation modes like transimpedance amplifier mode and non-inverting amplifier mode.

In addition to these changes above, we corrected the mistakes that we made in the first high speed circuit. The details of each stage will be explained in the following sections.

3.2.1.1 Power Supply

Power supply with its cables radiates both differential mode and common mode noise. To suppress such noise, we use cascaded choke coils to suppress the common mode noise and chip EMI filters to suppress the normal mode noise. Figure 24 shows two parallel cascades; one for the positive side and the other for the negative side of the power supply. We use choke coil model DLW5BSN351SQ2L from Murata Company that has 350 ohm at 100 MHz, and we use chip EMI filter, model NFM21CC222R1H3 from Murata Company. The frequency characteristics of choke coils and the chip EMI

filters are shown in Figures 25 and 26 for different models from. The graphs are copies from [56].

In addition to the power supply noise, ICs, PCB tracks, etc will add more noise to signals. To minimize such EMI signal distortion, a ferrite bead with three decoupling capacitors has been connected at the power supply input of each IC. The configuration of this filter is shown in Figure 27. The bead resonates at 200MHz and it will block all harmonics that have frequencies around 200 MHz. Figure 28 shows the frequency characteristics of different ferrite bead models. The two pole low pass filter will block all high frequency harmonics from going out of any IC to the power supply.

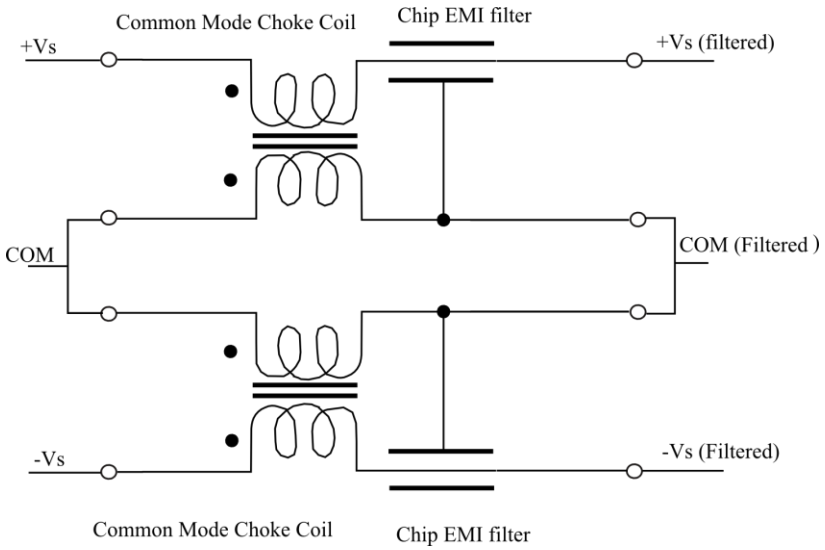

Figure 24: Power supply noise suppression configuration. Choke coil and chip EMI filter are connected in cascade for each power pole to suppress both normal and common mode noises.

Two types of capacitors (i.e., Tantalum (1µf) and Multilayer Ceramic Capacitors (MLCC) (.1µf)) are used; the first works optimally at high frequencies and the other at low frequencies [57], [58]. The .1 µf MLCC is used at every supply voltage connected to resistors.

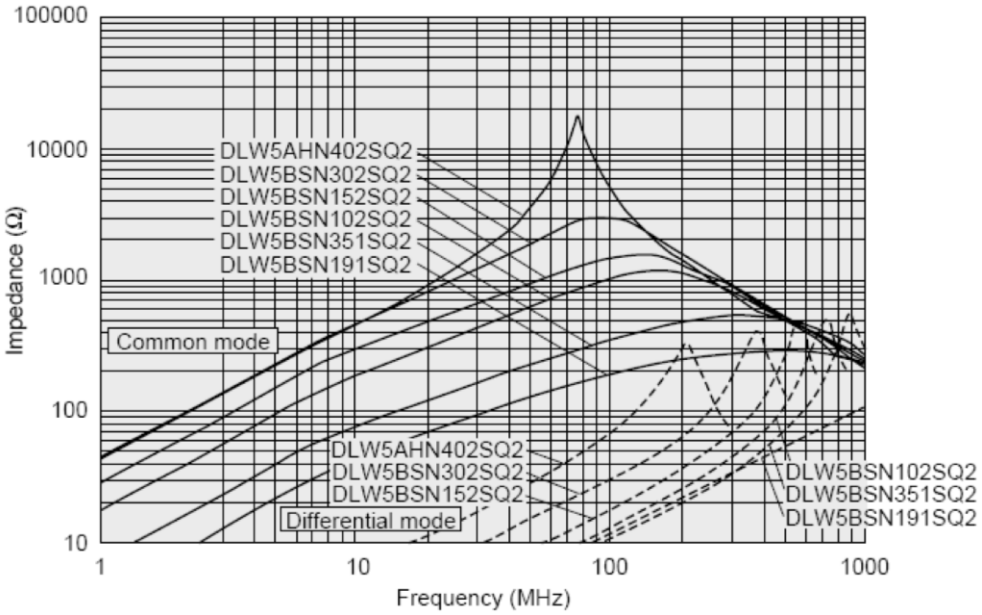

Figure 25: Choke coil frequency characteristics of different models from Murata Manufacturing Company. We use the model DLW5BSN351SQ2L. The graph is a copy from [59].

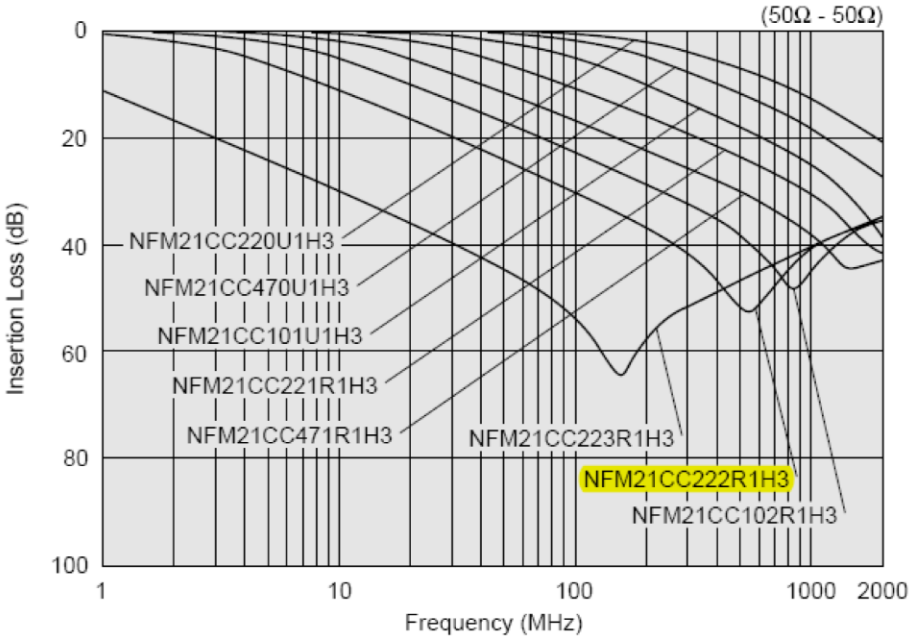

Figure 26: Chip EMI filter frequency characteristics of different models from Murata Manufacturing Company. We use the model NFM21CC222R1H3. The graph is a copy from [56].

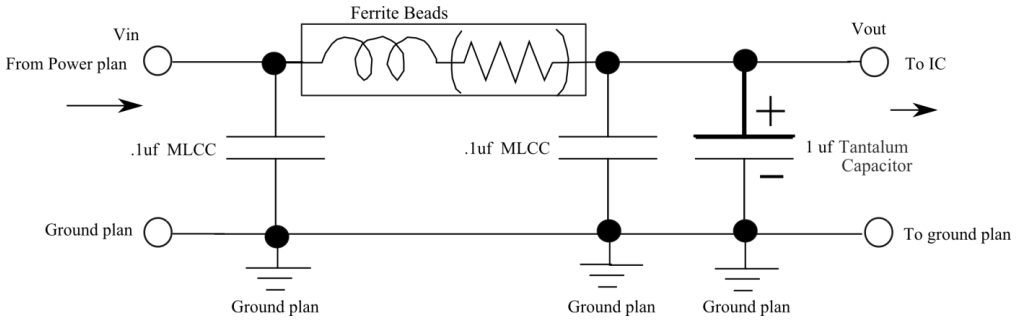

Figure 27: Ferrite bead and three decoupling capacitors form high frequency signals block to or from any IC in the circuit.

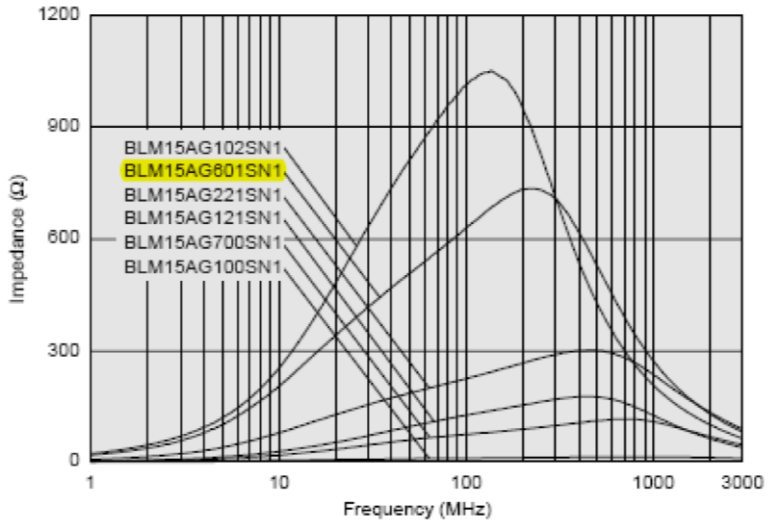

Figure 28: Ferrite bead frequency characteristics of different models from Murata Manufacturing Company. We use the model BLM15AG601SN1. The graph is a copy from [57].

3.2.1.2 Laser Driver Circuit

As mentioned above, our system must work in the MHz range because of the small size and fast speed of droplets, particles or cells under investigation. Therefore, we have to modulate our lasers with sine wave signals that have frequency up to 100MHz. For this purpose, we choose the high performance 3-channel laser diode driver with oscillator (EL6245 Elantec Semiconductor). The operating circuit of the driver is shown in Figure

29. The driver works as a voltage-controlled output current source. The control is performed using external resistors. We use variable resistors to give us the flexibility to adjust operating parameters such as light intensity, modulation frequency and amplitude etc. The output current of each control channel is determined by the value of the resistors connected to INR, IN2, and IN3 terminals. The output current per channel can be calculated as follows:

$$I_{out} = \frac{V_{cc}}{R_{inx}} * 100 \quad (39)$$

The driver has a 500MHz built-in sinusoidal oscillator that can modulate the diode current up to 100 mA peak to peak. To operate the oscillator, the terminals the pins OSCEN, OUTEN1 and OUTEN2 are held high (*Vcc*). The modulation frequency and amplitude can be controlled using the variable resistors connected to pins RFREQ and RAMP, respectively. The drive can be enabled and disabled by connecting the pin EN to high or low, respectively. Both the rise and fall times when enabled and disabled are .8 nsec. If we want to modulate the laser by an external square wave generator that oscillates between low (0V) and high (*Vcc*) levels, we have to connect the oscillator output to one of the pins OUTEN1 or OUTEN2; in this case, the built in oscillator will be disabled; the input current of the INR pin must be adjusted to allow the minimum required output current using its variable resistor; the maximum allowable or required output can be adjusted using the variable resistors of the pins IIN1 or IIN2 depending on which cannel we use to drive OUTEN1 or OUTEN2, respectively. Note: never exceed the maximum operating current of the laser diode under use for any mode of operation

(i.e., DC, internal sinusoidal modulation, or external square wave modulation). As shown in Figure 29, the decoupling configuration shown in Figure 27 is used at the two biasing pin of the drive *VCC*. The pin PDIN, VOUT, and VREF are connected to the high level because they are not used. Because the driver is still under property [54]. A laser diode current can be monitored using the voltage drop across a 1 Ω resistor connected in series with the laser diode.

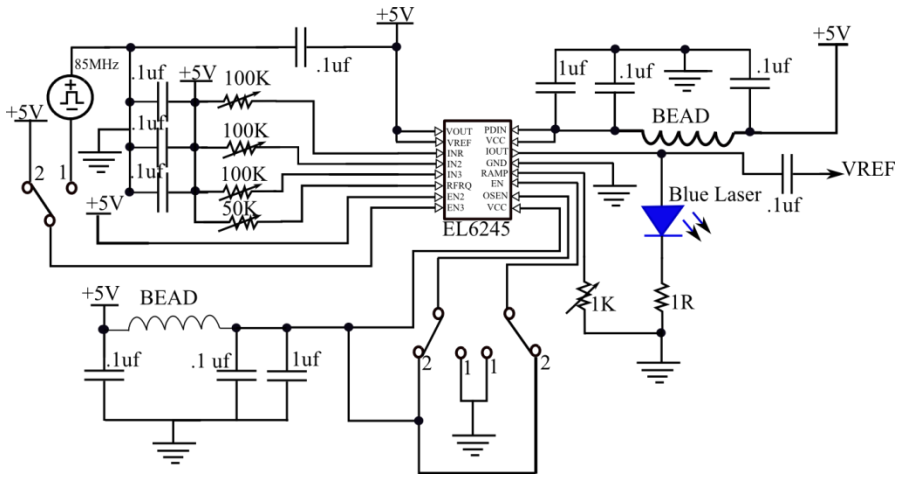

Figure 29: Laser diode driver circuit. Surface mount variable resistors are used to allow a flexible adjustment of operating parameters. The noise suppression block of Figure 27 is used at all power pins.

3.2.1.3 Analog Multiplier Circuit

The four-quadrant analogue multiplier chip IC model AD835500 MHz is used in the multiplier circuit is shown in Figure 30. It is capable of multiplying signals from DC up to 500MHz. The IC is suitable for our high speed cytometry application due to its low distortion ($\leq 0.05\%$ for 0 dBm input) and wide operating frequency range [55]. The circuit multiplies a reference signal with the multiplexed signal. The reference signal is the laser modulation signal, and it is taken as the voltage at the anode of the laser diode.

This signal is capacitively-coupled (.1µf) to the multiplier to eliminate the DC component from the reference signal. The other input signal to the multiplier is the multiplexed amplifier output that contains all frequency signals. When the two input signals are multiplied, the multiplier output will contain all harmonics represented in equation (34). A low pass filter with a cut off frequency, fc, of 200 KHz connected in series with the multiplier will eliminate all frequencies higher than f_c.

Defining the quantities *X=(X1-X2)* and *Y=(Y1-Y2)*, the current outputs of the multiplier *W* and *Z* can be written as [60]:

$$W = \frac{X * Y}{(1V)^2} * 4mA \tag{40}$$

$$Z = -\frac{X * Y}{(1V)^2} * 4mA \tag{41}$$

The 4 mA is an internal scaling factor when input is ±1 V. Because these two output-currents will flow in the two 50 Ω resistors, the differential output voltage will be:

$$V_{diff.} = \frac{X * Y}{(1V)^2} * 400mV \tag{42}$$

For proper use of the multiplier circuit, the input must not exceed the clipping level of ±1.3 V at each input channel. At this value the distortion levels become very high [60]. To minimize the noise generated by the multiplier IC, the noise suppression block of Figure 27 is used at all power input pins.

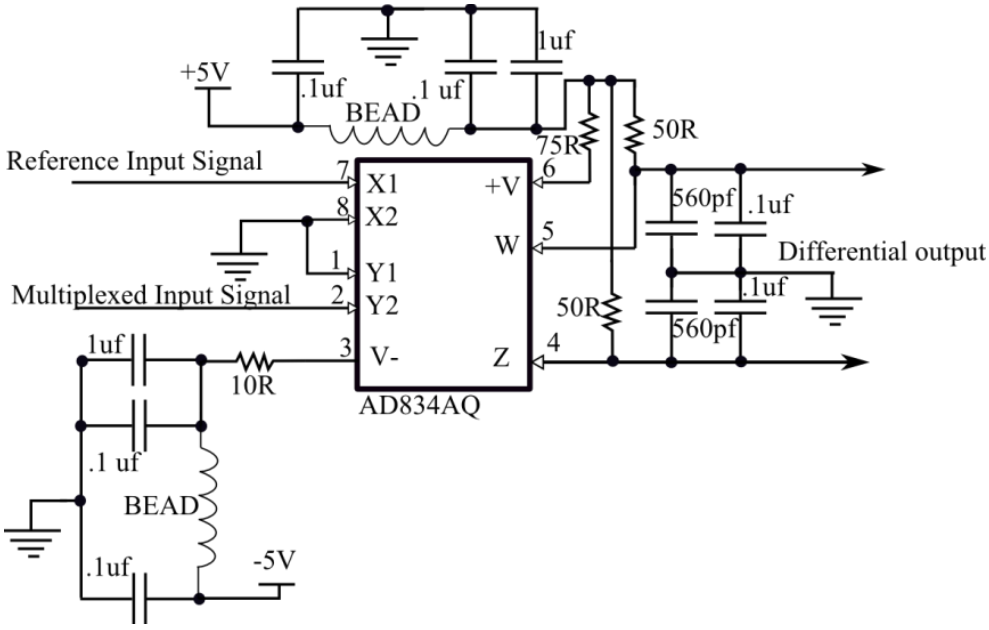

Figure 30: 500 MHz analogue multiplier circuit. One input is the reference that is taken at the anode of the laser diode via a coupling capacitor. The other input is the multiplexed output of the amplifier circuit shown in Figure 31. The noise suppression block of Figure 27 is used at all power pins.

3.2.1.4 Wide-Band Amplifier Circuit

In our final version of the FDM control circuit, we use the high gain bandwidth product (1.6 GHz), low-noise (4.8nV/√ Hz), FET-input operational amplifier (OPA657, Texas Instruments). However, because of its low bandwidth of 10 MHz when used in the trans-impedance amplifier mode, we use this amplifier in non-inverting amplifier mode shown in Figure 31, which has up to 200 MHz with gain equal to 10 [27]. We also noticed that in the TIA mode it oscillates very often above feedback resistor values of 7 KΩ because it is uncompensated amplifier chip. In the TIA mode we are not able to get it to work with PMTs as light detectors, but no oscillation is noticed when used in the NIA mode. Because of the available resistor values of 470 Ω and 47 Ω, we set the gain to 11 at

which the measure bandwidth shown in Figure 51 is 70 MHz. Reducing the gain can increase the band width. The noise suppression block of Figure 27 is used at all power pins.

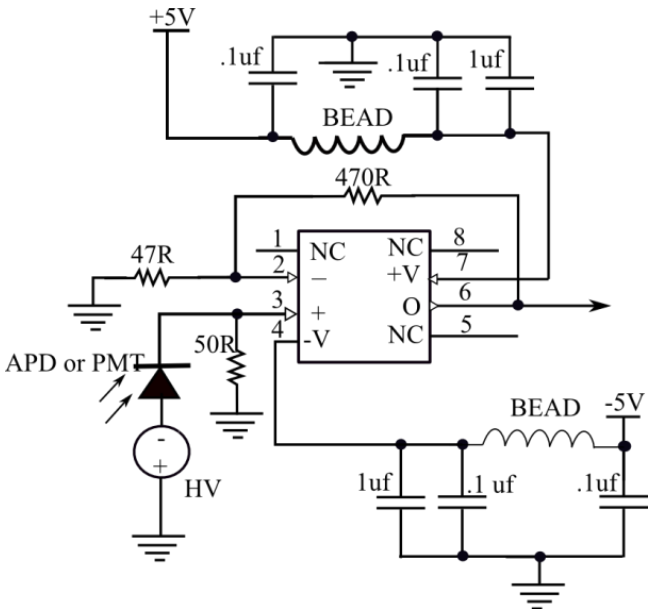

Figure 31: Wide band non-inverting amplifier circuit. The gain is set to 11 at which the circuit BW is set to about 70 MHz. Reducing the gain can increase the band width. . The noise suppression block of Figure 27 is used at all power pins.

3.2.1.5 Instrumentation Amplifier Circuit

Because the output of the multiplier stage is weak (10s mV) and in differential mode, the instrumentation amplifier is needed to amplify and convert it to a single mode signal. We use the AD622N (Analog-Devices) because it has the required band width of 800MHz, low cost, and requires one external resistor to set its gain 2 to 1000. The Instrumentation amplifier circuit is shown in Figure 32. An SMT variable resistor (0- 1 KΩ), $R_{G,}$ is used to adjust the gain. Table 2 presents the gain versus resistor value of the instrumentation amplifier [61]. The noise suppression block of Figure 27 is used at all power pins.

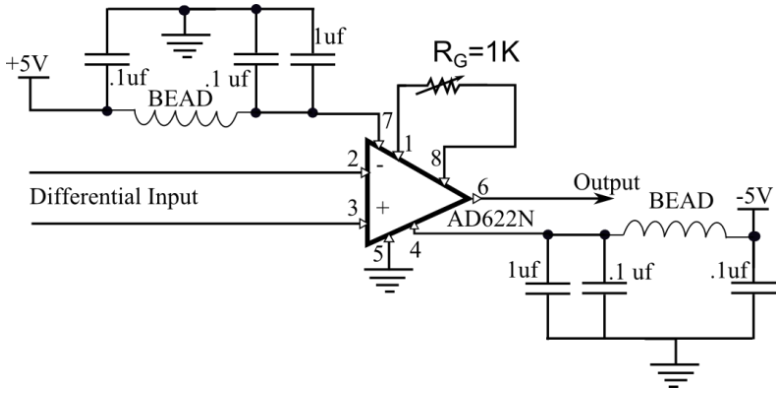

Figure 32: Instrumentation amplifier circuit. Because the output signal of the multiplier is in a differential and weak, the instrumentation amplifier is used to amplify it. The gain can be set by the resistor $R_{G.}$ The noise suppression block of Figure 27 is used at all power pins.

Table 2: Resistor values versus calculated and desired gains of the AD622N (Analog-Devices) instrumentation amplifier [61].

Desired Gain	Table Value of RG, Ω	Calculated Gain
2	51.1 k	1.988
5	12.7 k	4.976
10	5.62 k	9.986
20	2.67 k	19.91
33	1.58 k	32.96
40	1.3 k	39.85
50	1.02 k	50.5
65	787	65.17
100	511	99.83
200	255	199
500	102	496.1
1000	51.1	989.3

3.2.1.6 Square Wave Voltage Controlled Oscillator

As shown in Figure 29, the laser diode can be modulated with an external square wave oscillator through the laser drive (EL6245, Elantec). Figure 33 shows the circuit of

dual square wave generator up to 85 MHz using the voltage controlled oscillator chip model SN74S124D.

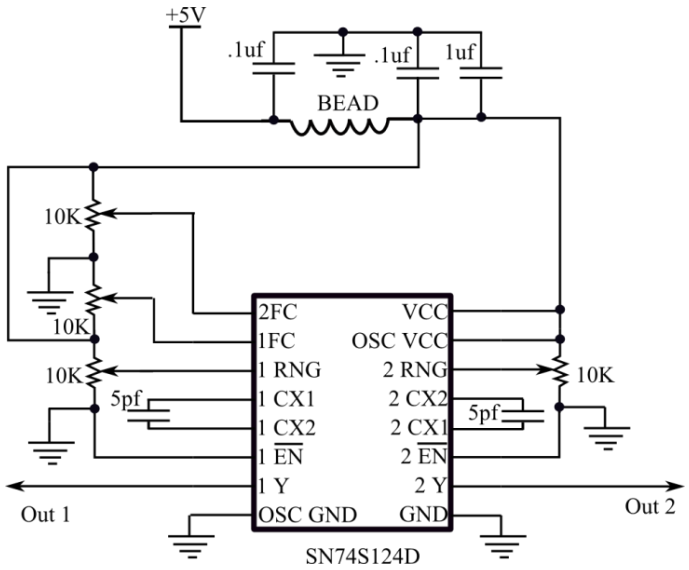

Figure 33: Dual square wave generator up to 85MHz using the voltage controlled oscillator chip (SN74S124D, Texas Instrument).

However, we are able to operate the square wave oscillator circuit only up to 18 MHz. Some undetermined parasitic capacitance in our PCB is limiting the maximum oscillation frequency. For each oscillator the frequency range and set value can be adjusted using two potentiometers. The capacitance of the capacitor connected between the pin CX1 and CX2 determines the maximum oscillation frequency. The noise suppression block of Figure 27 is used at all power pins.

3.2.2 PCB Layout

Pad2Pad Company allows the use of their free software with the condition that the user has to manufacture the Gerber files that allow the user to manufacture anywhere else. Therefore, we decided to use the FreePCB software the generated Gerber files

without any constraint, so all subsequent PCB layouts are generated using FreePCB software version 1.359.

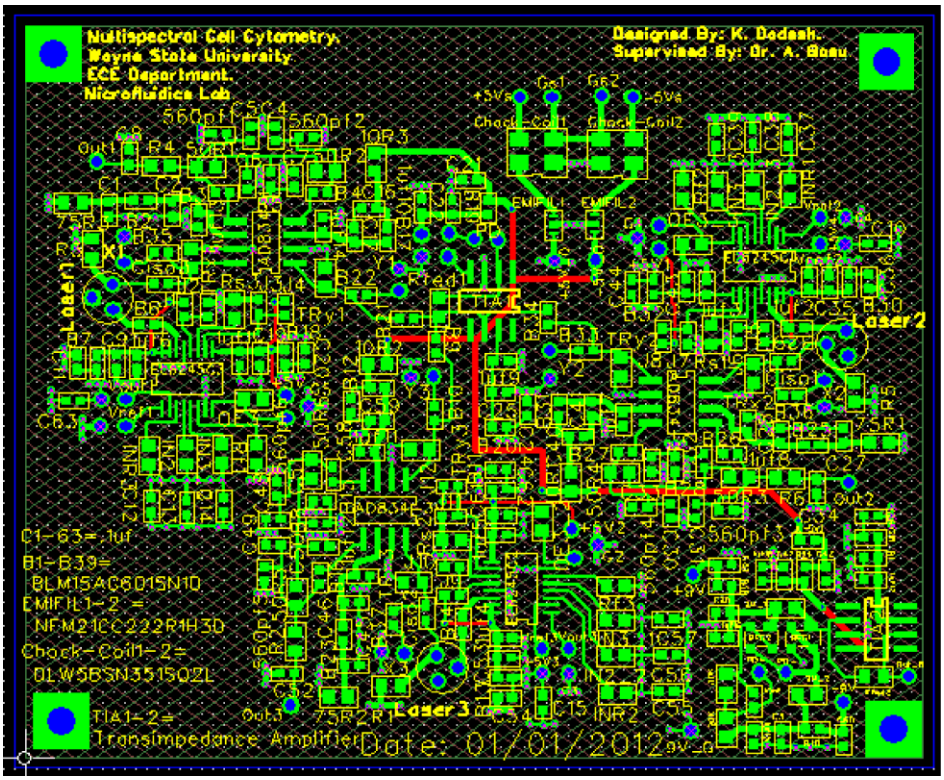

Figure 34: PCB layout of the first version of the high speed circuit. It is made of 4-layers; one of the middle layers is the ground plan and the other plan is the positive power potential.

Figure 34 shows the first 4-layer PCB layout of the schematic of the high speed circuit shown in Figure 22. The dimension of this design is 91.9 mm width and 73.2 mm height. Figure 35 shows the modified 4-layer PCB layout of the circuit schematic shown in Figure 23. The modified PCB has 140.5 mm in width and 84.5 mm in height, 1 oz copper weight, 0.062 in material thickness, and FR4 material type. Figure 36 show the cutouts we made in the second PCB version to eliminate stray capacitance between IC pins and internal layers that usually happens at high frequencies.

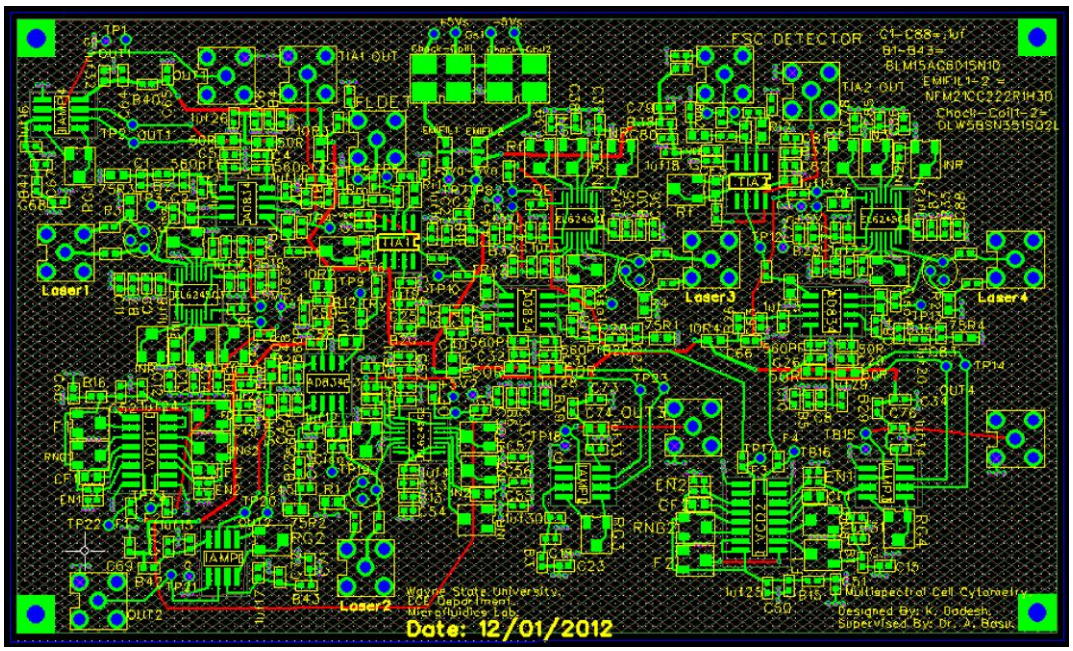

Figure 35: PCB layout of the second version of the high speed circuit. Some modifications to the first version are added. A complete stage for forward scatter measurements and Instrumentation amplifier circuits and are added.

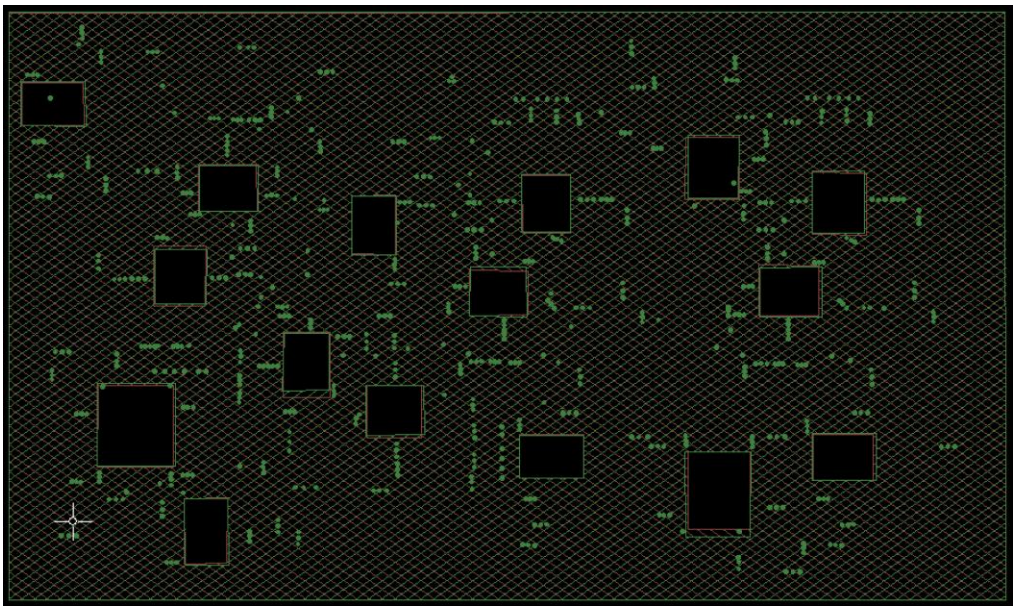

Figure 36: PCB cutouts in middle plans are made underneath all ICs to eliminate stray capacitances between IC pins and internal layers.

CHAPTER 4: PHOTOMETRY EXPERIMENTAL RESULTS

The preliminary results that we published so far, and the attempts found in the literature have motivated us to peruse further investigations in this regard. A proof of concept for the application of the FDM technique with absorbance photometry was published in EMBS 2011 conference [13]. This work showed the ability of the technique to simultaneously discriminate between the absorbance of red, green and blue lights with red, blue, or green FD&C dyes in continuous and droplet microreactor flow systems. We extended the work that by incorporating a detailed time and frequency domain analysis and investigating extra four chemical colors.

4. Absorbance Photometry

The details of the circuit used in this experiment are presented in section 3.1.1. Here we are presenting the experimental results using the photometry-FDM system.

4.1.1 FDM Absorbance System Design and Operation

The multispectral FDM photometry system shown in Figure 27 is designed and implemented to be compact and low cost. Figure 37A illustrates the block diagram. The emissions from the three LEDs are coupled into a single 1 mm polymer optical fiber (Industrial Fiber Optics) using a 3x1 optical coupler (IF-543, Industrial Fiber Optics) and are guided to a detection cell. The flow cell consists of a polyethylene cross junction (Value Plastics) where two optical fibres are affixed to the upper and lower ports, while the sample flows from the left to the right ports. The upper fiber transmits light into the detection cell, and the lower fiber collects the scattered light and guides it to a high-speed photodiode (PD) detector housed in a fiber-optic package (IF-D91, Industrial Fiber

Optics). The PD provides fast rise and fall times (~5ns) and wide spectral range (400-1100 nm).

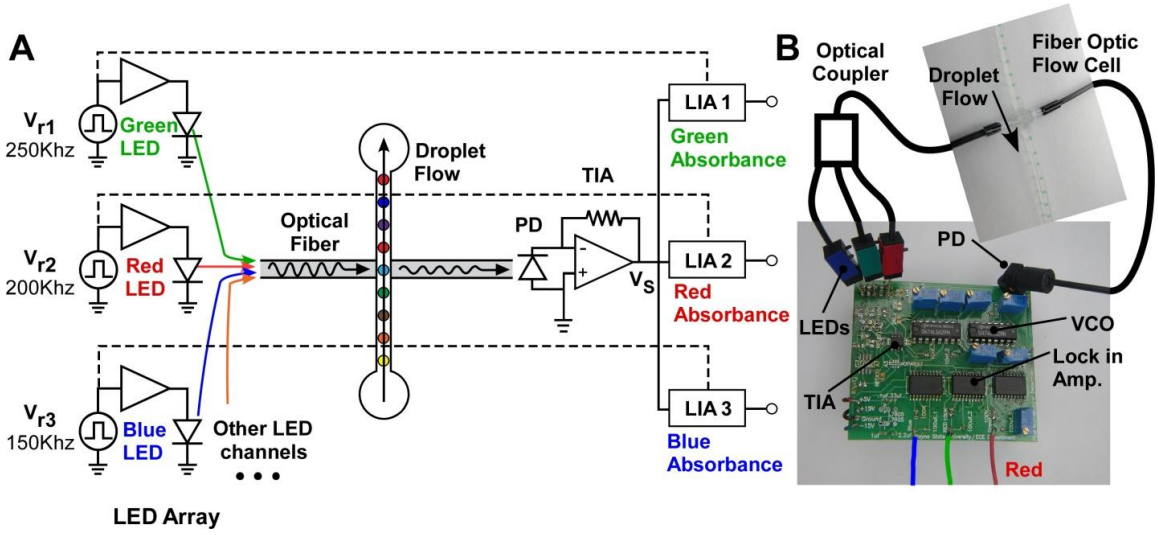

Figure 37: A) A schematic diagram of a multi-spectral absorbance detection system using FDM. Absorbance at red (636 nm), green (574 nm), and blue (470 nm) wavelengths are simultaneously monitored using a simple modulation/demodulation scheme. This approach can be economically scaled to include many LEDs spanning a wide spectral range. B) Photo of the implemented circuit. It is implemented using low cost electronic components and flow cell. The 1x3 optical fiber coupler is drawn schematically because of its large size.

According to Beer's Law, light absorption by the sample reduces the amplitude of each LED depending on the sample's absorption coefficient at the corresponding wavelength. The ratio of transmitted to incident light is $I_T/I_O = 10^{-\alpha l}$, where α is the absorption coefficient, and *l* is distance the light travels through the material (i.e., the path length). When the signal from each LED is extracted, each channel provides a measurement of the absorbance at a specific wavelength.

Figure 37B shows the FDM-detection circuit implemented in a compact, double layer

printed circuit board (PCB). The board can be divided into three main sections. The first contains three VCOs that generate three reference square wave signals, the second contains three lock-in amplifiers, and the third section contains the photodiode and transimpedance amplifier**.**

4.1.2 Results and Discussion of the Photometry-FDM system

4.1.2.1 Time and Frequency Domain Measurements

Time and frequency domain measurements, taken at the output of the TIA, validate the principles of FDM and its ability to multiplex light signals and perform multispectral photometry. In the control experiment, a deionized water sample is passed through the detection cell, and the photodetector signal is recorded using a digital oscilloscope with a 100 MHz sampling rate. Figure 38A shows the TIA time-domain signal when the green LED is modulated by a 150 KHz square wave, while the blue and red LEDs are off (no multiplexing). Distortions in the square wave voltage signal can be attributed to the exponential current-voltage characteristic of the emitting LED. When the LEDs are driven by a square wave voltage signal, the Taylor series expansion of the diode current contains even harmonics which are apparent in the frequency spectra (Figure 39A, spectra 3). These harmonics are acceptable because they are later filtered out by the lock in amplifier. Similarly, Figures 30B-C show the frequency spectra due to the red LED modulated at 200 KHz, and the blue LED modulated at 250 KHz. When all three LEDs are modulated simultaneously, the resulting signal at the photodiode (Figure 38D) reflects the time-domain superposition of the three channels.

The frequency spectra of the time domain signals in Figures 29A-29D are shown in Figures 30A-30C, respectively. To record the frequency spectrum, all three LEDs are activated and the voltage signal is acquired at a high sampling rate. The signal is then converted to the frequency domain using Matlab's Fast Fourier Transform (FFT) function. The results for the red, green, and blue channels are shown in Figures 30A, 30B, and 30C, respectively. Beginning with the red channel, Figure 39A shows five spectra, one at each stage within the detection system. Signal (1) is the 200 KHz square wave generated using the voltage controlled oscillator circuit to pulse the red LED at this frequency.

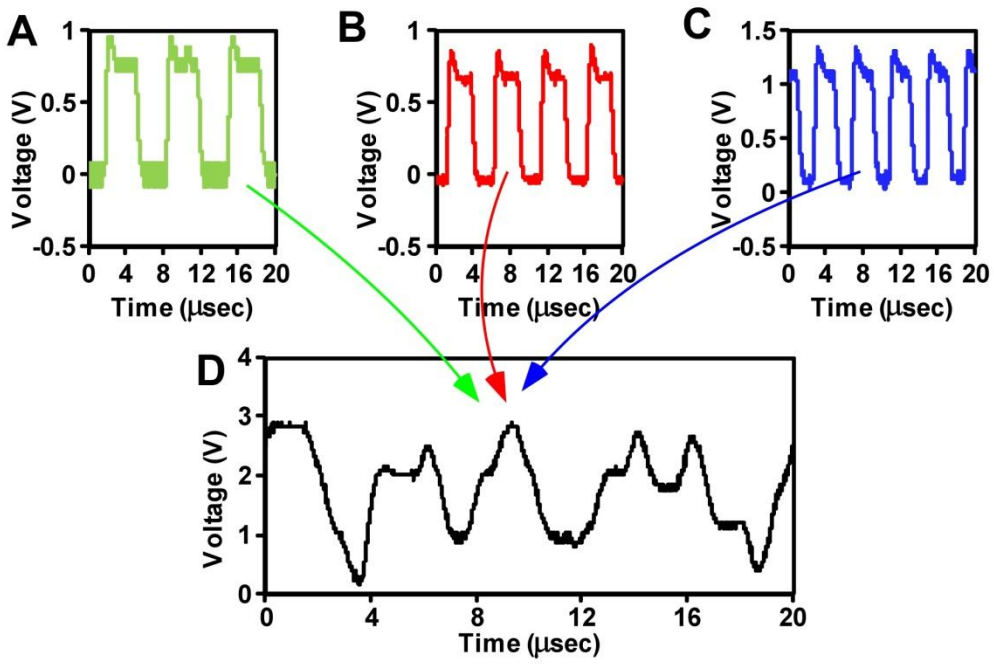

Figure 38: *Time domain signals of the transimpedance amplifier when: A) only the green LED was pulsed at 150 KHz. B) Only the red LED was pulsed at 200 KHz. C) Only the blue LED was pulsed at 250 KHz. D) All LEDs were pulsed at the previously mentioned frequencies simultaneously. This graph represents a multiplexed signal containing absorbance measurement on all three colors.*

As expected from equation 5, only odd multiples of the fundamental frequency exist (i.e., 1 x 200 KHz, 3 x 200 KHz, and so on). Signal (2) is taken at the PD output, and therefore contains components from all three frequency channels. In addition to the expected odd components, signal (2) has extra even harmonics of the three light signals (i.e., 2 x 150 KHz, 2 x 200 KHz, and 2 x 250 KHz). As discussed above, these are due to the nonlinearities of the light detectors. For PDs the incident-light energy is proportional to the generated current. If we modulate the electric field of the light signal with a sine wave with frequency f_m, the generated current will be proportional to the square of the this sine wave. Using simple trigonometric relations, we end up with $2*f_m$ component that appears in all of the PD output signals. This effect is again illustrated in signal (3), which shows an even harmonic (2 x 200 KHz) at the PD output when only the red LED is illuminated. Signal (4), taken at the output of the lock-in amplifier, shows the product of the reference signal (1), and the multiplexed PD signal (2). Signal (4) contains the summations and differences of all of the components available in signals (1) and (2), including inter-channel crosstalk harmonics. For example, the difference of the modulation frequencies 200 KHz and 150 KHz results in a harmonic at 50 KHz. This is the first component one can see in signal (4) after the low frequency components (i.e., near DC). Signal (5) is the final output signal, taken after the low pass filter has removed the high frequency components from (4). The output signal consists of two components: i) *The desired signal*: the product of odd components of the reference signal (1) and the PD signal (2) produced by the red LED; and ii) *Crosstalk components*: the product of harmonics which overlap with other frequency channels. For example, the third

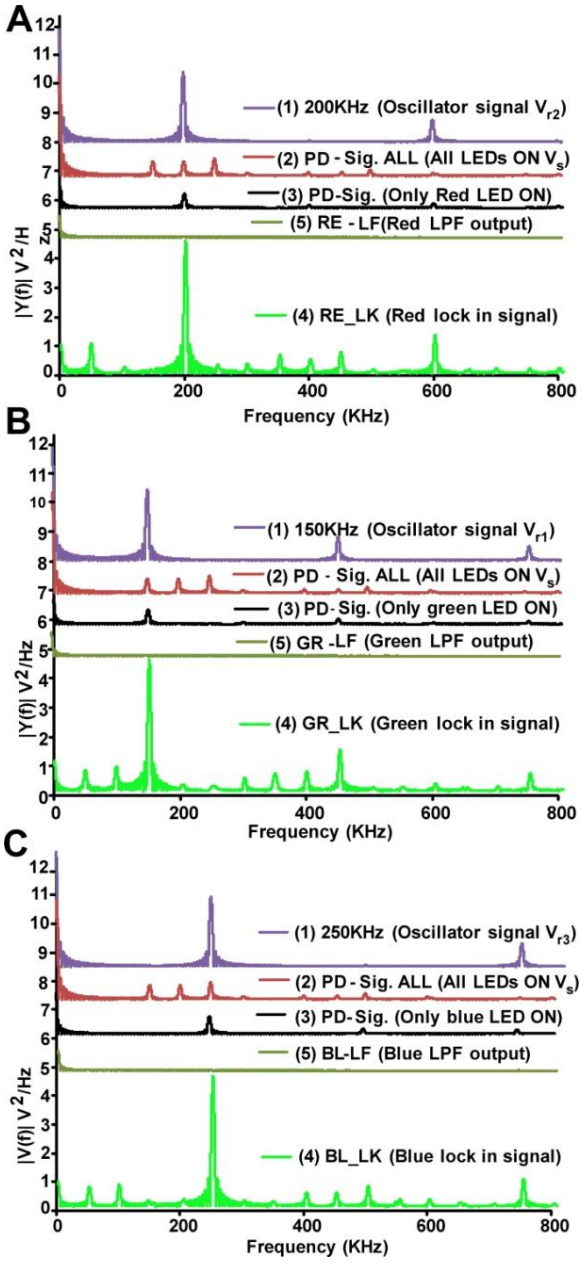

Figure 39: Results of the Fast Fourier Transform (FFT) analysis of time domain signals produced using a Matlab algorithm. Five signals in each graph: (1) oscillator electrical signal, (2) photodiode (PD) signal when three LEDs were on, (3) photodiode (PD) signal when only one LED was on, (4) lock-in output signal, and (5) low pass filter (LBF) output signal. A) Red LED signals at 200 KHz, B) green LED signals at 150 KHz, and C) blue LED signals at 250KHz. Note: all signals are shifted up differently to avoid overlapping.

harmonic of the 250 KHz reference signal coincides with the fifth harmonic generated by the green LED, which was modulated at 150 KHz. These crosstalk components are typically quite small because amplitudes of the higher harmonics degrade by 1/*N*, where *N* is the harmonic number. The crosstalk can also be eliminated entirely by carefully selecting multiplexing frequencies so that their integer harmonics do not coincide. Any two frequency components which have a frequency separation less than the bandwidth of the low pass filter will affect the measurements, so this must also be taken into account when selecting multiplexing frequencies. Figures 40B-40C show the frequency domain of the green (150 KHz) and blue (250 KHz) signals, respectively.

4.1.2.1 Multispectral Absorbance Photometry of Organic Dyes

This section demonstrates multiplexed absorbance photometry of single-phase flow injected samples, as well as discrete droplet microreactors containing several colored dyes. We use four dyes, Xylene cyanol, Orange G Sodium Salt, Bromophenol Blue, and Cresol Red, all of which are commonly used as markers in electrophoresis and other assays. For each dye, a high molarity stock solution (1-3 mM) is serially diluted with DI water to a minimum concentration of 1 μM. For each concentration, the FDM system provides three simultaneous absorbance measurements, one for each LED channel. The absorbance is calculated using the Beer-Lambert law, $AU = -\log_{10}(V/V_0)$, where V is the channel's output voltage when the flow cell contains sample, and V_o is the voltage when the flow cell contains only DI water.

Figures 31A-31D demonstrate the ability to simultaneously perform three wavelength absorbance measurements without crosstalk. Within the linear concentration

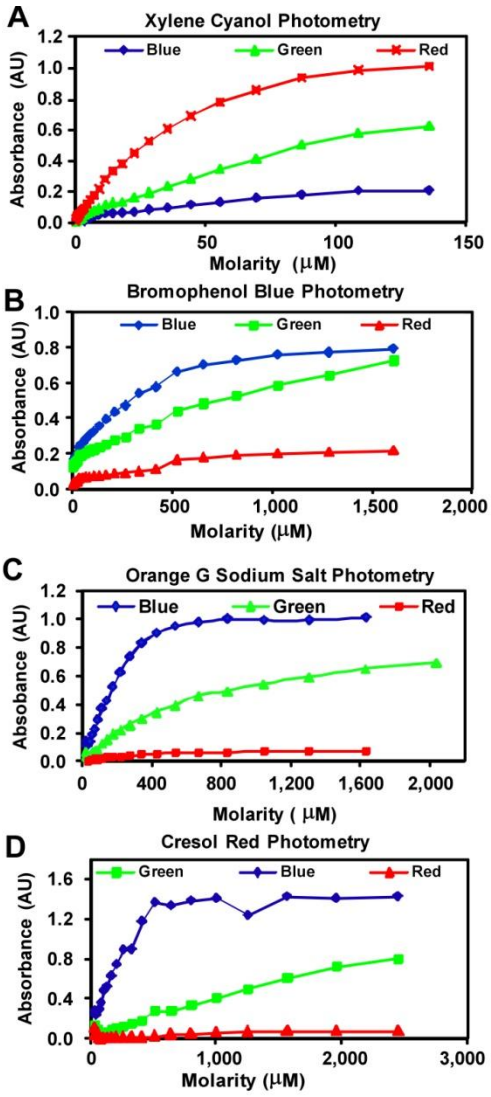

Figure 40: Multiplexed absorbance measurements of four chemeical colors: A)Xylene cyanol; B) Bromophenol Blue; C) Orange G Sodium Salt; D) Cresol Red.

range, approximately 15mM - 100µM, the absorbance characteristic of the four colors follow Beer's law, which correspond to a dynamic range of 1 AU. The lower limit of detection (LOD) is set by the length of the interrogation window, in this case ~1mm. Like other absorbance photometers, the LOD can be exponentially improved (according to Beer's law) by increasing the length of the flow cell. Xylene cyanol, a blue dye, absorbs red light much stronger than the blue light (Figure 40A). The Xylene Cyanol

absorbance at about 90µM is .93, .50, and .17 AU for red, green and blue lights, respectively. This behavior is expected as Xylene Cyanol is known to absorb strongly at 634 nm, less at 574 nm, and the least at 470 nm [62]. The absorbance of bromophenol blue at 90 µM is .07, .22, and .31 AU for red, green and blue lights, respectively. The absorbance of Orange G sodium salt at 90 µM is .02, .08, and .37 AU, respectively. Finally, the absorbance of cresol red at 90 µM is .003, .05, and .36 AU, respectively. In contrast to Xylene Cyanol, the three dyes bromophenol, Orange G sodium salt, and cresol red, absorb blue light more strongly than red (Figures 9B-D).

4.1.2.2 Time Analysis of Droplet Microreactors

In digital or droplet-based microfluidics, aqueous droplets in an immiscible carrier fluid serve as reaction containers for biochemical assays [63-64]. The droplets can be of miniscule volume , and specific chemical reactions may be initiated by merging droplets with each other or an aqueous stream [64]**.** Monitoring reactions in droplets typically involves a flow through setup, similar to cytometers, where droplets serially pass by a detection cell [4], [65]. In such systems, high-speed multiplexed photometry allows us to efficiently perform multiparameter, high throughput analysis in a single, compact window. Figures 10A-6C demonstrates the ability of the FDM photometer to perform high speed multispectral absorption measurements on droplets, and distinguish their contents. Droplet microreactors (radius 1mm) containing allura red, blue #1, and green (i.e. a mixture from blue #1 and yellow #5) FD&C dyes (12.5% v/v) are dispersed in oleic acid using a T-junction [4]. The flow of the two immiscible phases at the two inlets of the junction generates a stream of droplets. The droplets are then flowed past the

detection system at a throughput of 12 drops/sec. The absorbance of each droplet is quantified by comparing the light signal while the droplet is in the detection cell, to that of the base carrier fluid. The absorbance is measured simultaneously in each of the three LED channels, providing a multiparameter profile of each droplet.

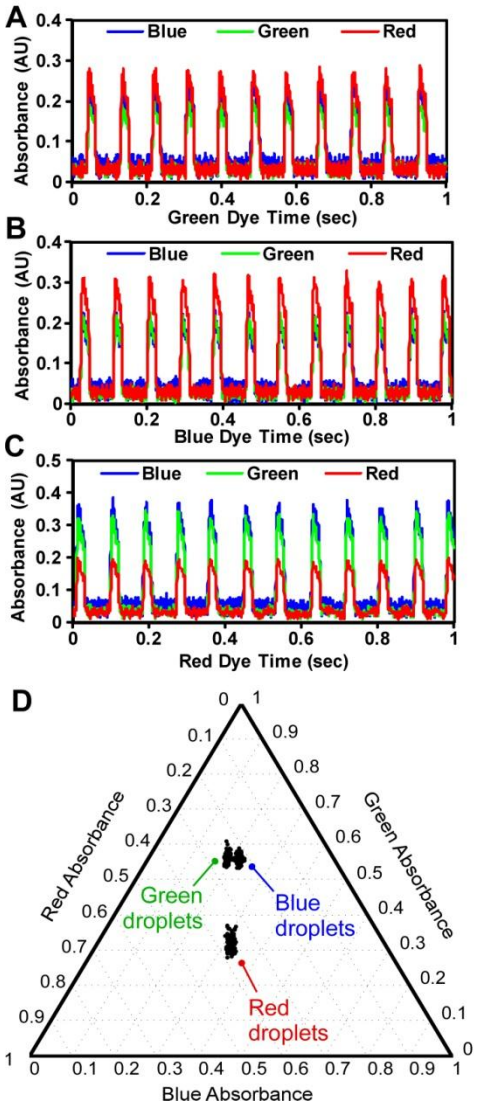

Figure 41: Inline, multispectral analysis of droplet microreactors using the FDM photometer for; A) Green food Dye, B) Blue food Dye, and C) Red food Dye. D) A triangle diagram that indicate three different populations.

The droplets are plotted on a triangle scatter diagram which displays the three-dimensional profile in a compact 2D space (Figure 41D). The three types of droplets can be distinguished as individual populations in the diagram. In this way, multispectral photometry can be used to identify droplet populations, so long as the important wavelengths can be identified a priori. The absorbance profiles of the three dyes agree with the expected values for each dye. Although the current fluidic setup limited the throughput to 12 drop/sec, we expect the circuit to be able to handle 1-2 orders of magnitude higher. The measurement bandwidth of the system was found to be 160 Hz.

CHAPTER 5: FLUORIMETRY EXPERIMENTAL RESULTS

5.1 Low Speed Laser Induced Fluorescence FDM System (FDM-LIF)

5.1.1 System Concept and Experimental Setup

A comparison of a conventional two-color LIF system and the corresponding FDM-LIF system is shown in Figure 42. The conventional system (Figure 42A) requires two PMTs, each with a dedicated high voltage power supply, filter, and optical path. In the FDM-LIF system (Figure 42B), fluorescence signals are frequency multiplexed on a single PMT. Two reference oscillators modulate two laser diodes (f_1=1 KHz, f_2=1.5 KHz) with λ_1=405 nm and λ_2=532 nm, respectively, which excite fluorescein and rhodamine-6G florescent dyes. As a result, the complex PMT signal contains two frequency channels representing the fluorescence excited by λ_1 and λ_2, respectively. To extract the two channels, we utilize two lock-in amplifiers which are referenced to the oscillator electrical signals f_1 and f_2. Such a phase sensitive approach reduces electrical noise by several orders of magnitude. The system components consists of a single PMT and inexpensive microelectronic chips (i.e., two lock in amplifiers [48] and two oscillators), which is more compact and less expensive than the conventional system.

The blue and green lasers are combined externally and passed to fluorescence port of an inverted microscope. A high pass dichroic mirror and a triple band-stop filter (Figure 43), installed in the filter cube, were used to excite the dyes and remove the excitation wavelengths, respectively. Fluorescence signals from both dyes were detected using a single PMT. The PMT current signal was converted to a voltage by a high speed,

low noise transimpedance amplifier with 100 kΩ feedback resistances (OPA380, Texas Instruments). The signal contains multiplexed frequency harmonics of the two excited fluorophores. These are then demodulated by phase-sensitive detection using two LIAs and two electronic low pass filters. The LIAs were referenced to the same signals driving the lasers. This phase sensitive approach can increase S/N ratio by up to 100dB [66].

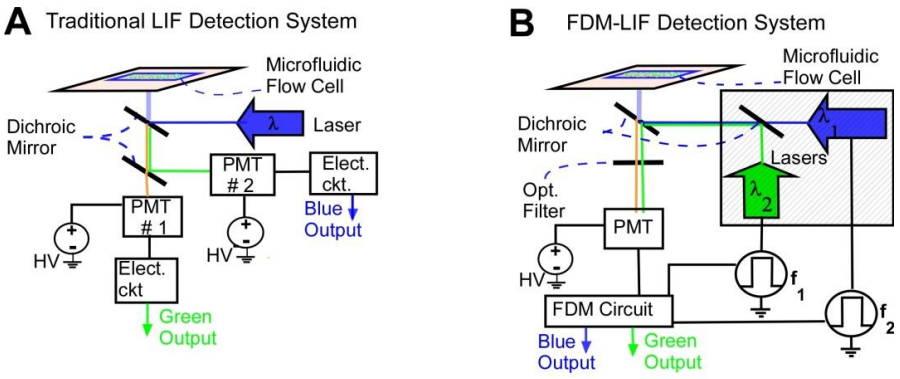

Figure 42: Comparison between A) a conventional LIF detection system and B) the FDM-LIF detection system. The conventional system requires two PMTs, two high voltage power supplies, and corresponding optical components. It uses one excitation source. The FDM system requires only one PMT, one high voltage power supply, and one optical filter set. It uses two laser diode excitation sources. This approach has lower cost because PMTs are typically the most expensive and bulky part of the detection system. This system distinguishes fluorophores based on their excitation spectra.

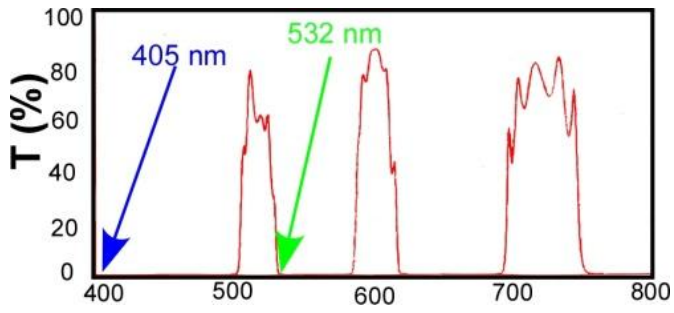

Figure 43*: Spectrum of the triple band pass band filter. We used blue laser (λ=403 nm) and green laser (λ=532 nm) for excitation. The emitted fluorescence is in the 500-520 nm range for fluorescein and 580-610 nm for rhodamine-6G.*

5.1.2 Results and Discussion

Figures 35A-35B show alternating aqueous droplets of fluorescein and rhodamine-6G which were generated in a microfluidic tertiary junction with oleic acid as the carrier fluid at a rate of one drop per second. Figure 44A shows the generation of the fluorescein droplet while Figure 44B shows a subsequent rhodamine-6G droplet. Rhodamine-6G is known to associate with fatty acids, and it leaches into the carrier fluid.

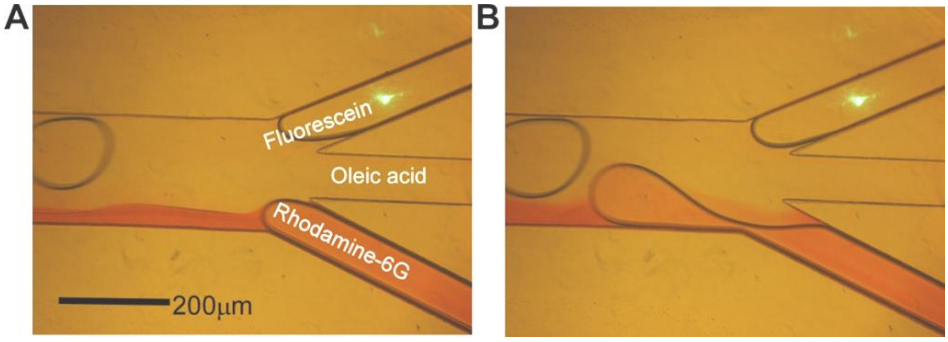

Figure 44: Alternating droplets between A) fluorescein and B) rhodamine-6G that were generated in a microfluidic tertiary junction with oleic acid as the carrier fluid. The photos show the rhodamine-6G dissolves in the carrier fluid.

The FDM-LIF system was used to detect and distinguish the alternating droplets shown in Figures 46A-45C. The two laser detection spots are slightly offset to qualitatively show how fluorescence emission changes with time. The photos qualitatively show the relative florescence emission of rhodamine-6G, oleic acid, and fluorescein, respectively.

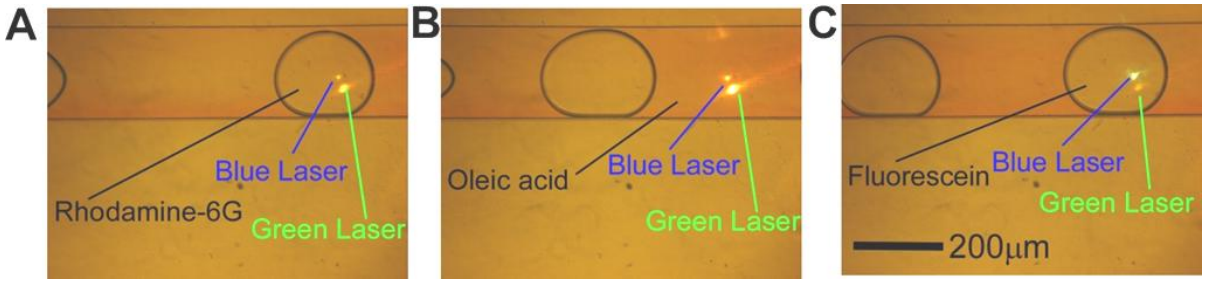

Figure 45: Florescence emission of the droplets of: A) Rhodamine-6G. B) Oleic acid. C) Fluorescein. The dissolved rhodamine-6G in the oleic acid causes the green laser to excite the carrier fluid.

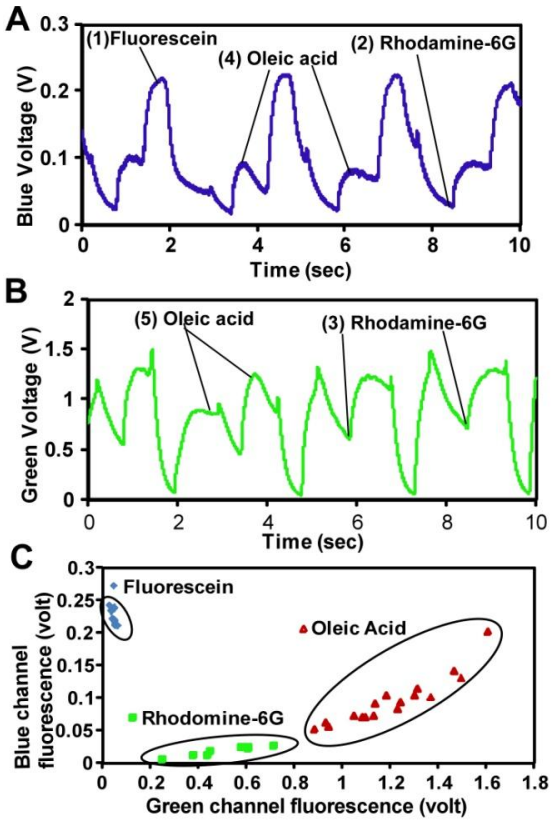

Figure 46: (A-B) multiple fluorescence output signals detected using the FDM-LIF system. (1) Fluorescein emission due to blue laser excitation; (2&3) Rhodamine-6G emission due to blue and green laser excitations, respectively. Since the rhodomine-6G leaches into oleic acid, the oleic acid emission appears stronger than the rhodomine-6G droplet (4&5) oleic oil emission due to blue and green lasers excitations, respectively. (A) Blue channel. (B) Green channel. (C) Scatter plot showing 3 distinct clusters measured using the FDM-LIF system. The blue cluster is fluorescein; the green cluster is rhodamine-6G, and the red cluster is the oleic acid.

Figure 46 demonstrates the crosstalk-free fluorescence signals in both channels after demodulation. A total of 5 distinct fluorescence levels are observed in the two channels. Droplets of fluorescein, known to excite in the blue wavelengths, show a high fluorescence in the blue channel and very little fluorescence in the green channel. In contrast, rhodamine-6G exhibits large fluorescence in the green channel, but little in the blue channel. The oleic acid carrier fluid, which contains rhodamine-6G, shows a high degree of fluorescence in the green channel, and also some in the blue channel (due to auto-fluorescence). In addition, the fluorescence varies between plugs because of diffusive effects. Nonetheless, the three components can be distinguished by plotting the fluorescence from both channels on a scatter plot (Figure 46C). Three clusters can be seen: the blue cluster represents the fluorescein droplets, the green cluster represents the rhodamine-6G droplets, and the red cluster represents the segments of oleic acid carrier. Note that the oleic acid and rhodamine-6G droplet clusters are close to one another because they both contain rhodamine-6G. This can be avoided in the future by using a dye which does not partition to the carrier fluid. However, this scatter demonstrates the ability of the FDM-LIF detection system to distinguishing unique samples. Due to the low cost of the system and its electronics, we believe it can be extended to additional fluorophores. The motivation for this was indicated earlier: a system with n fluorophores can detect up to 2^n unique populations.

5.2 A 40 MHz Frequency Multiplexed Electronic System for Multicolor Droplet Flow Cytometry

In the previous section, low frequency and low speed FDM-LIF system was implemented and tested. Although it shows the ability of the FDM technique to distinguish electronically between two alternating droplets, it lacks the measurement bandwidth required for high speed cytometers (~200,000 cell/sec) due to its low modulation frequencies. To overcome this limitation, we developed a new circuit topology which improves the measurement bandwidth by >30,000X, enabling multicolor detection at 200,000 cells/sec as needed for flow cytometry.

5.2.1 System Concept and Experimental Setup

The schematic diagram shown in Figure 47 consists of three-stage circuit that modulates three excitation small size laser diodes (450/520/680nm) at unique carrier frequencies: 25MHz, 32MHz, and 40MHz. The lasers are combined and directed into the fluorescence port of an inverted epi-fluorescence microscope, using a three color optical combiner shown in Figure 48, and focused into the sample by a 40X objective. Consequently, each fluorophore in the detection window is modulated at a unique frequency.

The fluorescence emissions pass through a multi-band-stop emission filter which removes the excitation signals (Figure 49), and are then detected by a single PMT. The PMT signal, containing all three fluorescence channels, is de-multiplexed using a heterodyne demodulator circuit which emulates a multi-channel lock-in detector. The demodulator consists of a 500 MHz four-quadrant analog multiplier, model AD834

(Analog Devices), and a low pass filter. The details of the control circuit operation are presented in section 3.2.

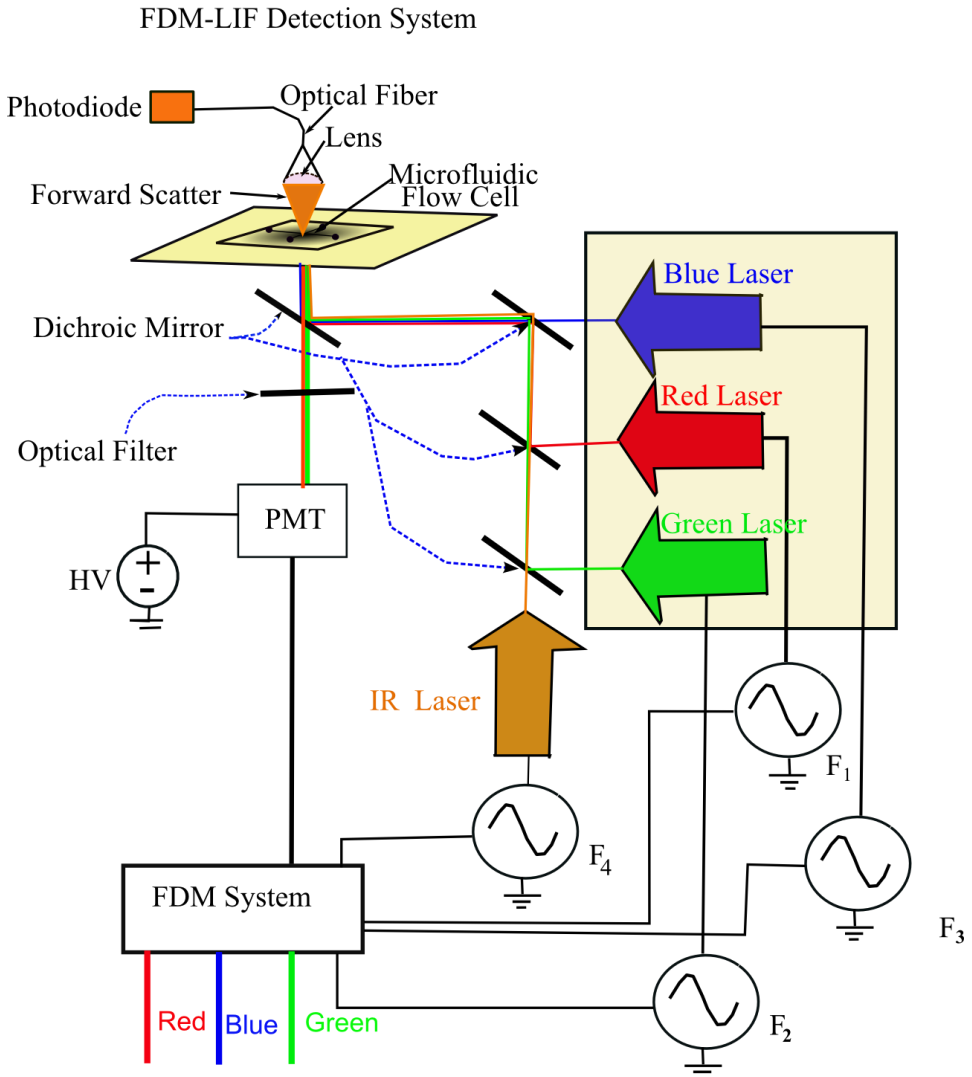

Figure 47: A Concept figure of the proposed FDM system. The system requires only one PMT with one high voltage power supply and one photodiode. Four lasers can modulated at four different frequencies. Three lasers are used for as excitation sources and the fourth is used to measure the forward scatter. Thus, optical components are minimized while still allowing multiple excitation sources.

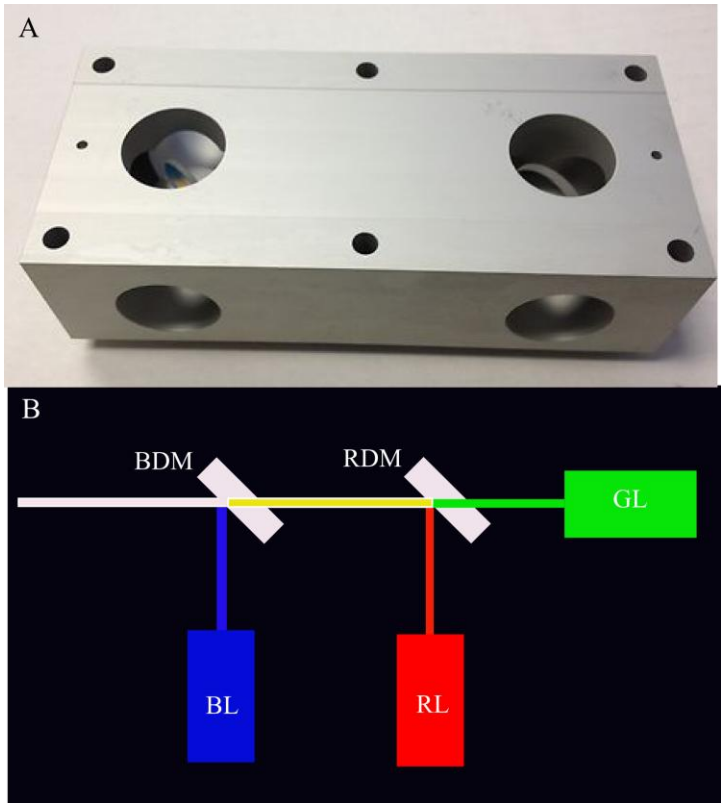

Figure 48: A) Three laser beam combiner B) Operation principle of the beam combine. Red and blue dichroic mirrors are installed at 45^{o}angle inside aluminum frame.

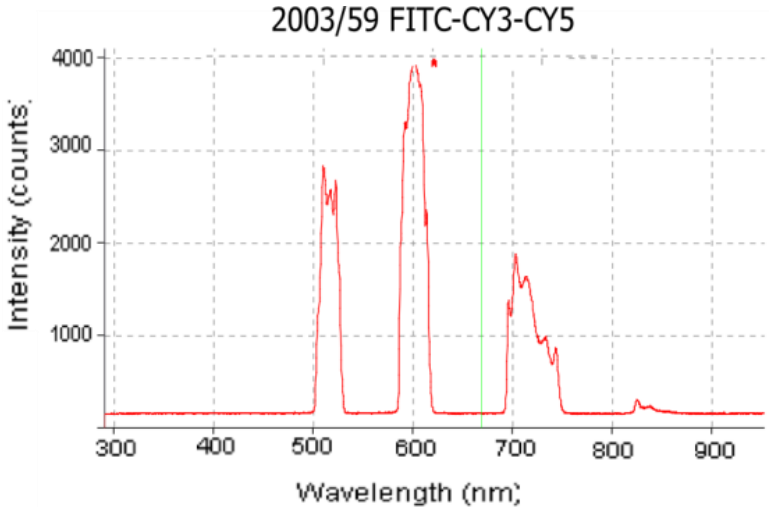

Figure 49: Spectrum of the multi-band stop filter used to remove the excitation signals. Our experiments used the blue (λ=450 nm) red (λ=680 nm) lasers for excitation.

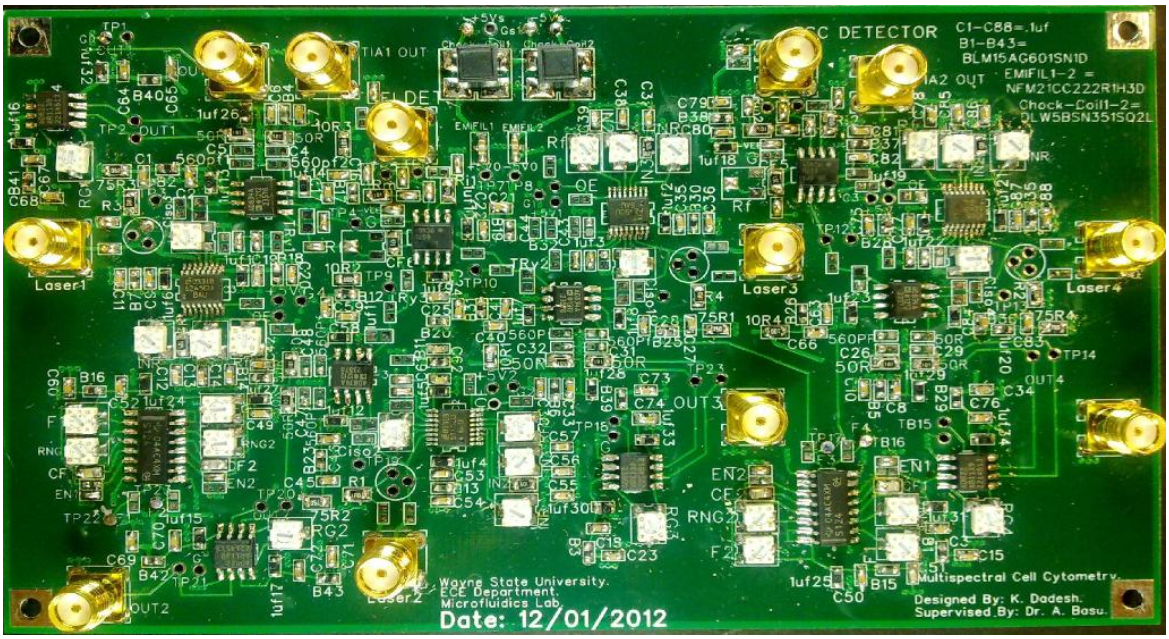

Figure 50: PCB layout for the FDM system. All components are surface mount technology (SMT). Four laser drivers, model EL6245 (Elantec), with up to 500 MHz sinusoidal oscillators onboard are used to modulate laser diode currents. They can be driven using four external square wave voltage controlled oscillators, SN74S124D. Two low noise amplifiers with 1.6 GHz gain-bandwidth product are used to amplify the detected multiplexed high frequency light signals. Four 500 MHz analogue multiplier, AD834 (Analog Devices), and four low pass filters are used as heterodyne demodulators for each channel. Four instrumentation amplifiers, AD622 (Analog-Devices), are used to amplify the four DC differential outputs. Input and output signals can be accessed via SMA connectors. Variable SMT resistors are used to adjust modulation frequencies and amplitudes.

The PMT signal is amplified using the NIA circuit stage that has the frequency response sown in Figure 42, and then down-converted using three analog multipliers referenced to the three respective oscillators driving the laser diodes. The three multiplier outputs are then low-pass filtered with a 5 µsec time constant to remove any crosstalk from the other channels. The three outputs represent the 3 fluorescence channels. A fourth channel is implemented to measure forward scatter signals.

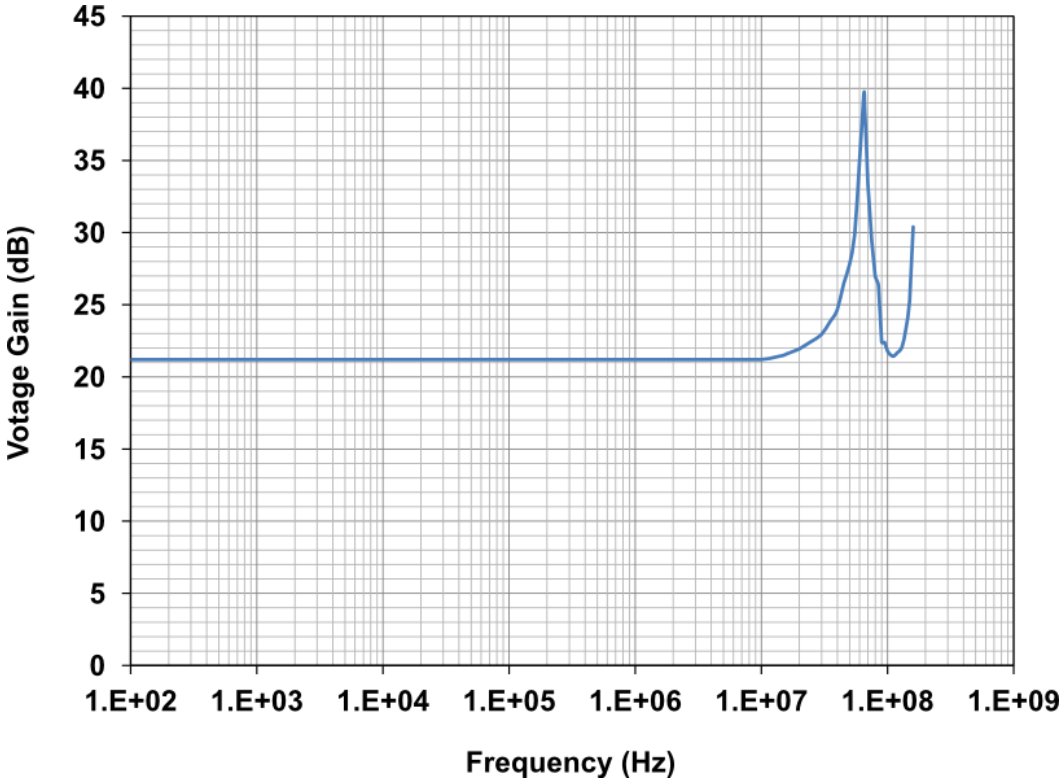

Figure 51: Frequency response of the NIA circuit stage. The high Q of the amplifier can be controlled by changing external resistor values.

5.2.2 Results and Discussion

5.2.2.1 Distinguishing Alternating Droplets

To demonstrate high-speed detection of droplets, two of the three channels (450@25 MHz and 680nm @ 40 MHz) are successfully used to discriminate alternating droplets containing two different fluorophores: Fluorescein and Alexa 680. Figure 50 shows a picture for the developed PCB. The droplets are generated by an alternating drop generator which is currently limited to 300 drops/sec (Figure 52).

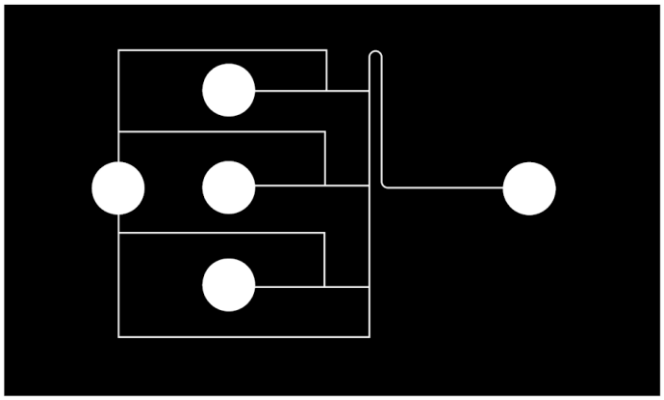

Figure 52: Schematic of alternating drop generator which can operate up to 300 drops/s.

Figure 53 shows the output of the two frequency channels, demonstrating that our FDM system is capable of electronically distinguishing between the two droplet populations flowing at 300 drops/sec. Figure 54 is a scatter for the plotted data of Figure 53 that shows the two populations, one containing fluorescein and the other Alexa 680.

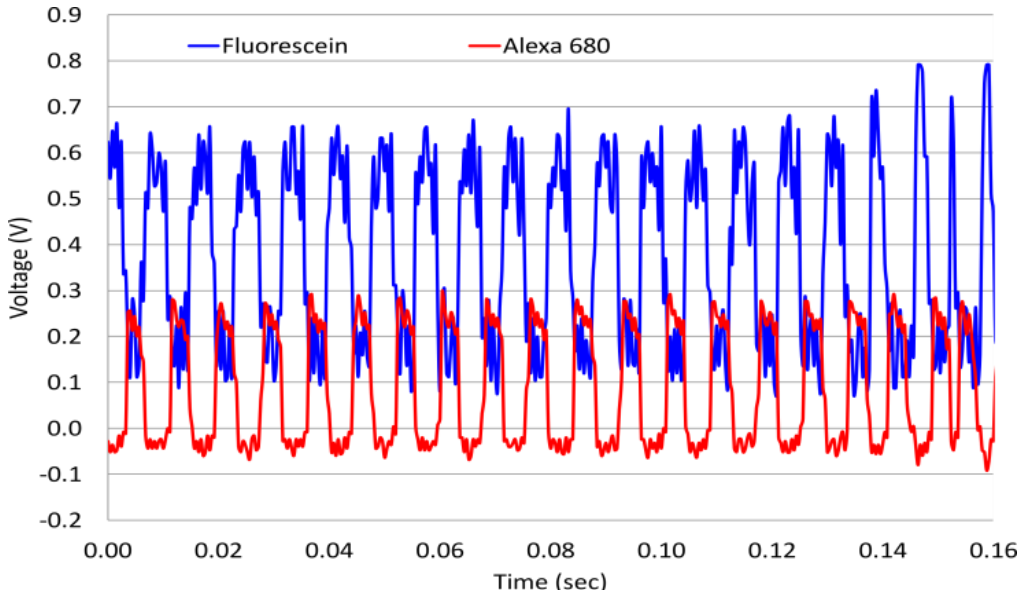

Figure 53: Detection of alternating droplets of Fluorescein and Alexa 680 at a rate of 300 drops/sec. The drop generation rate is limited by the microfluidic chip design.

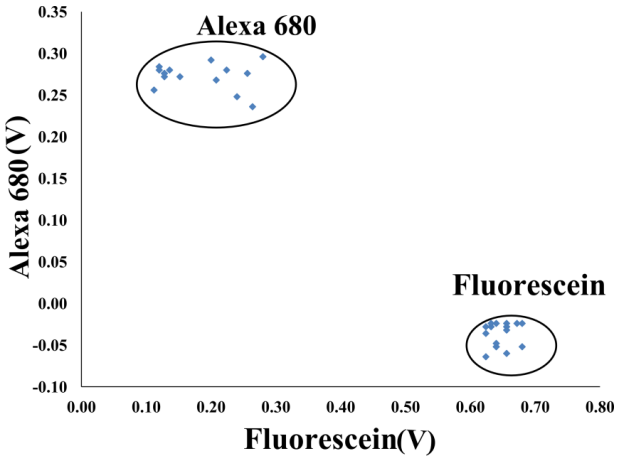

Figure 54: A scatter graph of the plotted data in Figure 53 showing two distinct populations of Alexa 680 and Fluorescein.

5.2.2.2 Detection Speed Limit

To demonstrate higher speed detection, we used a second ultra-high speed generator which generates single droplets at 2,800 drops/s (Figure 55). These drops can also be readily detected by our FDM system as shown in Figure 56, which demonstrates a crosstalk free bandwidth of >200 KHz.

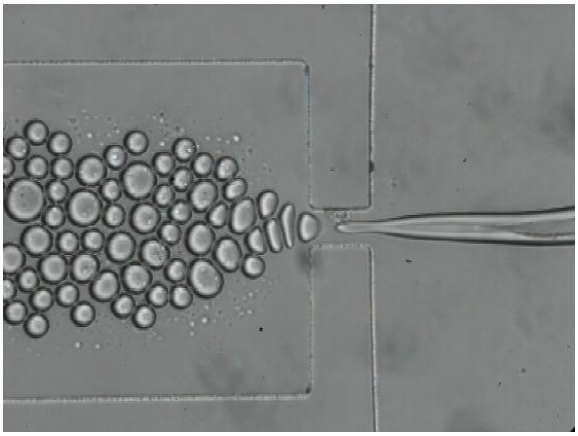

Figure 55: High-speed fluorescein droplet generator, operating at up to 2,800 drops/sec

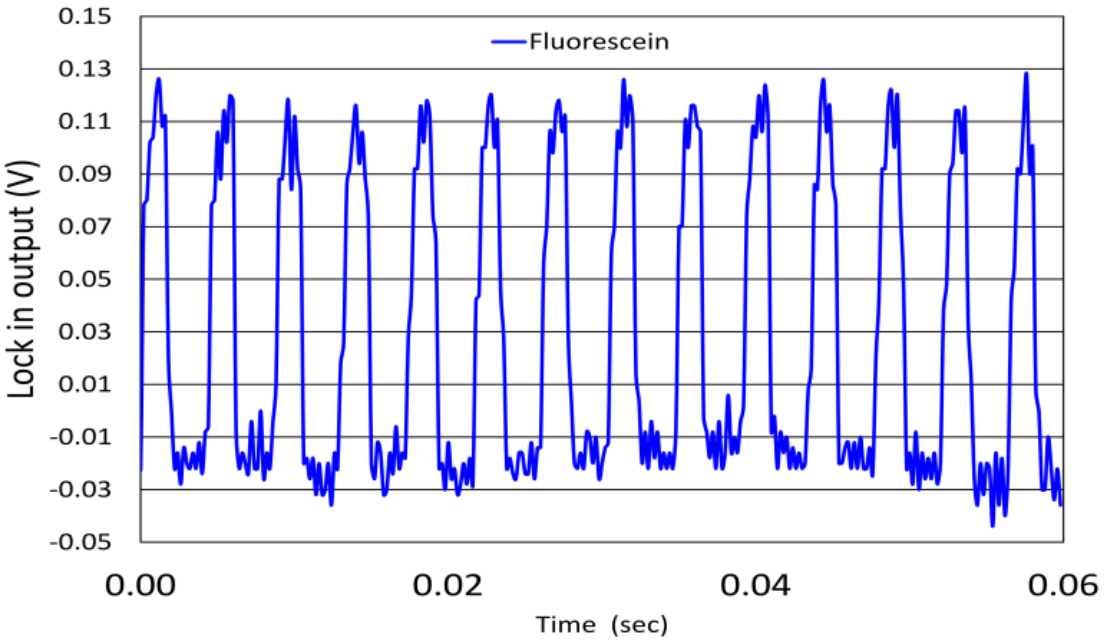

Figure 56: High speed detection (2,800 drops/sec) of Fluorescein generated by the high-speed drop generator suggested by Anna et al 2003 [35]*. It is expected that our FDM system can work even one order of magnitude higher due to the 15MHz frequency separation between channels.*

5.2.2.3 Limit of Detection (LOD), Sensitivity and Cross talk

The limit of detection (LOD) was found by testing a serial dilution beginning with 3 mM fluorescein stock solution. The output voltage of the blue channel was measured versus molarity and the lowest detectable molarity was defined as that which generated a signal to noise ratio of 2. The results (Figure 48) show that the LOD of this channel is 30 nM. Similarly, for the red laser excitation channel, we used an Alexa 680 solution of 2 mM with subsequent serial dilutions. Figure 58 shows the measured results and indicates the LOD is 2 μM.

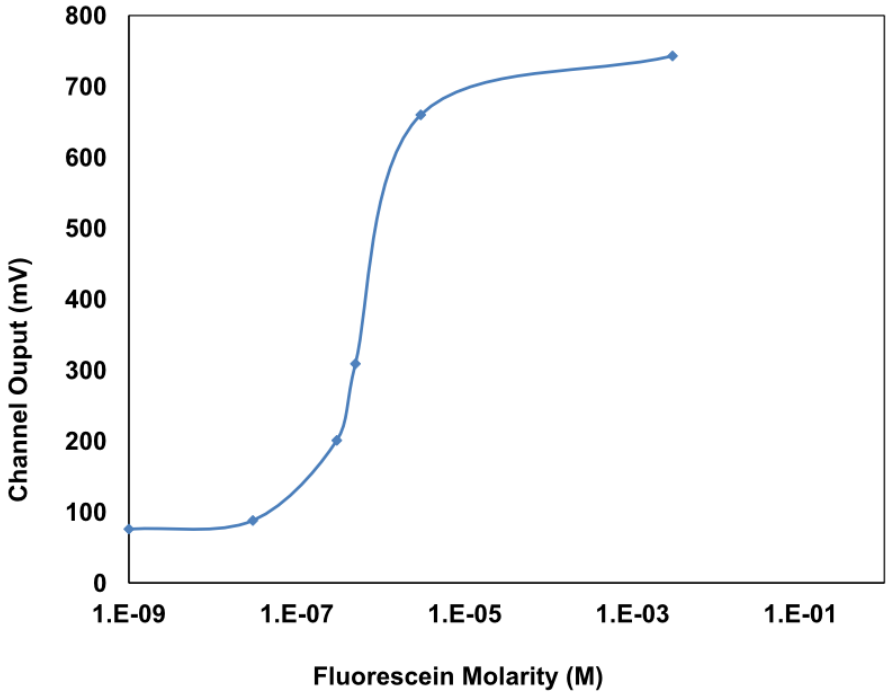

Figure 57: Fluorescein molarity verses blue laser channel output voltages of the FDM-LIF system.

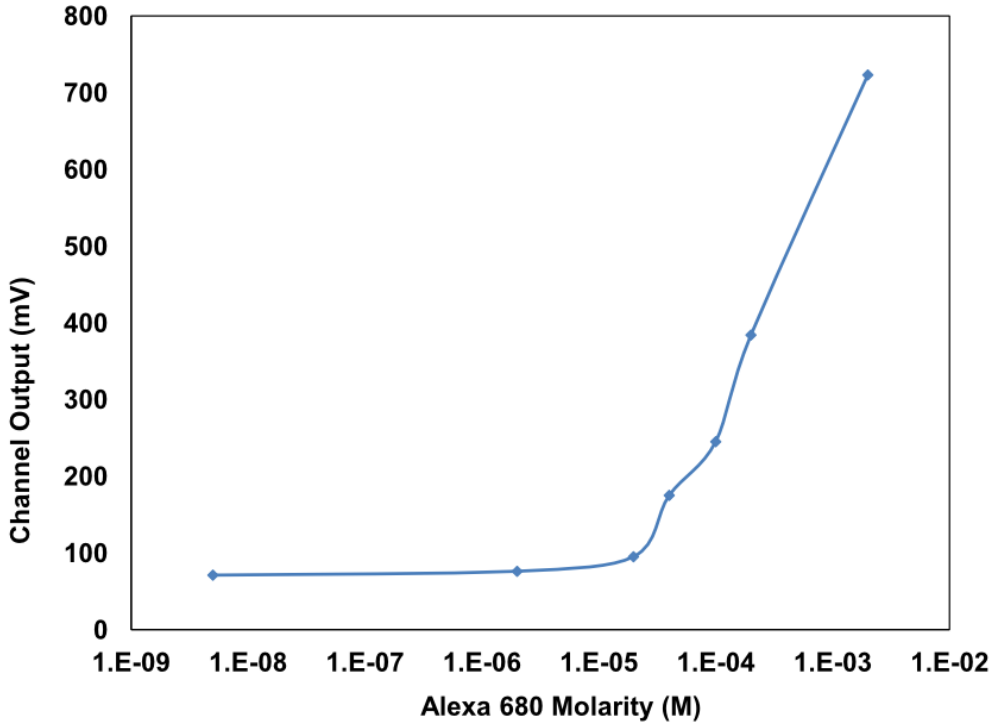

Figure 58: Alexa 680 molarity verses red laser channel output voltages of the FDM-LIF system.

Figure 59 shows a cross talk measurement between the blue laser channel and red laser channel for different molarities. The measurement reveals no cross talk between the two channels. However, Figure 60 reveals a cross talk between the two channels for different Alex 680 molarities. The cross talk is due that the Alexa 680 is weakly excitable by the 450 nm blue laser. Therefore, to overcome such excitation overlap, fluorophores with sharp excitation lines such as lanthanide ions are the best candidate material in use with FDM-LIF system. The optical properties of lanthanide ions such compound-independent emission spectra, large Stokes shift upon excitation make them useful in many industrial applications like optical fibres, computer displays, fluorescence satins for cell imaging…etc [67].

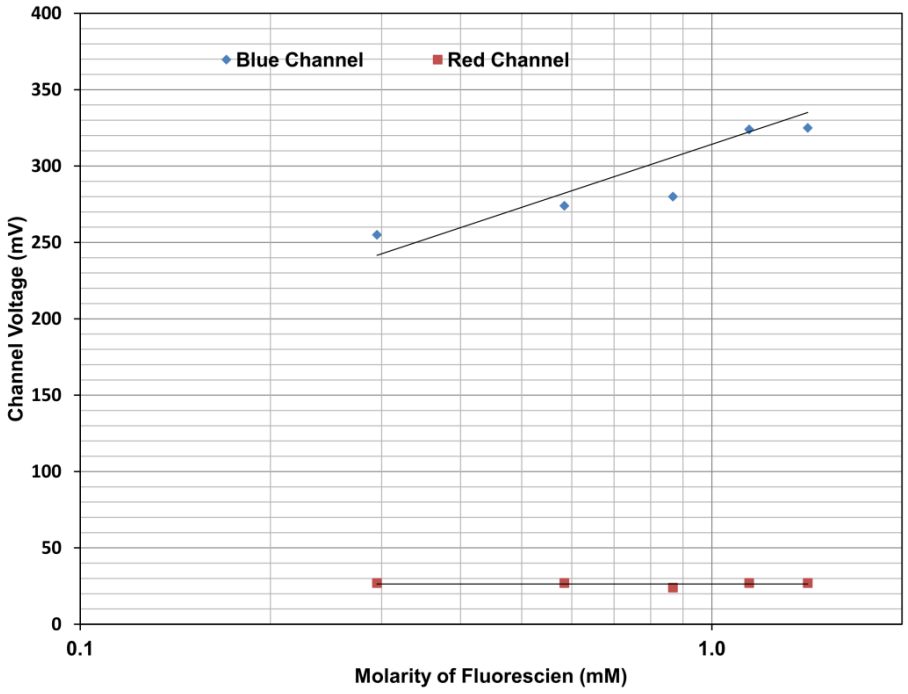

Figure 59: Cross talk measurement between blue and red laser channels at different Fluorescein molarities.

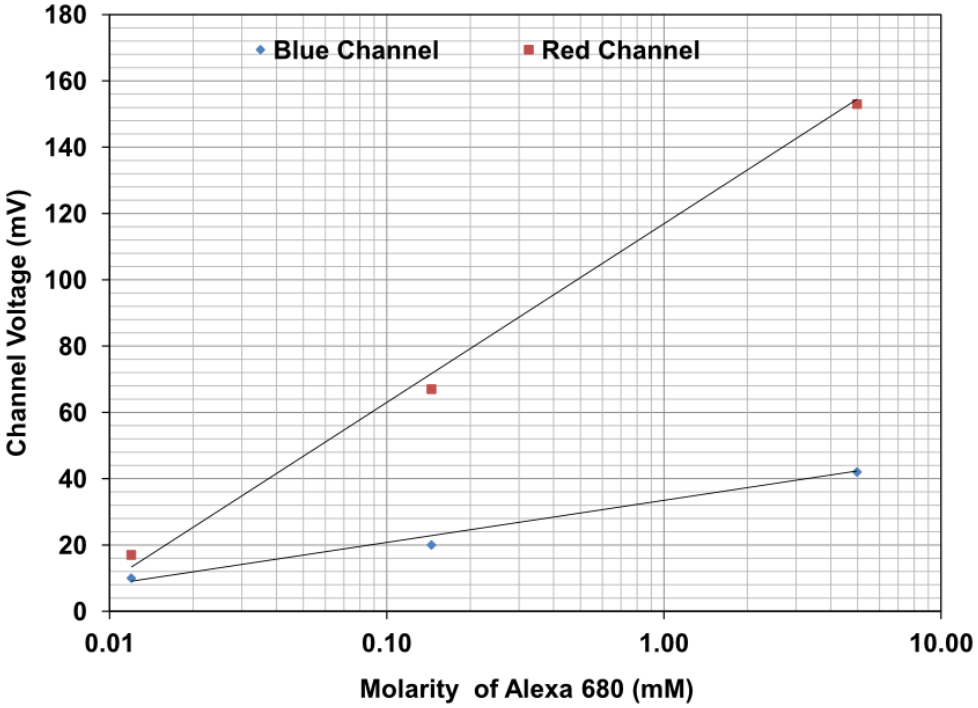

Figure 60: Cross talk measurement between blue and red laser channels at different Alexa 680 molarities. The graph reveals that Alexa 680 is excitable by blue 450 nm laser.

CHAPTER 6: APPLICATION TO CELL CYTOMETRY

6.1 Old Imunocytometry System

To demonstrate the use of the FDM-LIF detection system in a cell cytometry application, we installed the system in an old Becton Dickinson Imunocytometry System (model FACScan) shown in Figure 61. The FACScan had a defective laser light source shown in Figure 62, and was retrofitted for this project. It has four PMTs on board; three are for fluorescence lights detection, and the forth is for side scatter light detections as shown in Figure 63. It has also a PD for the forward scatter light detection as shown in Figure 64. It has a complete fluidic system with a hydrodynamic flow focusing cell as shown in Figure 65.

Figure 61: An old BD Immunocytometry system model FACScan. It has had a malfunctioning laser light source, and all other parts are completely functioning.

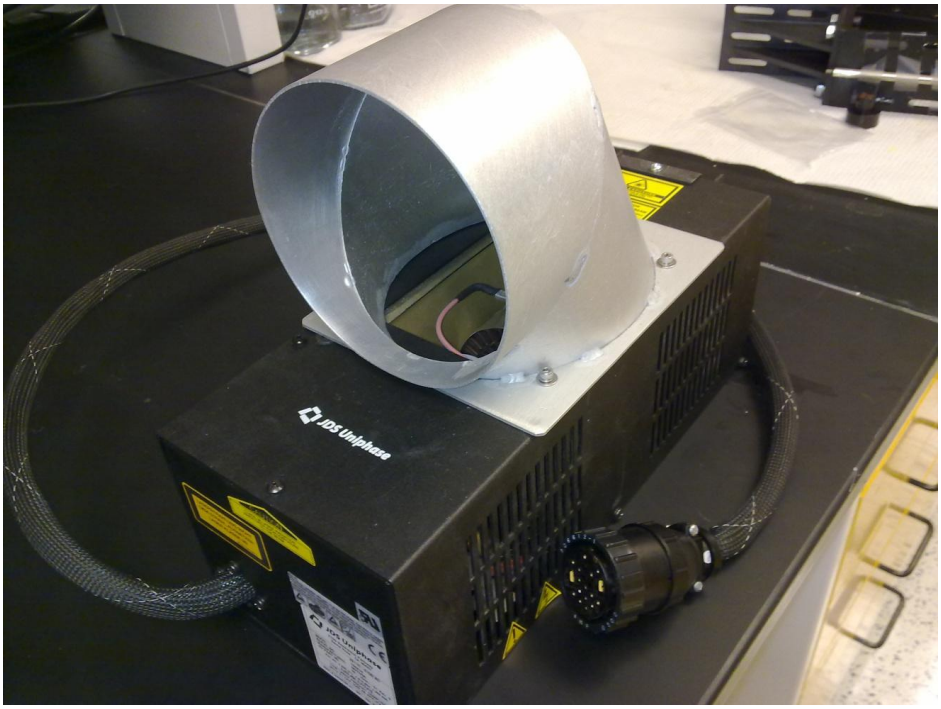

Figure 62: A defected laser light source originally installed in the BD cytometer. This laser has been removed, and our FDM-LIF system is installed instead.

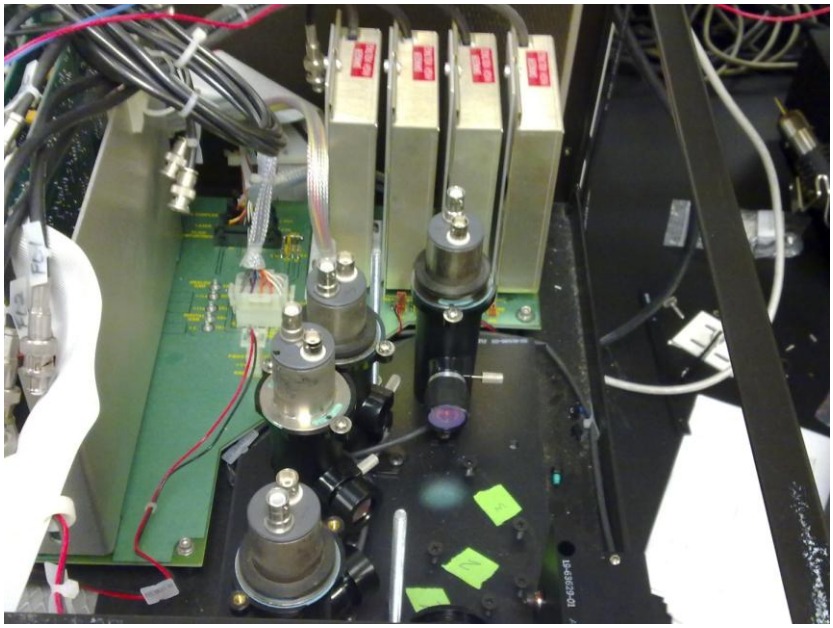

Figure 63: Four PMTs in the BD FACScan that will be replaced by one PMT using our FDM-LIF system.

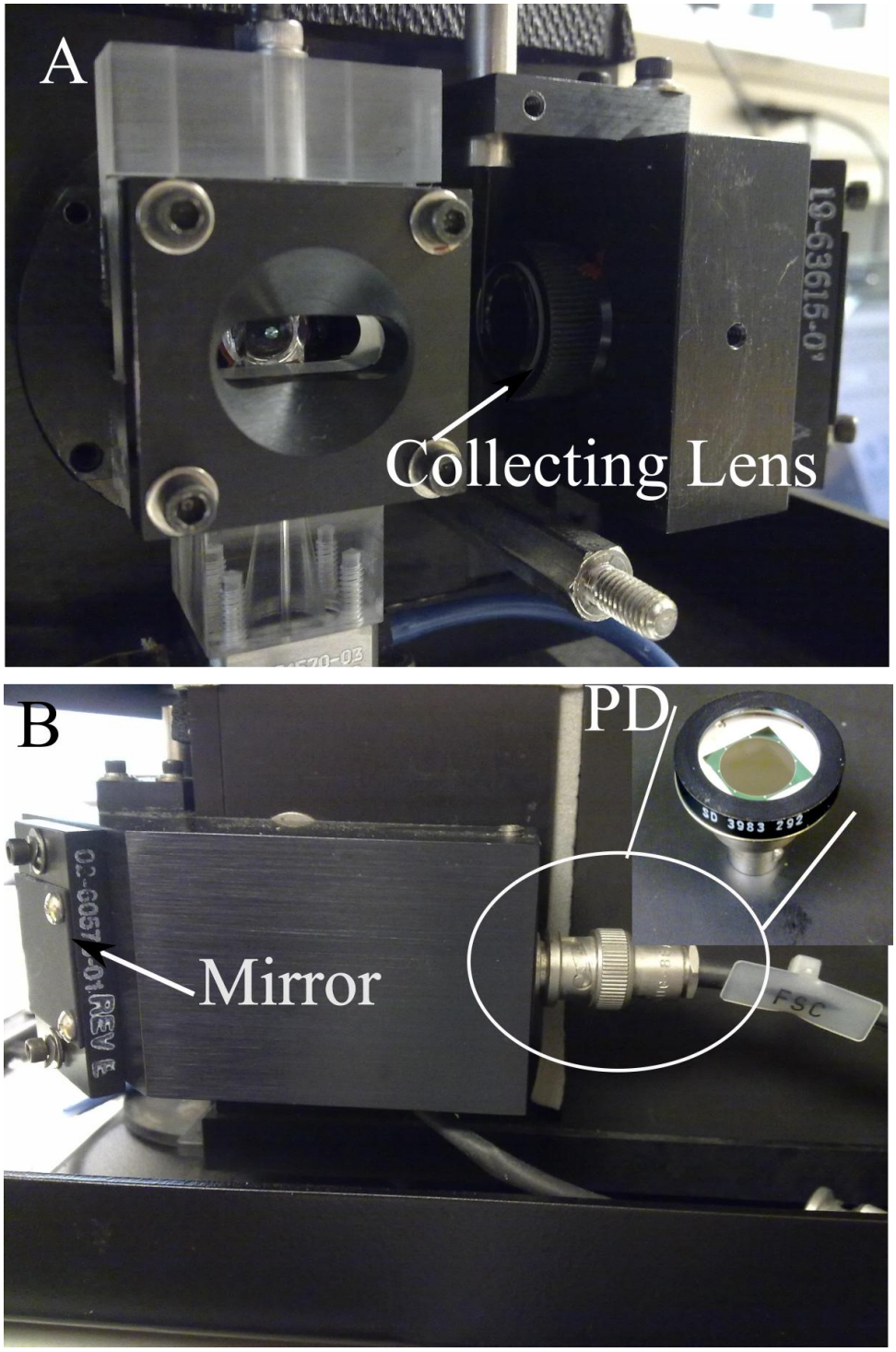

Figure 64: A PD in the BD FACScan that is used to detect the forward scatter light signals. Because it is a large PD, it cannot be used in our FDM-LIF system due to large capacitance.

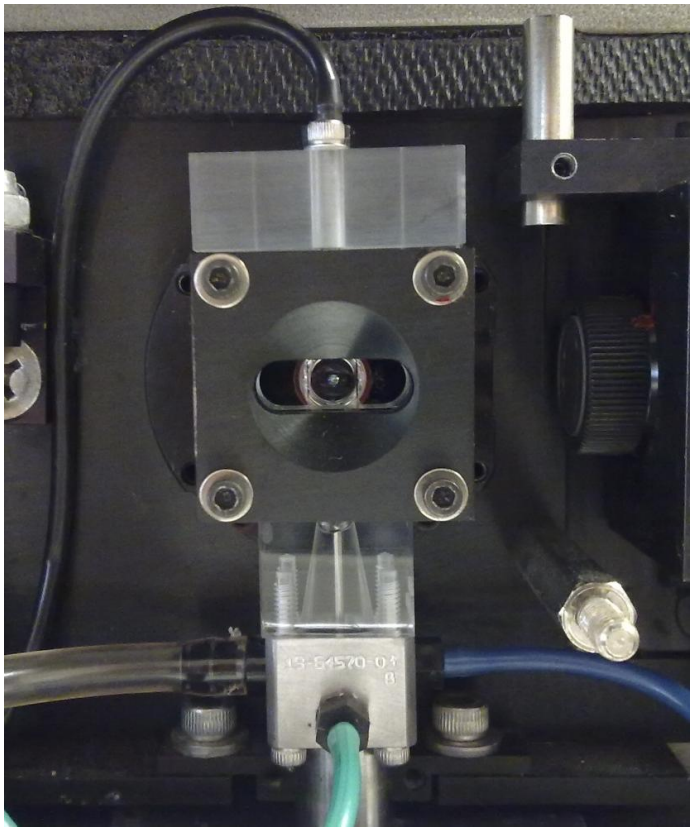

Figure 65: Hydrodynamic flow focusing cell used in the BD FACScan cytometer. It is a very important part in any cell cytometer. It focuses cells in a single file form to, individually; expose each cell to excitation light.

6.2 FDM-LIF System Installation in the Old Imunocytometry System

Figure 66 shows a schematic diagram of the optical setup for our beam combiner and the exciting optical setup in the cytometry instrument. Figure 67 shows a pictoral comparison between our FDM-LIF electronic system and the existing electronics of the Imunocytometry system. The comparison reveals that our electronic system is an order of magnitude smaller the Imunocytometry system (2000 cm^3 vs. 20000 cm^3). The main challenge in installing our system in the old BD cytometer is the positioning and alignment of the lasers. First, we use a Plexiglass sheet mounted on three adjustable

screws as an adjustable base. The three screws are used to adjust the level of the base in two directions. Figure 68 shows the leveling of the base. A triple beam combiner is mounted directly on the top of the base (Figure 69) at which we can adjust the position of the combined light beams at the center of the focusing lens.

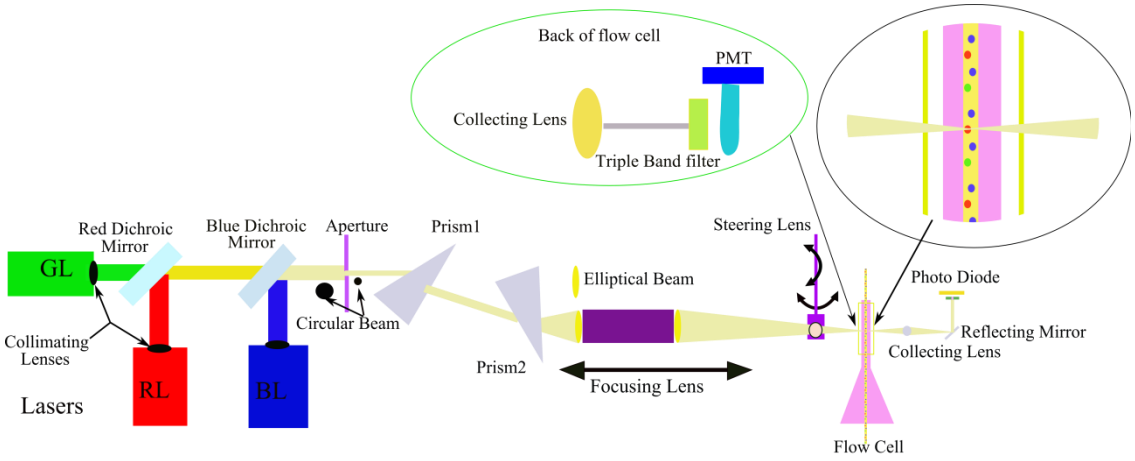

Figure 66: Optical setup including a laser combiner and the existing optical setup in the FACScan Imunocytometry instrument

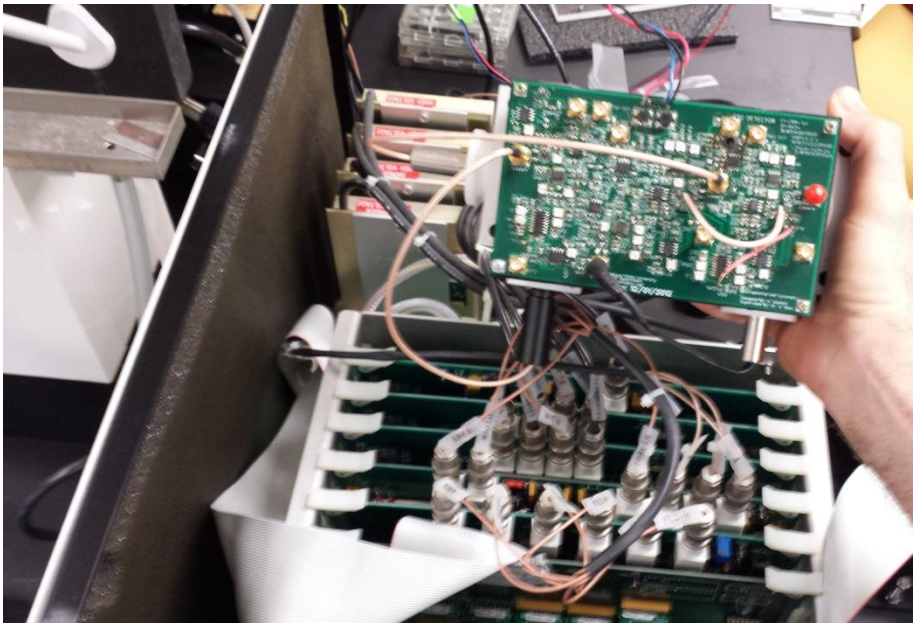

Figure 67: A picture comparison between our FDM-LIF electronic system and the exciting electronics of the Imunocytometry system.

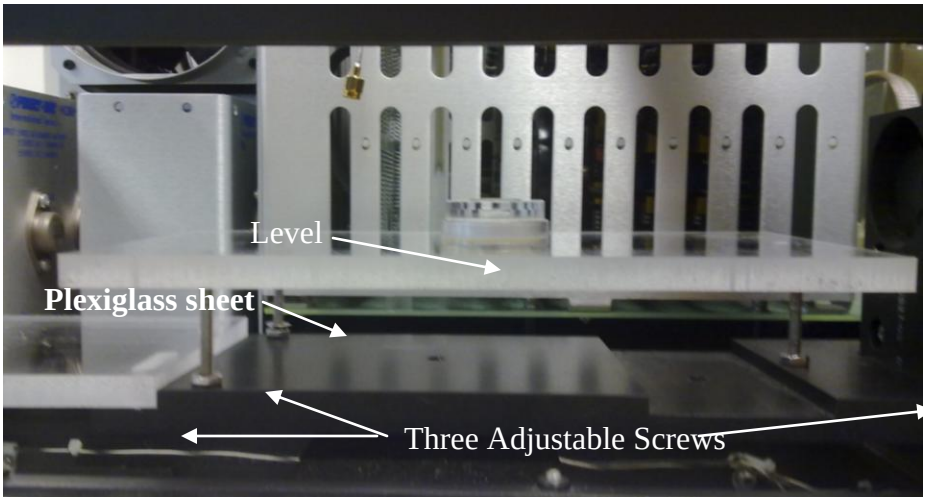

Figure 68: Plexiglass sheet mounted on three adjustable screws used base for lasers.

The combined light beam path passes thru two polarization prisms, focusing lens, and steering lens as shown in Figure 70. The two polarization prisms convert a circular beam to elliptical one. The focusing lens focuses the beam at target cells in the middle of a flow channel. The steering lens directs the focused beam at the right position inside the flow cell.

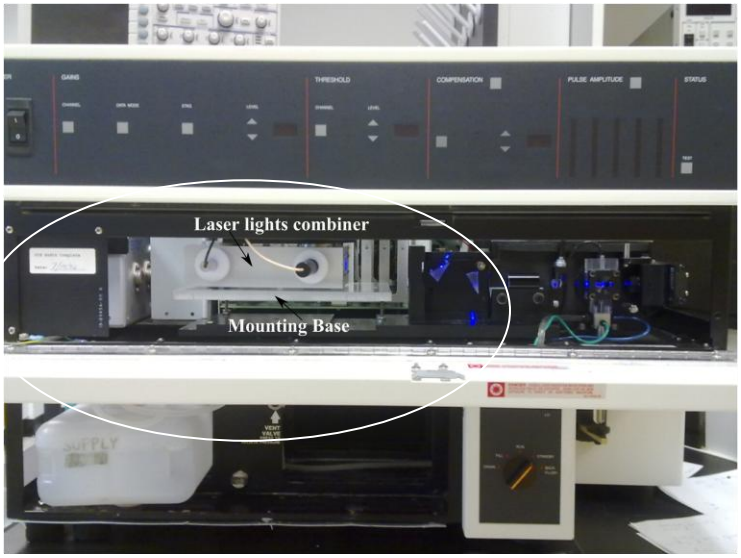

Figure 69: Laser lights combiner mounted on an adjustable base. Three laser lights can align collinearly.

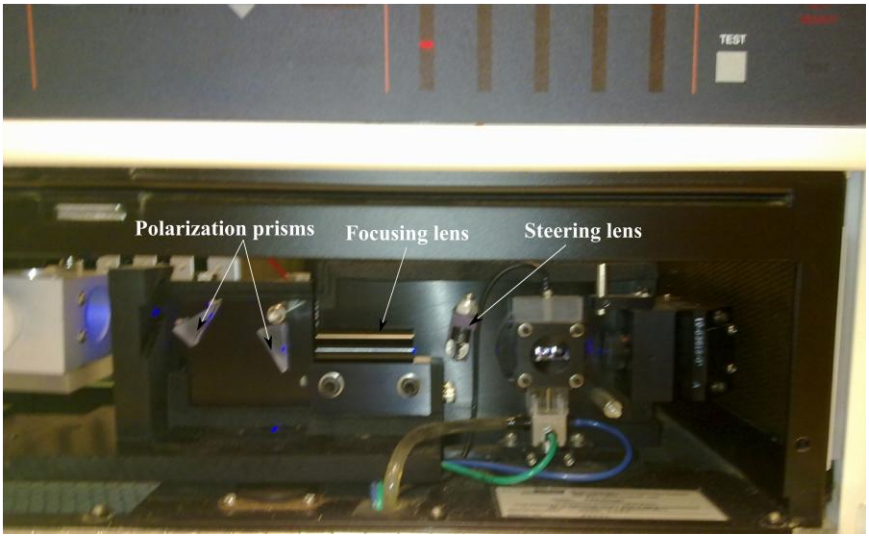

Figure 70: Combined light beam path through two polarization prisms, focusing lens, and steering lens.

In order to achieve a focused beam at the target cells flow, the combined beam has to be perfectly aligned to the centre of the focusing lens. For this purpose, we machined a setup of two parallel disks with fixed distance apart and a tiny hole in the middle of each (Figure 71). The setup replaces the focusing lens, and the combined beam is allowed to pass thru the two centre holes, which confirms the alignment of the beam at the centre of the focusing lens as shown in Figure 72.

Once the beam is aligned, the focusing and steering lenses must be adjusted. A fine screw is used to push the focusing lens to the left side against a spring which holds the lens still in place. The BD alignment microscope shown in Figure 73 is usually used to monitor the adjustment process of the beam intersection with flowing cells. Since we did not have access to this instrument, we performed the alignment manually. We passed large polymer microspheres (polydisperse) of 9.9 µm diameter in the flow cell, and by trial and error we adjust both focusing and steering lenses until we notice

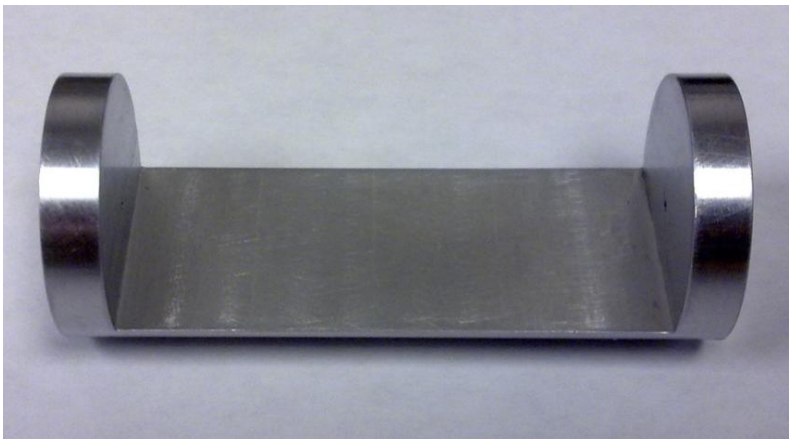

Figure 71: Two parallel disks are machined with a hole in the centre of each one to adjust the combined laser beam in the center of the focusing lens.

pulses proportional to the passing microspheres in forward and side scatter of a green laser (520 nm) light signals. This confirms that the focused beam intersects with the passing microspheres.

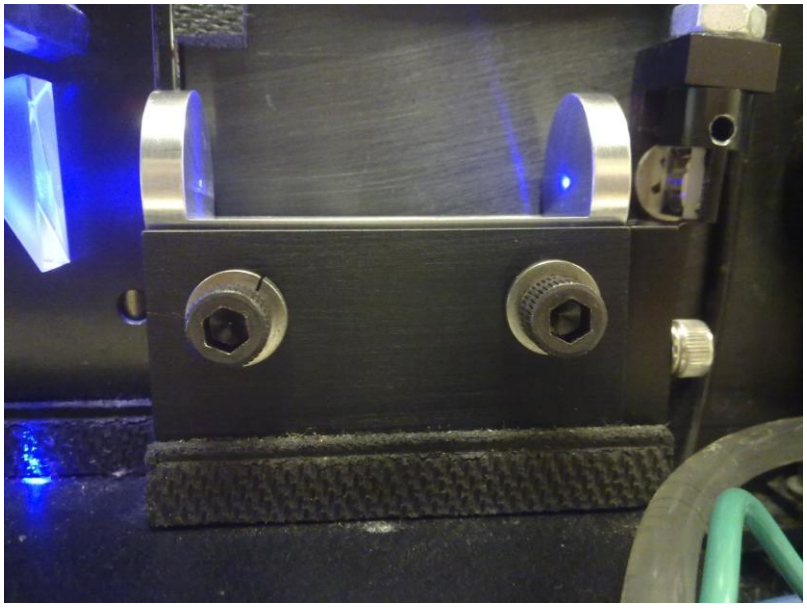

Figure 72: Placement of two disks in place of the focusing lens to align the combined beam in the centre of the focusing lens.

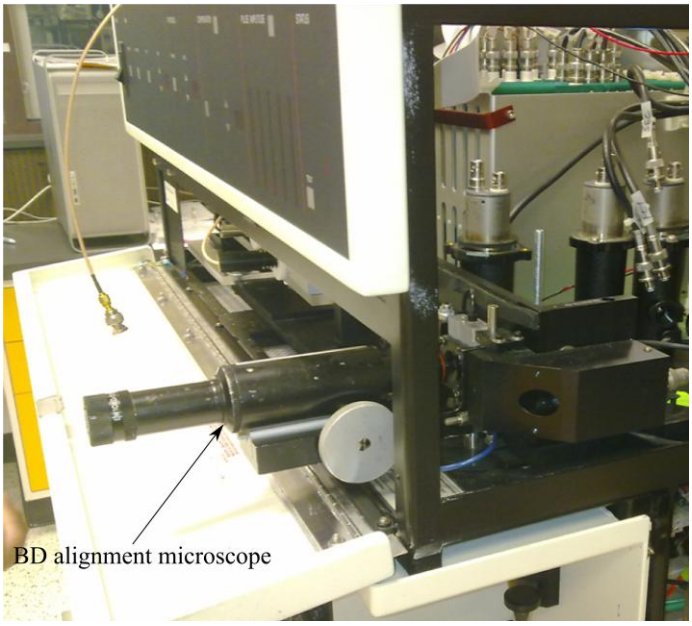

Figure 73: Alignment microscope mounted on a flow cell. It is used to help in monitoring the focusing process.

We note that the green laser is used to detect both the forward (FSC) and side scatter (SSC) signals. The SSC signal is detected using the same PMT used to detect fluorescence signals; however the FSC must be detected using a separate avalanche photodetector (APD). The green laser has 520 nm wavelength, and the laser diode is modulated with a 16 MHz sinusoidal wave. This wave is used as a reference signal in two separate heterodyne demodulators, one each for the FSC and SSC signals. The forward scatter signal is detected using a non-inverting amplifier stage that uses the OPA657 (Texas Instruments) operational amplifier. A plastic 1 mm fiber optic is used to direct the forward scattered light towards an APD as shown in Figure 74. The side scatter light signal is detected using the same PMT that we use to detect fluorescence signals. The PMT with a triple band filter is shown in Figure 75. The triple band filter that has the

spectral response shown in Figure 49 passes the green (520 nm) light and blocks other excitation wavelengths.

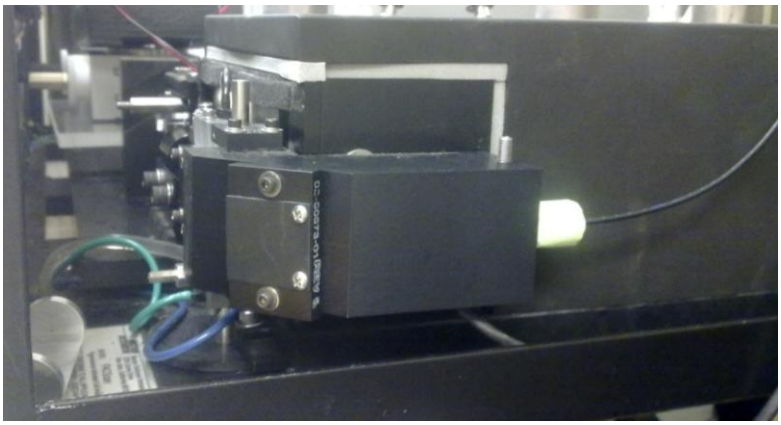

Figure 74: 1 mm plastic fiber optic is used to direct the forward light scatter to a PD.

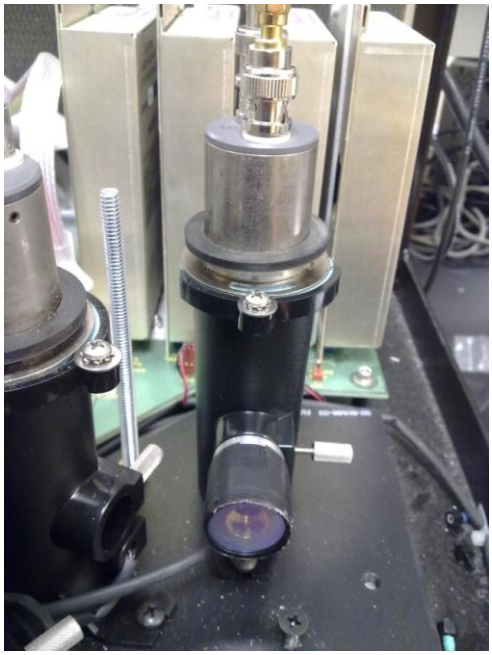

Figure 75: A PMT and triple band filter setup used to detect fluorescence and side scatter signals. The spectral response of the triple band filter is shown in Figure 49. The PMT is made by Hamamatsu Company, model R928. The spectral response of the PMT is shown in Figure 2.

6.3 Experimental Results

The next step after installing the LIF-FDM system and aligning the lasers is to test the alignment with microspheres of 9.9 μm diameter. The green laser is dedicated for forward and side scatter measurements. By passing the microspheres, adjusting both the focusing lens on the cytometer and the collimating lens in the laser module is possible to measure both forward and side scatter signals as shown in Figure 76.

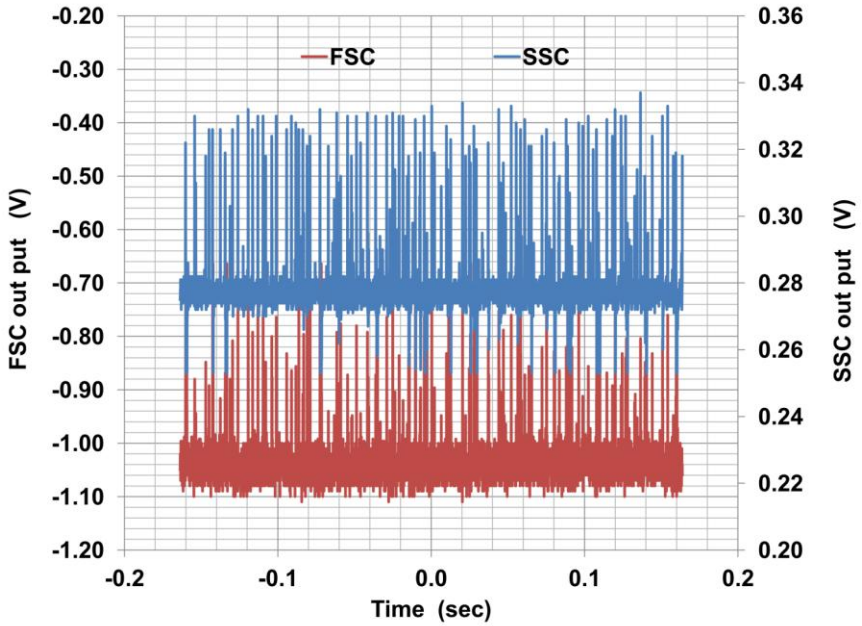

Figure 76: Forward and side scatter signals when microspheres of 9.9 μm diameters are passing in the FACScan Imunocytometry system with the LIF-FDM system.

To test fluorescence signals, a solution containing 1 mM fluorescein is passed in the system. Figure 77 shows the output amplified fluorescence signal detected by the PMT. It also shows the FFT of the output signal at which we see a peak at the excitation modulation frequency (25 MHz) and another noise peak corresponding to the peak at

about 65 MHz in the amplifier frequency response shown in Figure 51. Because the fluorescein solution is filling the whole flow channel, sharp focusing is not critical.

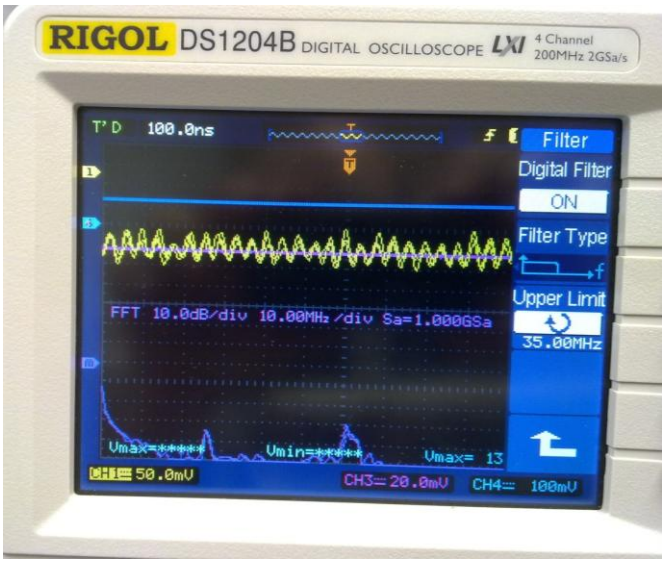

Figure 77: Fluorescence signal detected with the PMT when fluorescein solution is passed thru the flow cell.

In order to test the system with microspheres, two fluorescent beads are prepared. The first one is BD™ CompBead Anti-Mouse Ig,k attached to Alexa Fluor® 680 Goat Anti-Mouse IgG (H+L), and the second one is BD™ CompBead Anti-Mouse Ig,k attached to Alexa Fluor® 430 Goat Anti-Mouse IgG (H+L). The first assay is excited with a red laser diode (680 nm) and the second one is excited with a blue laser diode (450). The excitation-emission spectra of these two assays are shown in Figure 78. Negative microspheres are added to gate other channels using the FSC and SCC signals. As shown in Figure 79 the green light is sharply focused to hit the microspheres, and so the FSC and SSC signal are measurable. However, due to static nature of the laser light combiner, it is not possible to align the blue and red lasers, and no fluorescence was detected. To

overcome this issue, a dynamic optical combiner, where each laser can be adjusted independently, must be used. We leave this issue to future work.

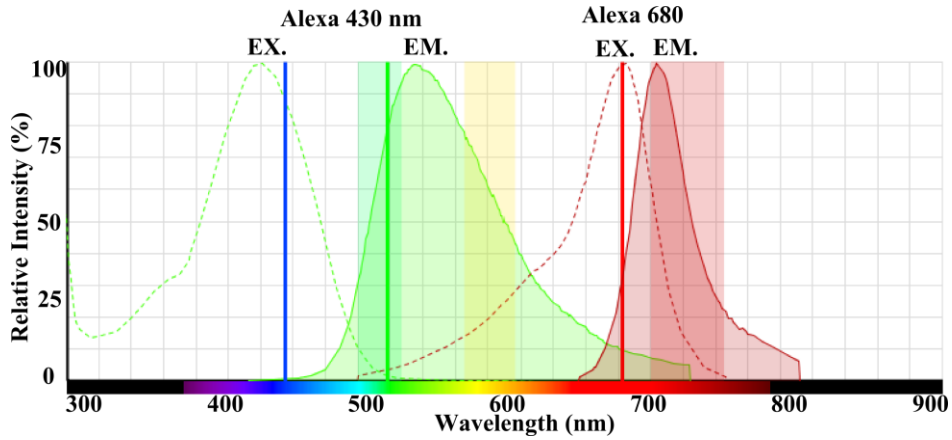

Figure 78: Excitation and emission spectra of the fluorescence test assay. Three lasers are used, so the 450 nm and the 680 nm lasers are used to excite the Alexa 430 and Alexa 680, respectively, and the 520 nm laser is used to measure the forward and side scatter signals. A triple band emission filter is used to eliminate the two excitation lasers and allow the green laser to collect the side scatter light.

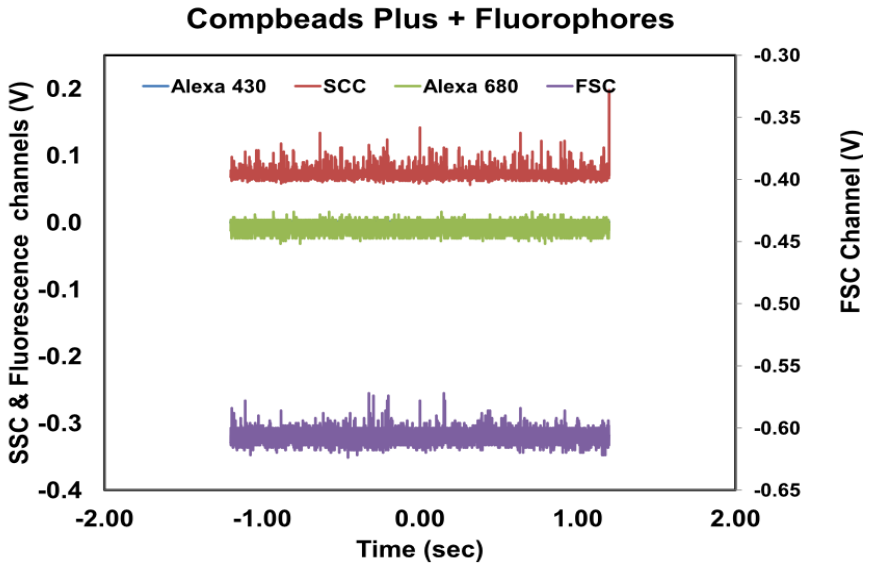

Figure 79: Side scattered light signals when microspheres of 9.9 µm diameter are passing.

CHAPTER 7: CONCLUSIONS

When used with monochromatic LED or LD-based light sources, FDM can provide multi-spectral measurement in a single optical window by replacing optical filtering components with an electronic filtering technique. Using the FDM technique with high modulation frequencies enables high-speed multispectral photometry of liquid samples, discrete droplet microreactors, as well as cells in sheath flow. It can also be used with high-speed multispectral fluorimetry for cell cytometry applications. This can potentially provide several benefits in point of care systems: 1) *Scalability*: Additional channels can be added economically, and LEDs and LD with a wide spectral range (200-2000nm) are commercially available. 2) *Low cost*: The system requires only a single light detector and interrogation window, and it is based on low-cost optoelectronics components. It is also simple, compact and consumes low power (<2W). 3) *Sensitivity*: Lock-in detection inherently reduces measurement noise up to 100dB, potentially enabling nanomolar sensitivity [37].

The FDM technique is tested in both absorbance photometry and fluorimetry applications and found to be feasible in reducing system complexity and cost. In absorbance photometry we were able to multiplex three LED lights with frequencies as high as 250 KHz of square wave modulation signals. Our prototype is able to simultaneously discriminate between three different analytes. Using a triangle diagram, we were able to see three different clusters.

The FDM-LIF technique presented here enables us to perform multiplexed LIF detection using a single PMT and multiple excitation lasers instead of multiple PMTs and

one excitation laser. PMT's are typically the most expensive and bulky components in a multicolour detection system; therefore, this approach can reduce the size and cost of multicolor systems. When tested with microdroplet flows, the FDM-LIF detector was able to discriminate three different clusters; one cluster represents fluorescein, the second is for rhodamine-6G, and the third is the carrier fluid. Since it distinguishes samples based on excitation spectra, it can resolve fluorophores with overlapping emission spectra [6]. However, overlapping excitation spectra is a problem in the FDM-LIF system, and any assay must be prepared using fluorophores with minimal excitation overlap. Therefore, fluorophores with sharp excitation lines such as lanthanide ions are the best candidate material in use with FDM-LIF system [67].

To enhance our FDM-LIF system performance, a four layer FDM-PCB control circuit has been developed to control (or modulate at three distinguished frequencies up to 100MHz) three different lasers, convert light scattered signals to voltage signals via a light detector and a TIA or NIA, and demodulate the multiplexed signal into three different channels. The circuit was found to be operational using good quality single mode laser diodes. The actual NIA stage has 100 MHz bandwidth and 21 dB gain.

The developed FDM-LIF system is used for high-speed detection of droplets; two of the three channels (450@25 MHz and 680nm@40 MHz) are successfully used to discriminate alternating droplets containing two different fluorophores: Fluorescein and Alexa 680. The droplets are generated using an alternating drop generator which is currently limited to 300 drops/sec. As a measure of detection limit, the system is able to

detect a single droplet at 2800 drops/sec produced using a high speed droplet generator suggested by Anna et al., 2003 [35].

In the effort of applying our developed FDM-LIF system to cell cytometry, we installed the system in an old cell Becton Dickinson Imunocytometry System (model FACScan). The old laser light source in the instrument is replaced with our three combined lasers and their control circuit. The four PMTs onboard are replaced by only one PMT with a triple band filter. This PMT, along with the FDM-LIF circuit, can be used to detect all fluorescence and the side scatter signals. The forward scatter light signal is collected using fiber optical cable and directed to a separate APD and detection electronics. We successfully demonstrated the detection of the forward and side scatter signals. The fluorescent measurements, however, were unsuccessful but can be addressed by improving optical alignments of the laser in future work.

REFERENCES

[1] S. Fantini, M.-A. Franceschini, J. S. Maier, S. A. Walker, B. B. Barbieri, and E. Gratton, "Frequency-domain multichannel optical detector for noninvasive tissue spectroscopy and oximetry," *Optical Engineering*, vol. 34, no. 1, pp. 32–42, 1995.

[2] F. Komurian-Pradel, G. Paranhos-Baccalà, M. Sodoyer, P. Chevallier, B. Mandrand, V. Lotteau, and P. André, "Quantitation of HCV RNA using real-time PCR and fluorimetry," *Journal of virological methods*, vol. 95, no. 1, pp. 111–119, 2001.

[3] M. O'Toole and D. Diamond, "Absorbance based light emitting diode optical sensors and sensing devices," *Sensors*, vol. 8, no. 4, pp. 2453–2479, 2008.

[4] V. Trivedi, A. Doshi, G. Kurup, E. Ereifej, P. Vandevord, and A. S. Basu, "A modular approach for the generation, storage, mixing, and detection of droplet libraries for high throughput screening," *Lab Chip*, vol. 10, no. 18, pp. 2433–2442, 2010.

[5] Y. Suzuki, H. Hori, M. Iwatsuki, and T. Yamane, "A four-wavelength channel absorbance detector with a light emitting diode-fiber optics assembly for simplifying the flow-injection analysis system," *Analytical sciences*, vol. 19, no. 7, pp. 1025–1028, 2003.

[6] W. Schmidt, "A high performance micro-dual-wavelength-spectrophotometer (MDWS)," *Journal of Biochemical and Biophysical Methods*, vol. 58, no. 1, pp. 15–24, 2004.

[7] N. R. D. Aslund and K. S. Carlsson, "Apparatus for quantitative imaging of multiple fluorophores," 1994.

[8] K. Carlsson, “Signal-to-noise ratio for confocal microscopy when using the Intensity-modulated Multiple-beam Scanning (IMS) technique,” *Micron*, vol. 26, no. 4, pp. 317–322, 1995.

[9] K. Carlsson, “Confocal scanning microfluorometry of dual-labelled specimens using two excitation wavelengths and lock-in detection technique,” *Micron*, vol. 24, no. 6, pp. 603–609, 1993.

[10] K. Carlsson, N. Åslund, K. Mossberg, and J. Philip, “Simultaneous confocal recording of multiple fluorescent labels with improved channel separation,” *Journal of microscopy*, vol. 176, no. 3, pp. 287–299, 1994.

[11] K. Carlsson and A. Liljeborg, “Simultaneous confocal lifetime imaging of multiple fluorophores using the intensity-modulated multiple-wavelength scanning (IMS) technique,” *Journal of microscopy*, vol. 191, no. 2, pp. 119–127, 1998.

[12] G. Kurup and A. S. Basu, “Multispectral Absorbance Photometry with a Single Light Detector Using Frequency Division Multiplexing,” 2010.

[13] K. M. Dadesh, G. K. Kurup, and A. S. Basu, “High speed low noise multiplexed three color absorbance photometry,” in *Engineering in Medicine and Biology Society,EMBC, 2011 Annual International Conference of the IEEE*, 2011, pp. 39 – 42.

[14] R. Ziemer and W. H. Tranter, *Principles Of Communications: System Modulation And Noise*, 6th ed. John Wiley & Sons, 1976.

[15] PerkinElmer-Optoelectronics, “Silicon Avalanche Photodiodes,” 2000.

[16] PerkinElmer-Precisely, “Avalanche Photodiodes: A User’s Guide,” 2003.

[17] Hamamatsu-Photonics, “Photomultiplier tubes basics and applications,” 2006.

[18] Hamamatsu-Photonics, “Photomultiplier Tubes,” 2008.

[19] R. E. Simpson, *Introductory electronics for scientists and engineers*. Prentice Hall, 1987.

[20] J. H. Scofield, “Frequency-domain description of a lock-in amplifier,” *American Journal of Physics*, vol. 62, no. 2, pp. 129–132, 1994.

[21] G. C. Bjorklund, “Frequency-modulation spectroscopy: a new method for measuring weak absorptions and dispersions,” *Optics Letters*, vol. 5, no. 1, pp. 15–17, 1980.

[22] M. Nakamura, K. Aiki, N. Chinone, R. Ito, and J. Umeda, “Longitudinal-mode behaviors of mode-stabilized Al x Ga 1-x As injection lasers,” *Journal of Applied Physics*, vol. 49, no. 9, pp. 4644–4648, 1978.

[23] S. Kobayashi, Y. Yamamoto, M. Ito, and T. Kimura, “Direct frequency modulation in AlGaAs semiconductor lasers,” *Quantum Electronics, IEEE Journal of*, vol. 18, no. 4, pp. 582–595, 1982.

[24] W. Lenth, “Optical heterodyne spectroscopy with frequency-and amplitude-modulated semiconductor lasers,” *Optics letters*, vol. 8, no. 11, pp. 575–577, 1983.

[25] K. Razdan and D. A. Van Baak, “Demonstrating optical beat notes through heterodyne experiments,” *American Journal of Physics*, vol. 70, p. 1061, 2002.

[26] P. C. D. Hobbs, *Building electro-optical systems: making it all work*. Wiley, 2009.

[27] Texas-Instrument, “1.6GHz, Low-Noise, FET-Input Operational Amplifier,” 2008.

[28] Texas-Instrument, “Transimpedance Considerations for High-Speed Amplifiers,” 2009.

[29] A. Krishan, H. Krishnamurthy, and S. Totey, *Applications of Flow Cytometry in Stem Cell Research and Tissue Regeneration*. Wiley-Blackwell, 2011.

[30] P. K. Chattopadhyay, C. M. Hogerkorp, and M. Roederer, “A chromatic explosion: the development and future of multiparameter flow cytometry,” *Immunology*, vol. 125, no. 4, pp. 441–449, 2008.

[31] V. Kapoor, V. Karpov, C. Linton, F. V. Subach, V. V. Verkhusha, and W. G. Telford, “Solid state yellow and orange lasers for flow cytometry,” *Cytometry A*, vol. 73, no. 6, pp. 570–577, Jun. 2008.

[32] Y. Xia and G. M. Whitesides, “SOFT LITHOGRAPHY,” *Annual Review of Materials Science*, vol. 28, no. 1, pp. 153–184, Aug. 1998.

[33] Y. Tung, “PDMS-based opto-fluidic micro flow cytometer with two-color, multi-angle fluorescence detection capability using PIN photodiodes,” *Sensors and Actuators B: Chemical*, vol. 98, no. 2–3, pp. 356–367, Mar. 2004.

[34] P. Garstecki, M. J. Fuerstman, H. A. Stone, and G. M. Whitesides, “Formation of droplets and bubbles in a microfluidic T-junction—scaling and mechanism of break-up,” *Lab on a Chip*, vol. 6, no. 3, pp. 437–446, 2006.

[35] S. L. Anna, N. Bontoux, and H. A. Stone, “Formation of dispersions using ‘flow focusing’ in microchannels,” *Applied physics letters*, vol. 82, p. 364, 2003.

[36] L.-H. Hung, K. M. Choi, W.-Y. Tseng, Y.-C. Tan, K. J. Shea, and A. P. Lee, “Alternating droplet generation and controlled dynamic droplet fusion in

microfluidic device for CdS nanoparticle synthesis," *Lab on a Chip*, vol. 6, no. 2, pp. 174–178, 2006.

[37] Microchem, "NANO SU-8: Negative Tone Photoresist Formulation." 2002.

[38] C.-C. Chang, Z.-X. Huang, and R.-J. Yang, "Three-dimensional hydrodynamic focusing in two-layer polydimethylsiloxane (PDMS) microchannels," *Journal of Micromechanics and Microengineering*, vol. 17, no. 8, p. 1479, 2007.

[39] C. Simonnet and A. Groisman, "Two-dimensional hydrodynamic focusing in a simple microfluidic device," *Applied Physics Letters*, vol. 87, no. 11, pp. 114104–114104–3, 2005.

[40] F.-C. Chang and Y.-C. Su, "Controlled double emulsification utilizing 3D PDMS microchannels," *Journal of Micromechanics and Microengineering*, vol. 18, no. 6, p. 065018, 2008.

[41] X. Mao, J. R. Waldeisen, and T. J. Huang, "'Microfluidic drifting'—implementing three-dimensional hydrodynamic focusing with a single-layer planar microfluidic device," *Lab on a Chip*, vol. 7, no. 10, pp. 1260–1262, 2007.

[42] S. D. Cusworth, J. M. Senior, and .S.E. Moss, "Multiplexing techniques for noninterferometric optical point-sensor networks: A review," *Fiber & Integrated Optics*, vol. 17, no. 1, pp. 3–20, 1998.

[43] A. D. Taylor, J. Ladd, Q. Yu, S. Chen, J. Homola, and S. Jiang, "Quantitative and simultaneous detection of four foodborne bacterial pathogens with a multi-channel SPR sensor," *Biosensors and Bioelectronics*, vol. 22, no. 5, pp. 752–758, 2006.

[44] B. Chance and N. Graham, “A Rapid Scanning Dual Wavelength Spectrophotometer,” *Review of Scientific Instruments*, vol. 42, no. 7, pp. 941 –945, Jul. 1971.

[45] G. Totschnig, D. S. Baer, J. Wang, F. Winter, H. Hofbauer, and R. K. Hanson, “Multiplexed continuous-wave diode-laser cavity ringdown measurements of multiple species,” *Applied optics*, vol. 39, no. 12, pp. 2009–2016, 2000.

[46] W. Schmidt, “A high-performance dual-wavelength spectrophotoometer and fluorometer,” *Journal of Biochemical and Biophysical Methods*, vol. 2, no. 3, pp. 171–181, 1980.

[47] M. P. Arroyo, T. P. Birbeck, D. S. Baer, and R. K. Hanson, “Dual diode-laser fiber-optic diagnostic for water-vapor measurements,” *Optics letters*, vol. 19, no. 14, pp. 1091–1093, 1994.

[48] L. Gianfrani, G. Gagliardi, M. van Burgel, and E. Kerstel, “Isotope analysis of water by means of near infrared dual-wavelength diode laser spectroscopy,” *Opt Express*, vol. 11, no. 13, pp. 1566–1576, Jun. 2003.

[49] D. B. Oh, M. E. Paige, and D. S. Bomse, “Frequency modulation multiplexing for simultaneous detection of multiple gases by use of wavelength modulation spectroscopy with diode lasers,” *Applied optics*, vol. 37, no. 12, pp. 2499–2501, 1998.

[50] I. Y. Eom and P. K. Dasgupta, “Frequency-selective absorbance detection: Refractive index and turbidity compensation with dual-wavelength measurement,” *Talanta*, vol. 69, no. 4, pp. 906–913, 2006.

[51] D. Izquierdo, M. Puyol, I. Salinas, R. Alonso, J. Alonso, C. Domínguez, and I. Garcés, “Dual-wavelength measurement system for absorbance chemical sensing,” *Measurement Science and Technology*, vol. 18, p. 3443, 2007.

[52] F. Wu, X. Zhang, J. Y. Cheung, K. Shi, Z. Liu, C. Luo, S. Yin, and P. Ruffin, “Frequency division multiplexed multichannel high-speed fluorescence confocal microscope,” *Biophysical journal*, vol. 91, no. 6, pp. 2290–2296, 2006.

[53] K. M. Dadesh and A. S. Basu, “Multicolor LIF Detection in A Single Optical Window Using Phase-Sensitive Multiplexing,” presented at the MicroTAS 2011, the 15th International Conference on Miniaturized Systems for Chemistry and Life Sciences, 2011, p. 3.

[54] Elantec, “EL6245C - Product Brief,” 2001.

[55] Analog-Devices, “500 MHz Four-Quadrant Multiplier,” no. Rev. E, 2008.

[56] Murata-C31E-NF, “Chip EMIFIL,” 2011.

[57] Murata-C31E-BL, “Chip Ferrite Bead,” 2011.

[58] TDK, “Multilayer Ceramic Chip Capacitors,” 2010.

[59] Murata-C31E-DL, “Chip Common Mode Choke Coil,” 2011.

[60] Analog-Devices, “500 MHz Four-Quadrant Multiplier,” no. Rev. E, 2008.

[61] Analog-Devices, “AD622N Instrumentation Amplifier,” 2012.

[62] H. Cartwright, “Color perception and factor analysis,” *J. Chem. Educ.*, vol. 63, no. 11, p. 984, 1986.

[63] A. S. Basu and Y. B. Gianchandani, “A programmable array for contact-free manipulation of floating droplets on featureless substrates by the modulation of

surface tension," *Microelectromechanical Systems, Journal of*, vol. 18, no. 6, pp. 1163–1172, 2009.

[64] A. B. Theberge, F. Courtois, Y. Schaerli, M. Fischlechner, C. Abell, F. Hollfelder, and W. T. S. Huck, "Microdroplets in microfluidics: an evolving platform for discoveries in chemistry and biology," *Angewandte Chemie International Edition*, vol. 49, no. 34, pp. 5846–5868, 2010.

[65] J. C. Baret, O. J. Miller, V. Taly, M. Ryckelynck, A. El-Harrak, L. Frenz, C. Rick, M. L. Samuels, J. B. Hutchison, and J. J. Agresti, "Fluorescence-activated droplet sorting (FADS): efficient microfluidic cell sorting based on enzymatic activity," *Lab Chip*, vol. 9, no. 13, pp. 1850–1858, 2009.

[66] L. Novak, P. Neuzil, J. Pipper, Y. Zhang, and S. Lee, "An integrated fluorescence detection system for lab-on-a-chip applications," *Lab on a Chip*, vol. 7, no. 1, pp. 27–29, 2007.

[67] J.-C. G. Bünzli and C. Piguet, "Taking advantage of luminescent lanthanide ions," *Chemical Society Reviews*, vol. 34, no. 12, pp. 1048–1077, 2005.

ABSTRACT

MULTIPLEXED PHOTOMETRY AND FLUORIMETRY USING MULTIPLE FREQUENCY CHANNELS

by

KHALED M. DADESH

August 2013

Advisor: Dr. Amar Basu

Major: Electrical Engineering

Degree: Doctor of Philosophy

Multispectral photometry and fluorimetry are useful for quantifying and distinguishing samples during flow injection analysis, flow cytometry, and ratiometric absorbance measurement. However, multispectral detectors, including spectrometers, typically require arrayed or multiple light detectors, optical components, and path alignments, all of which increases the size and cost of the detection system. Several previous efforts have attempted the use of time division multiplexing or frequency division multiplexing (FDM) techniques to minimize both size and cost of multispectral photometry equipment by using only a single light detector. Although many of these designs achieved low cost, they generally operated at <50 KHz, which limited the detection speed of the overall system. An alternative frequency multiplexing design operated at 3MHz; however, it required electro optical modulators [50], which are too expensive and bulky for portable applications. In contrast to both approaches, the

objective of this research is to use frequency division multiplexing to perform multispectral photometry and fluorimetry while achieving both low cost and high frequency operation (up to 100 MHz). The multiplexing is performed electronically using low cost optoelectronic sources, a single light detector, and a single high-throughput interrogation window. It enables us to perform multi-parameter biological analysis at lower costs and less complexity. Multiple monochromatic light sources, each with a unique wavelength, are electronically modulated at distinct frequencies, and their combined light emission is directed to the sample detection cell. The light transmitted by the sample (absorbance mode) or emitted by the sample (fluorescence mode) is directed to a single light detector. The received light is then converted to a voltage signal and demodulated into the frequency channels using phase-sensitive electronics. Each recovered channel therefore provides either absorbance or fluorescence at its respective optical wavelength. The system is designed to operate at high speed in order to be used in high throughput detectors such as flow cytometers. As a proof of concept, we apply the FDM technique in two detection systems: 1) a three-color absorbance photometry detector and 2) a two-color laser induced fluorescence (LIF) detector. In the first system, three LEDs are operated with 150 KHz, 200 KHz, and 250 KHz modulation frequencies, and the system achieves a 1 ms measurement time constant at an overall component cost <$10. We perform absorbance photometry of four different organic dyes in flow injected solutions and in discrete droplet microreactors with throughputs in the 10's of samples per second. In both cases, the system is able to simultaneously discriminate between them [13]. In the LIF system, first two laser diodes operated at 1 KHz and 1.5 KHz,

respectively, are used to excite fluorophores at the respective frequencies. This system is able to distinguish low speed (1 drop/sec) water-in-oil droplets containing fluorescein or rhodamine-6G generated in a microfluidic junction. Second two laser diodes operated at 25MHz and 40 MHz, respectively, are controlled using a developed high frequency FDM system to excite Fluorescein and Alexa 680 dyes at the respective frequencies. Because of the high frequency operation, this system is able to distinguish alternating high speed (300 drops/sec) droplets containing the two fluorescent dyes. In both case, the developed In previous experiments we use an inverted fluorescence microscope with a specific optical cube to excite dyes and collect fluorescence signals. These two FDM-LIF systems identify the different fluorophores based on their excitation frequency rather than their emission band, giving it a unique ability to distinguish fluorophores with overlapping emission spectra. However, overlapping excitation spectra is a problem in the FDM-LIF system, and any assay has to be prepared using fluorophores with minimal excitation overlap. Therefore, fluorophores with sharp excitation lines such as lanthanide ions are the best candidate material in use with FDM-LIF system. The system uses high frequency (100 MHz) modulation which enables multiplexed time constants on the order of 1 μs. Achieving this high bandwidth allow us to apply the system towards high throughput analysis such as cell cytometry, where it could substantially reduce cost and size of the system. Therefore, the FDM-LIF system is installed in an old BD bioscience cytometer, which is available in the cell cytometry laboratory in Karmanos Cancer Research Center (KCRC) located at Detroit Medical Center (DMC). A biological assay containing Alexa Fluor® 680 Goat Anti-Mouse IgG (H+L) and Alexa Fluor® 430 Goat Anti-Mouse IgG

(H+L) with BD™ CompBead Anti-mouse Ig, κ beads is tested using the FDM-LIF system. The system is capable to count the two different antigens simultaneously, which gives the possibility of incorporating this system in cytometers. This technology promises to reduce cost and complexity of future cytometers.

AUTOBIOGRAPHICAL STATEMENT

Khaled M. Dadesh; Ph. D. from Wayne State University, Electrical and Computer Engineering Department, 2013. M.Sc. and B.Sc from Tripoli University, Electrical and Electronic Engineering Department in 2003 and 1992, respectively. Worked as a researcher in the center for solar energy studies, Tripoli Libya from 1996 to 2006, and a faculty at Tripoli University from 2006 to 2008. Awarded a scholarship to earn the Ph. D. in electrical engineering from the US from 2008 to 2013.